Optimal Exploration Systems

by

Andrew T. Klesh

A dissertation submitted in partial fulfillment
of the requirements for the degree of
Doctor of Philosophy
(Aerospace Engineering)
in The University of Michigan
2009

Doctoral Committee:
Professor Pierre T. Kabamba, Co-Chair
Assistant Professor Anouck R. Girard, Co-Chair
Professor James J. Duderstadt
Emeritus Professor Elmer G. Gilbert
Associate Professor Ella M. Atkins
Associate Professor Emilio Frazzoli, MIT

A man's dream should exceed his reach, or what's a heaven for?

— Robert Browning

To my parents, my family and my friends.

Acknowledgments

It goes without saying that I have the deepest gratitude for the advice, teachings and comments from my two thesis advisers Professor Anouck Girard and Professor Pierre Kabamba and my thesis committee. From them I have learned to speak, write, listen, argue and, every once in a while, think.

My experience at Michigan would not have been complete if not for the guidance from many other advisers throughout the years: Dr. Duderstadt who let me play, Professor Washabaugh who gave me my first lab, Professor Cesnik who helped me build my first flying UAV, Professor Bernal who supported SpaceBubbles, Professor Atkins who brought me to flight and Professor Cutler who gave me access to space. I cannot thank you enough for the opportunities and words of wisdom you have given.

Professor Gilbert offered me extensive comments and a very precise understanding of optimal control. Without his help and time I would not have been able to complete this work.

Beyond these few, I must thank the entire student, faculty and staff body of the Aerospace Engineering department for making Michigan such a memorable experience. I should especially note Eric Gustafson and Amor Menezes for the debates, edits and arguments that helped us all survive. For John Chang, Baro Hyun and Sara Spangelo: your heroic efforts helped complete this thesis. To all the student groups I have been a part of, especially the SolarBubbles team, I thank you.

I am very grateful for the assistance from several entities which supported this work in part: The United States Department of Defense Air Force Office of Scientific Research,

the Air Force Research Lab, the Michigan Space Grant Consortium and NASA/Jet Propulsion Laboratory, the University of Michigan Aerospace Engineering Department, and the Rotorcraft Design Center.

Without the support of my friends and family scattered around the world I would never have started much less finished this work. Many thanks. This thesis is dedicated to you.

Preface

This dissertation was submitted at the University of Michigan in partial fulfillment of the requirements for the degree of Doctor of Philosophy in Aerospace Engineering, and defended on February 6, 2009. The doctoral committee was composed of Assistant Professor Anouck Girard, committee co-chair, Professor Pierre Kabamba, committee co-chair, Associate Professor Ella Atkins, Professor and President Emeritus James Duderstadt, Professor Emeritus Elmer Gilbert, and Massachusetts Institute of Technology Associate Professor Emilio Frazzoli. This thesis is a comprehensive work based on the following papers that have been published in journals and presented at conferences:

Publications

A. Klesh, A. Girard, P. Kabamba. "Cooperative Thermalling: Extending the Endurance of Unmanned Aerial Vehicles." Optimization and Cooperative Control Strategies: Proceedings of the 8th International Conference on Cooperative Control and Optimization, Lecture Notes in Computer Science, Springerman, 2009.

A. Klesh, P. Kabamba. "Solar-Powered Aircraft: Energy-Optimal Path Planning and Perpetual Endurance." AIAA Journal of Guidance, Decision and Control, 2009, Accepted.

A. Klesh, A. Girard, P. Kabamba. "Time-Optimal Path Planning for Autonomous Exploration." AIAA Journal of Guidance, Decision and Control, 2008, Submitted.

A. Klesh, T. Huntsberger, G. Woodward, B. Hyun, A. Girard, P. Kabamba. "Tactical Area Search with Non-Isotropic Sensors." IEEE Journal of Field Robotics, In Preparation.

A. Klesh, J. Chang, A. Girard, P. Kabamba. "Optimal Path Planning for Uncertain Exploration." IEEE Transactions, In Preparation.

Conferences

A. Klesh, P. Kabamba. "Energy-Optimal Path Planning for Solar-Powered Aircraft in Level Flight." AIAA Guidance, Navigation and Control Conference, 2007.

A. Klesh, P. Kabamba. "Solar-Powered Unmanned Aerial Vehicles on Mars: Perpetual Endurance." 58th International Astronautical Congress, 2007.

A. Klesh, A. Girard, P. Kabamba."Cooperative Thermalling: Extending the Endurance of Unmanned Aerial Vehicles." 8th International Conference on Cooperative Control and Optimization, 2008.

A. Klesh, A. Girard, P. Kabamba. "Real-Time Path Planning for Time-Optimal Exploration." AIAA Guidance, Navigation and Control Conference, 2008.

A. Klesh, A. Girard, P. Kabamba. "Path Planning for Cooperative Time-Optimal Information Collection." American Control Conference, 2008.

A. Girard, J. Hedrick, A. Klesh, B. Basso, J. Love. "Control of Mobile Sensor Networks: A State-Of-The-Art Review", ASME Dynamic Systems and Control Conference, 2008.

A. Klesh, D. Macy, P. Senatore, N. Rooney, J. Wiebanga, A. Smith. "SolarBubbles: An Autonomous Solar-Powered UAV." Autonomous Unmanned Vehicle Systems International, 2008.

A. Klesh, A. Girard, P. Kabamba. "Optimal Path Planning for Uncertain Exploration." Proceedings of the American Control Conference, 2009, Accepted.

E. Atkins, R. Eubank, A. Klesh. "A Reconfigurable Flight Management System for Small-Scale Unmanned Air Systems." AIAA Infotech, 2009, Accepted.

Z. Hasan, M. Faied, A. Klesh, A. Girard. "Distributed Heterogeneous Control of Mini-Flying Machines and Ground Robots", AIAA Guidance, Navigation and Control Conference, 2009, Accepted.

B. Hyun, A. Klesh, A. Girard. "Robotic exploration with a non-isotropic sensor." AIAA Guidance, Navigation and Control Conference, 2009. Accepted.

A. Klesh, T. Huntsberger, G. Woodward, P. Kabamba, A. Girard. "An Information-Based Adaptive Area Search Method", IEEE Conference on Decision and Control, 2009, In Preparation.

A. Klesh, S. Spangelo, P. Kabamba, A. Girard. "Exploration and Surveillance with Solar-Powered Aircraft." IEEE Conference on Decision and Control, 2009, In Preparation.

Table of Contents

List of Tables

Table

List of Figures

List of Appendices

Appendix

Abstract

This dissertation studies optimal exploration, defined as the collection of information about given objects of interest by a mobile agent (the explorer) using imperfect sensors. The key aspects of exploration are kinematics (which determine how the explorer moves in response to steering commands), energetics (which determine how much energy is consumed by motion and maneuvers), informatics (which determine the rate at which information is collected) and estimation (which determines the states of the objects). These aspects are coupled by the steering decisions of the explorer. We seek to improve exploration by finding trade-offs amongst these couplings and the components of exploration: the Mission, the Path and the Agent.

A comprehensive model of exploration is presented that, on one hand, accounts for these couplings and on the other hand is simple enough to allow analysis. This model is utilized to pose and solve several exploration problems where an objective function is to be minimized. Specific functions to be considered are mission duration and total energy. These exploration problems are formulated as optimal control problems and necessary conditions for optimality are obtained in the form of two-point boundary-value problems. An analysis of these problems reveals characteristics of optimal exploration paths. Several regimes are identified for the optimal paths including the Watchtower, Solar and Drag regime, and several non-dimensional parameters are derived that determine the appropriate regime of travel. The so-called Power Ratio is shown to predict the qualitative features of the optimal paths, provide a metric to evaluate an aircrafts design and determine an aircrafts capability for flying perpetually. Optimal exploration system drivers are identified

that provide perspective as to the importance of these various regimes of flight.

A bank-to-turn solar-powered aircraft flying at constant altitude on Mars is used as a specific platform for analysis using the coupled model. Flight-paths found with this platform are presented that display the optimal exploration problem characteristics. These characteristics are used to form heuristics, such as a Generalized Traveling Salesman Problem solver, to simplify the exploration problem. These heuristics are used to empirically show the successful completion of an exploration mission by a physical explorer.

Chapter 1

Introduction

1.1 Background

Humans have felt the drive to explore throughout history. In this dissertation, we deal with exploration defined as the augmentation of knowledge about a geographic area through the collection of information. The relationship between exploration and information is expressed in a quote by Thomas Jefferson who, in 1803, introduced the Lewis and Clark expedition by writing to Congress "An intelligent officer... fit for the enterprise... might explore the whole [Missouri River] line, even to the Western Ocean ... and return with the information acquired, in the course of two summers." The basic tenets of exploration can be distilled from this statement. The objectives of exploration are to:

- Investigate an area or objects of interest within an area (the *Mission*),
- Acquire and return information using a local topology (the *Path*),
- Satisfy constraints even in the presence of uncertainty and time limitations.

Current explorers, or *agents*, travel under seas (98), over land (59), in the air (96) and in outer space (121). While the environments, challenges and agents differ, the objectives of exploration remain the same.

In this dissertation, we seek to understand and exploit the couplings between the mission, the path and the agent of exploration. We first define these couplings in more explicit

terms.

1.2 Exploration and Information

Shannon (117) wrote that information is produced when "one message is chosen from a set of possible messages" and he introduced a theory to quantify this information. The earliest application of this theory was in the engineering of communication systems, which convey messages over a distance. We examine the engineering of information systems, not the meaning of information. As Shannon stated, "Frequently the messages have meaning; that is they refer to or are correlated according to some system with certain physical or conceptual entities. These semantic aspects of communication are irrelevant to the engineering problem" (117). In this work, the message is the state of a particular object of interest or area. Here, a state is a quantitative measure of an object, i.e., the size of an object, its position, its visibility, the value of its scientific interest, etc, described by real numbers or numbers of bits.

As shown in Figure 1.1, a communication process involves the encoding of a message by an information source and the resultant signal is sent over a channel by a transmitter. This signal may be corrupted by noise. A receiver (what we call an agent) receives the signal, decodes it, and extracts meaning. The information transmitted through this process is related to the probability of an intended message.

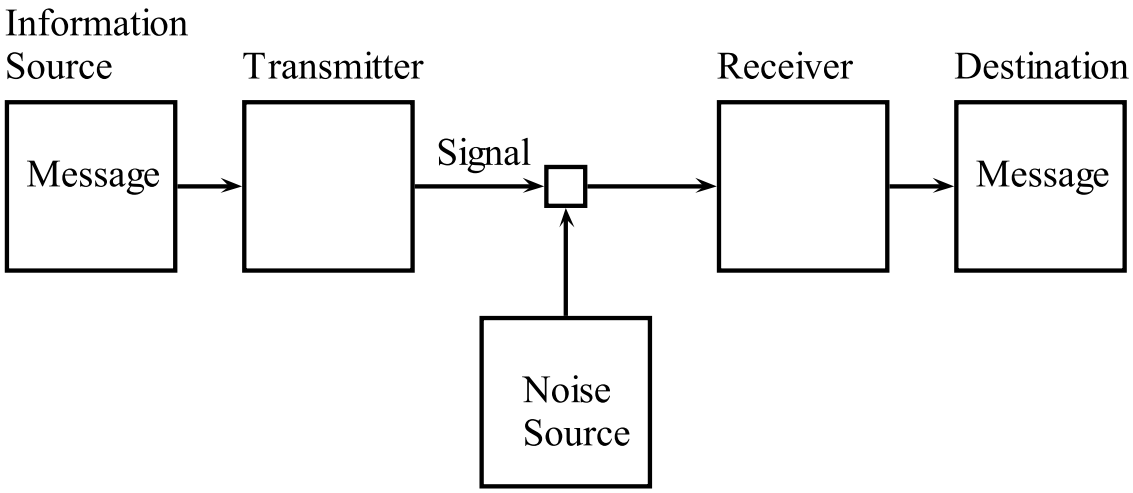

(a) Communication Model

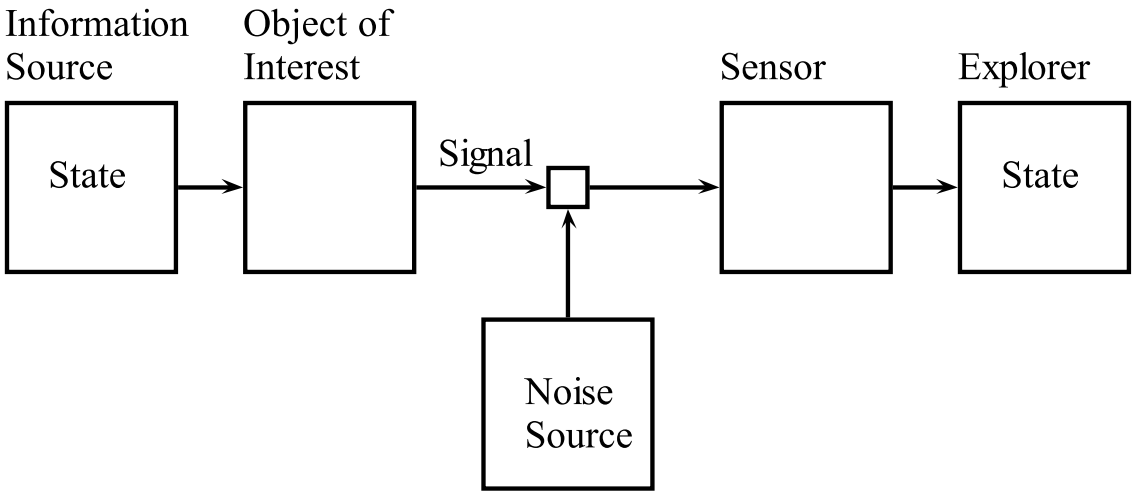

(b) Exploration Model

Figure 1.1 Schematic diagram of a general communication system (117) as related to an exploration system

Communication and exploration are similar in that they both require an agent to extract meaning from a signal. In the case of exploration, the agent is the explorer, the signal is the measurements from the sensors (e.g., visual/optical, radar or sonar), and the information is a measure of the probability distribution of the state of an object of interest, i.e., a measure of uncertainty.

However, exploration is distinct from communication. Specifically, an agent has to determine a path that is optimal (e.g., with respect to time or energy) subject to information constraints and estimate the state of the object of interest from the signal. That is, a communication receiver acts as a static explorer.

In this work, we view exploration as the collection of information for use in estimating a state of an object of interest. The amount of information that is collected about the probability distribution describing the state is a constraint on the optimal exploration problem. We assume that a fixed optimal code is used in all signal transmissions, hence we ignore coding in the analysis. We use Shannon's channel capacity equation as an example of how the information rate is bounded. The limits on information (here called informatics, i.e., the study of information systems), together with an analysis of agent kinematics and energy, optimization theory, and state estimation are the basis for our model of exploration.

1.3 Exploration and the Agent

An autonomous agent of exploration is a vehicle equipped with a payload to carry out the mission. Part of this payload is an onboard sensor, capable of collecting information from an exploration area and used for estimating states. The rate of acquisition of information is related to the distance between the sensor and the object of interest, i.e., we consider range-dependent sensing. In our model, decreasing this distance increases the rate at which information is collected. The vehicle, starting from an initial position, changes location with a speed appropriate to its kinematic capabilities, mission objectives and energy char-

acteristics. We refer to these energy characteristics as energetics as they describe the energy collected and lost by the vehicle.

Real-world sensors are imperfect, with a degree of accuracy often depending upon mission, path and vehicle characteristics. Trades between these characteristics can influence the capabilities of the agent and, as such, affect the completion of the mission. One such trade involves the aperture of the sensor. The sensor aperture is the angular range of possible relative azimuths (the angle between the agent's line of sight from its current position to the object of interest and the line along the agents heading), centered along the vehicle's heading, within which information can be collected. An isotropic sensor is able to collect information at all relative azimuths to the agent. Therefore, an isotropic sensor has a sensor aperture of 360 degrees. A more typical sensor is non-isotropic, and has a sensor aperture of less than 360 degrees.

Further sensor imperfections are include measurement noise and bandwidth limitations, i.e., restrictions on the information collection rate. These imperfections all affect the ability of the agent to accurately measure the state. Hence, to increase measurement accuracy, a filter is often required. This filter utilizes the information acquired along with noisy measurements to form an accurate state estimate.

Additional capabilities of the agent, including payload capacity, must also be considered. Each capability comes with a cost, both in mass and money. These costs must be balanced and can adversely affect exploration performance.

1.4 Exploration and the Environment

In this dissertation, the exploration environment includes an area to be explored and multiple objects of interest each having state attributes expressed parametrically by real numbers with known probability distributions. The agent that operates in the environment attempts to accomplish the pre-defined exploration mission objectives.

The following are assumptions related to the exploration problem presented in this dissertation. 1) The exploration area is located on a spherical planet in circular orbit around a star. 2) This planet has a spin-axis tilted with respect to the normal of the plane of its orbit. 3) The planet receives light in the form of energy waves traveling radially out from the center of the star. 4) The planetary exploration area is located in the vicinity of a specified planetary latitude and longitude. 5) The area is flat, i.e., within the area, the curvature of the planet is neglected. 6) The area is free of obstacles and 7) the agent can move freely within this area subject to its kinematics. Assumptions 1-4 affect the energy collection while 5-7 affect the vehicle path.

Various objects of interest with unknown states are located in the exploration area. These objects of interest have a pre-specified, fixed position with states that are time-invariant. Each object of interest is viewed as an omni-directional transmitter of a signal whose message contains information about the state parameter. Inherent object properties, including reflectivity, emissivity, and absorption, can increase or decrease the power of the signal in relation to the transmission channel noise, i.e., the measurement noise. The overall strength of a transmitted signal is the object's *visibility* and is expressed as the visibility parameter. An agent at a given distance from a highly visible object collects information faster than if the object is poorly visible. This visibility parameter is expressed as a constant for each object of interest.

The states of the object of interest are to be estimated by the agent with an acceptable level of variance of the estimation error. While not knowing where objects of interest may be located is a serious concern, even objects with known positions can present problems. Indeed, the sequence in which objects of interest must be investigated by an agent can determine the success of an exploration mission. Once this sequence of objects has been established, a path can be found that meets the requirements of the mission subject to the constraints.

1.5 Exploration and the Path

The exploration path is built from a time-history of the position of an agent. In a typical exploration problem, the decision of where to go strongly influences the quantity and quality of information received. This coupling of kinematics and informatics makes exploration problems particularly challenging: An optimal explorer must decide where to go so that the path followed is the most informative subject to mission requirements. Choosing the correct path, aligned with agent and sensor capabilities, is critical to mission success.

A path begins at the initial location of the agent within the exploration area. The entirety of the path is restricted to satisfy agent kinematic constraints. Control decisions made by the explorer alter the direction of the agent. A path that satisfies the mission requirements allows an agent traveling on that path to collect the pre-specified amount of information required by the mission objectives. Furthermore, a time-optimal or energy-optimal path meets these objectives while satisfying the requirements for optimality.

Unfortunately, the most informative path is often neither time-optimal nor energy-optimal. Worse, there is typically a trade-off between the amount of time to complete a mission and the amount of energy required (especially for solar-powered vehicles). As time and energy are often the expendables of an agent, finding an appropriate trade-off or weighting can be critical for mission success.

1.6 The Difficulty of Exploration

The relationships between exploration and information, the agent, the environment and the path have been outlined in the previous sections. These relationships must be considered when steering an agent in an uncertain environment along informative paths to meet mission objectives. The technical challenges of the exploration problem arise from the multiple couplings between several components: kinematics, informatics, energetics and state estimation. These components are linked by the control decisions of the agent, the design of

the agent and the environmental conditions. These interactions are illustrated in Figure 1.2.

This dissertation examines the relationship between the agent, the mission and the path by considering the trade-offs of agent performance and cost, a priori and a posteriori knowledge, and path duration and energy. A thorough understanding of these interactions allows significant exploration improvements. The difficulty in exploration arises from balancing these trade-offs while satisfying mission requirements.

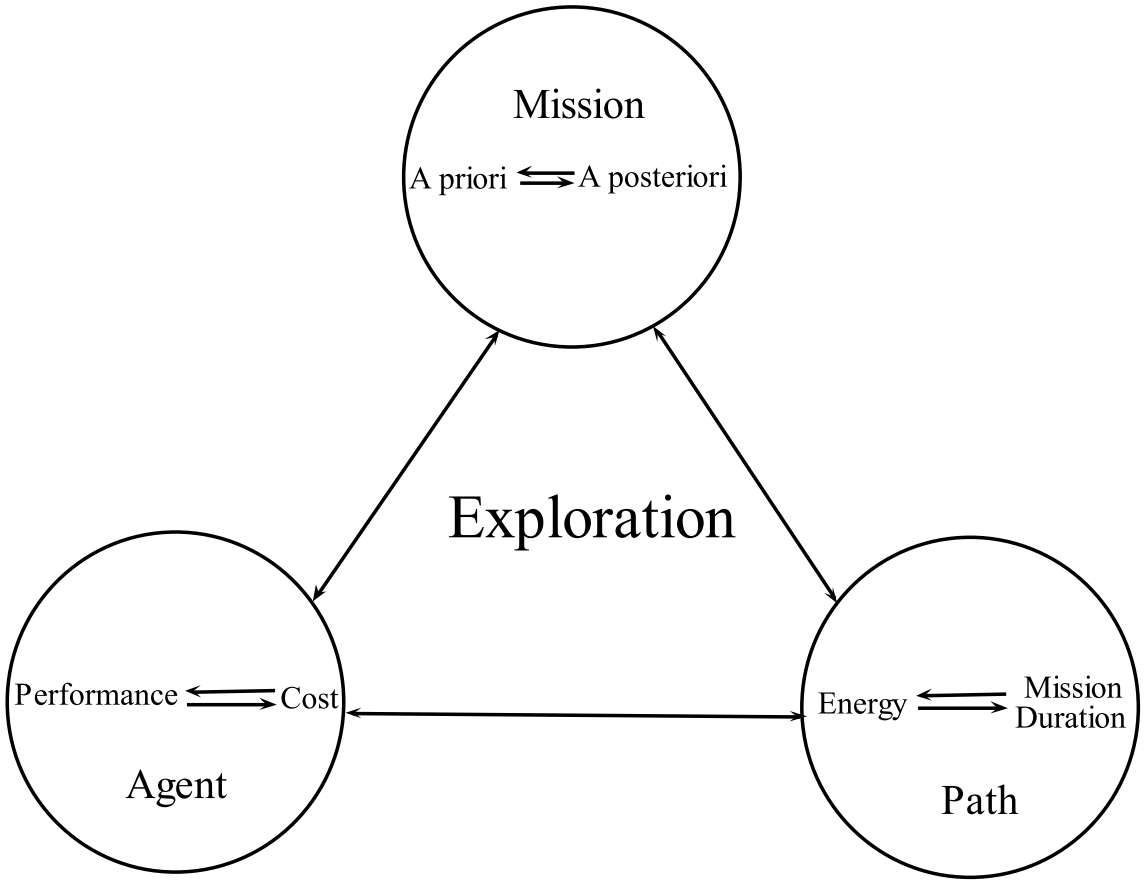

Figure 1.2 A model describing the three interacting components of exploration (Mission, Path and Agent) along with their subsequent trade-offs.

If a specific area is to be explored, the minimum amount of time, τ to collect at least I_f bits of information about objects of interest in the area, A, can be expressed as:

$$\tau = |A|/(VW_{is}(V, t_f \rightarrow \infty, I_f)), \tag{1.1}$$

where $A \subset \Re^2$ is the area to be explored, $V \in \Re^+$ is the velocity of the vehicle, W_{is} is the width of the sensor footprint where an object located within this footprint transmits information to the vehicle, t_f is the final time and I_f is the amount of information to be collected.

Exploration can become difficult if the time to explore an area approaches the maximum mission duration, T_M due to constraints, uncertainty, etc. Thus we define the difficulty of exploration $\delta \in \Re^+$ as:

$$\delta = \tau / T_M, \tag{1.2}$$

$$= \frac{|A|}{V W_{is}(V, t_f, I_f) T_M}. \tag{1.3}$$

If $\delta > 1$, the exploration problem cannot be solved with the current configuration. If $\delta < 1$, more trade-offs between the vehicle and sensor are available. In this dissertation, we study problems where $\delta < 1$ and examine how tradeoffs can affect the mission completion.

Consider a vehicle exploring at $V = 1m/s$ with $I_f = 1$bit, $W_{is} = 1m$ and $|A| = 100m^2$. With a maximum mission duration of $T_M = 50s$, $\delta = 2$. Since $\delta > 1$, the problem is too difficult and the mission will not be completed within the specified mission duration. The vehicle must increase its speed or increase the footprint width to decrease the difficulty of exploration.

This simple example highlights several component interactions within the exploration problem while providing a basic understanding of sensor, vehicle and environmental properties. Here, the trade-offs occurred in the mission objectives, i.e., T_M. Later we consider problems where trade-offs must occur at all levels of exploration.

Table 1.1 indicates the dependencies of the parameters of (1.3). The objectives of the mission then drive the trade-offs of the vehicle and the sensor.

Table 1.1 Dependence of Parameters Related to the Difficulty of Exploration

Parameter	Dependence
A	Environment:Area
V	Agent: Vehicle
W_{is}	Agent: Vehicle, Sensor
	Environment: Object of Interest
T_M	Mission Requirements

1.7 Problem Formulation and Original Contributions

To provide a specific platform from which to understand the inherent couplings in exploration, we use a solar-powered, fixed-wing, airborne explorer with range-dependent sensors mounted on a gimbal (i.e., banking the aircraft does not affect sensor pointing). The mission objectives are simple: to collect information to estimate the states of several objects of interest located in the area. The aircraft operates in an environment within which there are no obstacles. Simplifying assumptions are used in the following chapters to isolate and study particular couplings within the context of this mission.

As motivation, consider the following scenario. The *Mars Global Surveyor* has identified several potential objects of scientific interest on the surface of Mars. An airborne solar-powered explorer, capable of extended endurance and equipped with a radar sensor, is deployed in the area. The *Global Surveyor* communicates the location of the objects of interest to the explorer while noting that a dust storm is approaching (which motivates the need for a minimum time path). The explorer must then plan a path that accurately estimates the state of these objects of interest in a time-optimal manner, to avoid the dust storm, and in an energy-optimal manner, to maintain its endurance flight. This motivates the work presented in this dissertation.

Based on the integrated model to be presented in Chapter 3, the problem of exploration with a solar-powered aircraft is formulated as an optimal control problem with the steering decisions of the vehicle serving as the input. The present dissertation studies this optimization problem and provides the following original contributions:

- An integrated model of exploration accounting for couplings between the agent, mission and path is presented. These couplings rely on trade-offs between cost and performance, a priori and a posteriori knowledge, and time and energy (See Figure 1.2). A specific example of a solar-powered aircraft exploring Mars is used to illustrate the effect of these tradeoffs.

- Time-optimal exploration paths satisfying mission objectives are presented whose properties stem from analytic necessary conditions and simulation examples. Properties of these paths are used to formulate several heuristics to simplify and solve the time-optimal exploration problem.

- Energy-optimal paths for a solar-powered aircraft in level flight are presented and properties of energy-optimal paths are constructed. The so-called Power Ratio, a dimensionless parameter that can be computed before flight, is shown to correctly predict the regime of optimal flight. An analytic condition for perpetual endurance accounting for location, time of year, environment and aircraft parameters is presented. The condition requires the Power Ratio to exceed a threshold, the Perpetuity Threshold.

- A weighted cost function is used to find combination time-optimal and energy-optimal paths. Properties of these paths are discussed and used to couple energy-optimal flight to the exploration problem. For exploration paths, it is shown that exploration is driven more by time than by energy.

- A heuristic to simplify path planning when non-isotropic sensors are used is presented analytically and empirically.

- The fundamental contribution in this work is the recognition and exploitation of the coupling between information and exploration through considerations of the mission, path and agent.

The context and additional information pertinent to this problem is provided in the form of a literature review in Chapter 2. Chapter 3 provides the complete model used throughout the dissertation and additional background information for the methods used to solve the optimal exploration problem. Chapter 4 considers time-optimal exploration while Chapter 5 considers energy-optimal exploration. Chapter 6 exploits the properties derived in Chapters 4 and 5 to present time-optimal and energy-optimal exploration. Chapter 7 considers vehicle performance trade-offs while Chapter 8 presents conclusions and future work.

Chapter 2

Related Literature and Background

Exploration relies on several technical areas, each of which has a large body of recent literature. Although an exhaustive overview of the state of the art is beyond the scope of this chapter, a brief review of the most relevant literature and concepts follows. Section 2.1 describes some features of information theory. Autonomous vehicles are discussed in Section 2.2. As solar-powered aircraft are a focus in this dissertation, their history, design and optimization is discussed in Section 2.3. Section 2.4 covers optimization, estimation and optimal control. Section 2.5 surveys the field of exploration and information gathering.

2.1 Information Theory

Information is intuitively understood, but difficult to formulate mathematically. Shannon was the first to fully recognize that information is a measurable quantity related to a message being sent (117), that is, information is intrinsically related to the communication of messages.

Communication is the transmission of a coded message over a noisy path or channel to a receiver. Noise is a random additive process that disturbs or obfuscates the intended transmission. The message received may or may not be faithful to the original due to the added noise. A probabilistic decision must be made to recover the intended message from the set of possible messages based on the noisy signal that was received. The measure of

information from a given message can be regarded as the number of possible messages in the set when one message is chosen, all choices being equally likely. Intuitively, receiving the same message repeatedly increases the confidence and reduces the uncertainty that the recovered message is correct, so the total information acquired increases.

Shannon provided a bound on the rate at which information can be transmitted. This rate depends on the bandwidth, w, of the channel and on the strength of the signal-to-noise ratio, SNR (the ratio of the signal power to the noise power). The maximum information rate at which a channel can operate is defined by Shannon's channel capacity equation, $\dot{I} = w\log(1+SNR)$. Actual information transmission rates may be lower, but the channel capacity equation provides an upper bound. Multi-way channels are discussed in (132).

Fisher (46) introduced a different interpretation of information. He showed that it is additive, in that the information yielded from two independent experiments is the sum of the information from each of the experiments separately (74). Fisher's idea of information is connected to the inverse of a covariance, often used in estimation. Both definitions recognize information as conveying meaning (the compactness (53)) about a probability distribution.

From these definitions, information gathering is inherently a communication process. Something, perhaps an object of interest, is a message source. Observation of this object of interest requires the transmission of a signal over a noisy channel to a receiver or observer. The rate of information that can be collected from a sensor is governed by the signal-to-noise ratio and the specific way in which noise-affected-signal is processed. Roughly, the signal-to-noise ratio is a measure of the amount by which a signal is obfuscated in transmission. Noise or disturbances can increase through transmission distance, distortion, terrain occlusion, etc. Often, sensors are dependent upon geometry, emissivity and distance from the collector. Active sensors require a signal to travel to and from an object of interest (112). Passive sensors only collect signals.

2.2 Autonomous Vehicles

Autonomous vehicles are now widely available and used in many areas of society. In this section we focus on the control of autonomous vehicles rather than their design as we must choose control decisions for the vehicle serving as the agent of exploration.

The control of vehicles can be separated into several broad areas. A simple piloted vehicle has no autonomy: all decisions are made by a human pilot. An augmented vehicle is one where some tasks are performed automatically, such as with an altitude-hold autopilot (68), while others are performed by a pilot. A tele-operated vehicle requires a human to be operating the vehicle via a remote control. This type of control can introduce time-delays that can be detrimental to the mission (118), (7). A fully autonomous vehicle operates by pre-defined rules and algorithms that dictate its behavior and which can be adapted during the mission. Although various combinations and variants of these types of control can exist on the same vehicle (distributed by sub-system), in this dissertation, we discuss autonomous vehicles that make their own decisions based upon specified constraints.

Unmanned Aerial Vehicles (UAVs) and other autonomous systems are increasingly used for dirty, dull or dangerous missions (96). The most common use of these systems is the collection of data for Intelligence, Surveillance and Reconnaissance missions. We are particularly interested in missions where autonomous vehicles are tasked with exploring a given area. An example of such a mission involves Mars exploration where objects of interest have been located by the Mars Global Surveyor. The collection of a specified amount of information is performed using spacecraft, air vehicles and/or rovers.

Though we do not focus on cooperative control in this dissertation, the work is extensible to cooperative agents. Cooperative vehicles collecting information in an optimal manner have been considered in numerous papers (129), (53). The use of the information filter to share information between autonomous agents has yielded a decrease in the overall computation time and subsequent increase in performance. We seek to build upon this work by not considering how to maximize the amount of information collected, but only

requiring the collection of enough information to successfully determine states of objects of interest while performing under constraints (e.g., time, energy, etc).

2.3 Solar-Powered Aircraft

Although the current literature on solar-powered UAVs does not consider energy-optimal path planning or perpetual flight, a substantial body of work is available on the analysis and design of solar-powered aircraft. A brief review of this literature is as follows. The feasibility of solar-powered flight is reviewed in (64) and (56), and the history of solar-powered flight is discussed in (18), (33), and (9). Methods for analysis and design of solar-powered aircraft are discussed in (136), (85), (138), (18), (139), (124), (33), (20), (104), (130), (38), (48), (16), (137), (49), (100), (106), (39), (34), (93), (128), (40), (107), (9) and (41). Specifically, the design of solar-powered aircraft has focused on geometric configuration (20). Design of full aircraft systems can be found in particular in (33), (136), (85), (138), (20), (130), (48), (16), (49), (100), (106), (39), (93), (108).

Optimization for solar-powered aircraft is discussed in the literature. Most path planning has only considered minimum power consumption during level flight (85). References (130), (16) and (107) use an optimization procedure to design the aircraft based upon expected maneuvers and sunlight availability. Mission design is found in (41), (36), (55), (35) with particular emphasis on where and when to fly. In most references, efficiency through preliminary design is emphasized. Alternative methods to increase efficiency for solar-powered aircraft are discussed in (21), (30) and (37). Reference (37) achieves a 30% increase in efficiency by improving the cooling of solar cells. Energy-efficient flight is discussed in the literature on dynamic soaring (1), (2) and (3) and manned gliders (102) and (90). However, nowhere in the literature is there a study optimizing the flight path itself based upon the interaction of kinematics and solar energetics nor a design requirement for perpetual endurance for solar-powered flight.

2.4 Optimal Control and Estimation

Several broad works describing the methods of optimal control can be found in (23), (79), and (125). In general optimization problems, the goal is to minimize a cost function while satisfying some set of constraint functions. (125). In optimal control problems the cost and constraints depend on control functions that act through a system of differential equations. More specifically, constraints can be boundary conditions affecting the beginning or end of a trajectory, path constraints restricting states along the path, or control constraints limiting the range of control. Sometimes constraints are treated by adding terms to the cost function that express the degree to which the constraints are violated. The optimal controls formulated satisfy necessary conditions formed by Pontryagin and his coworkers (125).

A rough taxonomy of optimization problems is as follows. Optimization problems can be either deterministic or probabilistic. In the deterministic case, even though the problem data are described explicitly, parameters may be changing over time, such as in a path planning problem (23). The probabilistic case contain problems where data are uncertain. A large literature is devoted to the understanding of uncertain systems and how control can be maintained in the presence of uncertainty (75), (125).

Discrete time control and continuous time control differ in their form. Discrete time problems are formed of sequential decisions (17), while continuous time problems are described by differential equations (75). Another category includes static (80) and dynamic (134) problems. An example of a static problem is finding the dimensions of an object that maximize the volume under length constraints. Dynamic problems can be more difficult as the choice of control changes the system itself. Each of these categories can be mixed and matched as the situation requires with a large volume of literature devoted to particular instances of each.

An important aspect of stochastic control is estimation. For example, an observer is often used to estimate the state of the system when it cannot be directly measured. The most common type of observer is the Kalman Filter (66), which applies to linear systems. It has

a natural extension (58) to nonlinear problems and has many applications in estimation and control.

Other types of optimization problems have connections with exploration. An example is the Traveling Salesman Problem (TSP) where the salesman must visit every city in a country. The cost function is the total distance traveled, the order of the cities visited is the control and the objective is to minimize the total distance. The TSP been extensively studied in the literature and many variants exist. The full problem remains unsolved, although several heuristics and solutions for particular instances exist (78), (73), (81), (51), (103), and (109).

The objective of general optimal path planning is not to visit every point in an area, but to travel optimally between two points. The most relaxed (least constrained) problem is that with a free final condition: the optimal path has no prescribed destination. An interception problem constrains the final position of the vehicle, such as in missile terminal guidance problems (42). In the rendezvous problem, the final position and velocity are specified (71). It is the most constrained case considered in what follows.

Finding an optimal path can be challenging. Many methods exist for optimally solving the basic trajectory planning problem (23). However, not all of them solve the problem in its full generality. For instance, some methods require the workspace to be two-dimensional and the obstacles, if any, to be polygonal. Despite many external differences, the methods are based on few different general approaches: roadmap (76), (131), (83), cell decomposition (114), (115), (116), (131), (84), potential field (72), (77), (11) and probabilistic (67), (127). Optimal control approaches have also been studied in (43) and (122). The numerical method for finding optimal paths used in this thesis is discussed in Appendix B.

The use of optimal control to generate aircraft trajectories has been extensively covered in the literature by (23), (10), (26), and (123) as well as many others. Generally, the concern has been to fly in a fuel/energy-optimal manner (25), (110) and (113) or in a time-optimal manner (45). Multi-objective cost optimization, in this case for fuel and time, is discussed

in (133) and (32). Various methods have been employed to optimize aircraft trajectories, including necessary conditions (52) and parameter reduction (89).

2.5 Exploration

Exploration typically has a single goal: to accurately obtain, interpret and use knowledge about a given area. The information known beforehand, mission objectives and mission constraints may vary. Special problems of particular interest include reconnaissance (97) (collecting information about an object of interest and returning to a given location) and surveillance (14) (collecting information by loitering in the vicinity of an object of interest over a long period of time).

Other types of exploration are discussed in the literature. Area search problems, or area coverage problems, are concerned with visiting every point (140). Patrolling problems require coverage along a given path (4). Broadly speaking, area coverage problems are those in which an autonomous vehicle is tasked to cover a given area with its sensor footprint, or its information signature. The footprint is the area within which an appreciable amount of information can be collected. An example of this type of problem is the lawn-mower or the milling problem. The essence of this problem is to find the shortest or optimal path for a cutter such that every point in the area is within the path (8). The area may have obstacles or the vehicle constraints (95). Area coverage problems are addressed in (12), (13), (87). Additionally, emergency response coverage problems are addressed in (99).

A more complex problem occurs when the vehicle is unsure of its own location. The simultaneous location and mapping (SLAM) problem requires a vehicle to locate itself based on uncertain sensor measurements and previous mapping. Thus the SLAM system must collect information about the environment and its own positional relation to the environment. Many autonomous systems have been designed to account for SLAM techniques including underwater vehicles without global positioning systems (GPS), the tracking of

soldiers within buildings and ground or flying vehicles traveling in unknown areas. SLAM has been widely covered in the literature such as in (120), (19), (92), and (22).

Information based exploration has been discussed in a few papers in recent years, most notably in (63). Other information theoretic approaches have been applied to exploration in several papers including (82), (126), and (119). Alternative missions include area searches with SLAM (53), decentralized sensor control (31) and optimal sensor placement (86). Although the collection of specified amounts of information can be viewed as a goal of exploration, little work in the literature studies a path optimization problem whose constraints are information amounts about specific areas.

This work is concerned with exploiting the interaction between the facets of exploration (kinematics, estimation, informatics, energetics) as well as with how requirements for exploration are traded between the agent, mission and path. This is fundamentally the main contribution of this work.

The models used throughout this work along with the approach used in this dissertation are presented in the following chapter.

Chapter 3

Modeling and Approach

3.1 Introduction

In this dissertation, we consider a planet containing the exploration area, traveling in a circular orbit around a star with angular velocity Ω. The exploration area is in the vicinity of a specified planetary longitude and latitude. A reference frame located at this longitude and latitude has its x-axis oriented along an eastward vector, y-axis in the northern direction and z-axis vertically ascending. With respect to this reference frame, a line connecting the origin and the star has an azimuth and elevation $(\tilde{a}, e)$. Also defined in this reference frame are the locations of m objects of interest at positions $(a_j, b_j, 0), 1 \leq j \leq m$, each with p unknown states.

A single solar-powered aircraft explores the area, i.e., seeks to obtain accurate state-knowledge of the m objects of interest. The aircraft is equipped with onboard sensors mounted with a gimbal and outward facing with aperture α capable of collecting information at a rate that depends on the aircraft position $(x, y, 0)$ relative to the locations of the objects of interest. As we do not consider altitude effects on path planning for exploration, we refer to locations and positions throughout this dissertation in the $x-y$ plane of our reference frame. As a consequence, we drop the z-coordinate when referring to positions.

This model remains common throughout the work but further assumptions are made to analyze various subsystems. In this chapter, the complete model is discussed in detail and

the approach used for analysis is presented.

3.2 Modeling

The model consists of several parts: the vehicle model containing kinematics, informatics, detection and energetics, and the mission model including solar position and objects of interest. Each component is presented below. In each component, several assumptions are made. After presenting the component, we attempt to critique the assumptions made and asses 1) the level of realism and 2) how sensitive the results are to these assumptions.

3.2.1 Vehicle Models

The agent of exploration is a solar-powered aircraft. The kinematic model of the aircraft is presented along with the informatics and energetics.

Aircraft Kinematic Model

The bank-to-turn aircraft is assumed to fly in still air with coordinated turns and remain at constant altitude with zero pitch angle. The equations of motion are:

$$\dot{x} = V\cos\psi, \tag{3.1}$$

$$\dot{y} = V\sin\psi, \tag{3.2}$$

$$\dot{\psi} = \frac{g\tan\phi}{V}, \tag{3.3}$$

where x and y are the Cartesian coordinates of the vehicle, ψ is the heading angle, V is the speed, g is the gravitational acceleration of the planet and ϕ is the bank angle. Without (3.3), this model is the unicycle model (111). While the aircraft may bank, the onboard sensors are assumed to be gimballed and maintain their horizontal attitude, i.e., the field of

view is vertical descending, regardless of that of the vehicle. Vehicles without the need to bank (i.e., ground and underwater vehicles) are only modeled by (3.1) and (3.2).

This abstract model of a vehicle has often been used for path planning (43) and energetic (5) analysis. A full model of an aircraft would consider the effects of uncoordinated turns (slipping or skidding), non-level flight in unsteady air, effects of a changing weight distribution (due to resources being consumed) and many other nonlinear effects.

Gimballed sensors are often used by aircraft to maintain a sight-picture of the target, but gimbals can have singular points. Additionally, gimbals rotate at a finite rate often leading to delay between an aircraft maneuver and the corresponding gimbal response.

In this dissertation we are interested in planning the path of a vehicle that can maintain a sensor field of view. The forthcoming analysis remains insensitive to many of the assumptions made above to simplify the analysis. However, if the vehicle would operate in an area of unsteady air, path planning would become more difficult. We do not consider this in this dissertation as a great deal of literature is devoted to the effects of path planning disturbances (88).

Information Collection Model

We seek to collect a specified amount of information about each of the m objects of interest. Without loss of generality, we assume that the required amount of information to be collected is one bit for each object. To collect information, we use onboard active sensors, e.g., radar.

A key idea of this work is to recognize and exploit the similarity between communication and exploration. Specifically, exploration can be viewed as a communication process where the object of interest is the transmitter, the sensor is the receiver, the sensing process is the noisy communication channel, and the sensed signal carries information about the object of interest. Consequently, the maximum rate at which the sensor can collect information about the object of interest is in fact the capacity (117) and depends on the

signal-to-noise ratio of the channel through Shannon's equation. Two of the many possibilities for an information rate model include the Shannon and Fisher channel capacity rates (53). Here we use Shannon's channel capacity equation:

$$\dot{I} = w \log_2(1 + \text{SNR}), \tag{3.4}$$

where w is the channel bandwidth of the sensor and SNR is the signal-to-noise ratio.

Moreover, according to (112), a radar sensor on an aircraft located at Cartesian coordinates (x, y) and observing object j at Cartesian coordinates (a_j, b_j) provides a reading with signal-to-noise ratio of the form:

$$\text{SNR}_j = \frac{k_j^4}{((x-a_j)^2 + (y-b_j)^2)^2}, \tag{3.5}$$

where the visibility parameter k_j depends on the jth object.

A non-isotropic sensor cannot collect information at equal rates at all relative azimuths from the aircraft. $\Gamma_j(\Theta)$ represents the sensitivity of the sensor aperture to the relative azimuth $\Theta(x, y, a_j, b_j, \psi)$, and we assume that all radar sensing processes, viewed as communication channels with inherent coding, have the same bandwidth, w.

In this dissertation we use a specific non-isotropic sensor as shown in Figure 3.1 where we have constructed the aperture model:

$$\Gamma_j(\Theta(x, y, a_j, b_j, \psi)) = \frac{-1}{(1 + e^{(-(\Theta(x,y,a_j,b_j,\psi) - \alpha)/\beta)})} - \frac{-1}{(1 + e^{(-(\Theta(x,y,a_j,b_j,\psi) + \alpha)/\beta)})}, \tag{3.6}$$

where α is the angular range parameter, i.e., the width of the sensor cone for small β, or aperture, (65), β is the relative sharpness of the sensor cone and Θ is the relative azimuth between the aircraft and the object of interest. This equation can also be represented as the generic function $\Gamma_j(\psi, x, y, a_j, b_j, \alpha, \beta)$. $\Gamma_j(\Theta(x, y, a_j, b_j, \psi))$ can be regarded as the effi-

ciency of the sensor, from zero to one, as a function of the relative azimuth Θ. An isotropic sensor has a function such that $\frac{d\Gamma_j(\Theta)}{d\Theta} = 0$. It should be noted that Γ_j is a differentiable function which lends itself to analysis.

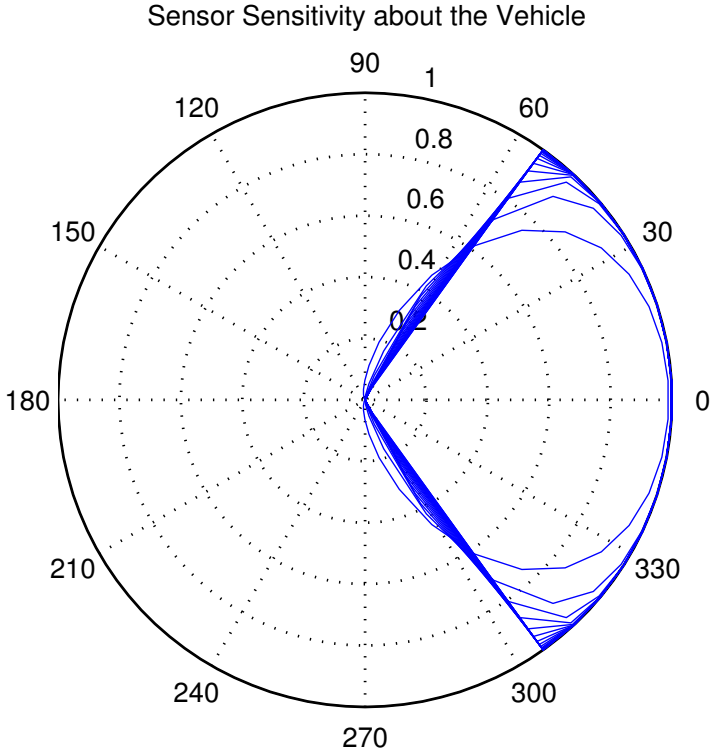

Figure 3.1 An example of the sensitivity, $\Gamma(\Theta)$, of the non-isotropic sensor to to the relative azimuth with $0.01 < \beta < 0.2$. The aircraft and sensor are aligned with the 0 degree axis.

Expanding on (3.4) and (3.5), the information collection model is as follows:

$$\frac{dI_j}{dt} = \Gamma(\Theta(x(t), y(t), a_j, b_j, \psi(t)))w\log_2(1 + \frac{k_j^4}{((x(t)-a_j)^2 + (y(t)-b_j)^2)^2}),$$
$$1 \leq j \leq m, \tag{3.7}$$

One difference between communication and exploration systems is that typically in communication systems *SNR* is large. In exploration systems, *SNR* is typically small. For analysis, we can simplify (3.7) by expanding $\log_2(\cdot)$ with a Taylor series assuming that the

SNR is small. The information collection rate becomes:

$$\frac{dI_j}{dt} = \Gamma(\Theta(x(t), y(t), a_j, b_j, \psi(t)))fracwk_j^4((x(t)-a_j)^2+(y(t)-b_j)^2)^2,$$
$$1 \leq j \leq m, \tag{3.8}$$

We assume here that collecting one bit of information is enough to achieve our mission objectives. Realistically, information is often changing, non-unique and non-additive. An appropriately detailed model of information collection is difficult to achieve, as has been shown in (19), so in this dissertation we use an abstracted model of information collection related to communication through Shannon (117).

Additionally, we use sensors that collect information at the channel capacity rate. Real sensor systems have filters, amplifiers and other stages that can corrupt a signal. These stages can be accounted for in the overall bandwidth of the sensor, modeled by w. Information collection and sensors are complicated components, each a field of study in it of itself. The abstract model presented here allows us to consider the finding of informative paths (here for given objects of interest, but expandable to a general system) while minimizing a cost.

Detection

The primary goal of exploration is to estimate the states of objects of interest. Unfortunately, exploration occurs in an environment that is known only by probability distributions and the *SNR* is finite. The measurement noise expressed in the *SNR* is assumed white and Gaussian with a variance of $R_v \in \Re^+$. Some environmental systems themselves may not be fully understood (such as the characteristics of the visibility parameter). This uncertainty is expressed as process noise, assumed white and Gaussian with variance $R_w \in \Re^+$. In this section we focus on objects of interest whose state can be represented by a real number.

The information collection model presented earlier does not allow the estimation of

states, i.e., we do not know the signal's meanings. To detect or recover the state even in the presence of noise, we make use of an optimal estimator, in this case, a Kalman filter. A typical Kalman filter can be used to estimate the state of the object, but has no inherent dependence on the sensor range (and thus, on kinematics). We address this problem as follows.

The general Kalman filter filtering problem has state dynamics expressed by:

$$\dot{z} = Hz + \tilde{w}, \tag{3.9}$$

$$\tilde{y} = Cz + v, \tag{3.10}$$

while the equations for the Kalman Filter are:

$$\dot{P} = HP + PH^T - PC^T R_v^{-1} CP + R_w, \tag{3.11}$$

$$\dot{\hat{z}} = H\hat{z} + K(\tilde{y} - C\hat{z}), \tag{3.12}$$

$$K = PC^T R_v^{-1}, \tag{3.13}$$

where the state of the object of interest, z, has additive Gaussian process noise $\tilde{w}$ with variance R_w. Here P is the covariance matrix of the state, H is a linear matrix of state dynamics, C is an output matrix of the sensors, R_v is the variance of the measurement noise, v is Gaussian noise with variance R_v, $\hat{Z}$ is the estimate of the state of the object of interest and $\tilde{y}$ is the measurement output.

This generic filter has no dependence upon range to the object of interest from the agent, a component of exploration. We now apply this general case to a specific formulation where z is an unknown constant parameter and the standard kinematic model formulated above is applied. Define R_{vj} as the variance of the measurement noise about a particular object of

interest as a function of range as:

$$R_{vj}^{-1}(t) = \frac{k_j^4}{((x(t)-a_j)^2+(y(t)-b_j)^2)^2}, \tag{3.14}$$

where $x(t)$ and $y(t)$ are obtained from (3.1) and (3.2). In this formulation, we assume that k_j is known.

Then (3.9) - (3.11) become:

$$\dot{x} = V\cos\psi, \tag{3.15}$$

$$\dot{y} = V\sin\psi, \tag{3.16}$$

$$\dot{z_j} = 0, \tag{3.17}$$

$$\tilde{y}_j = z_j + v_j, \tag{3.18}$$

$$\dot{P}_j(t) = -P_j(t)\sqrt{w}R_{vj}^{-1}(t)\sqrt{w}P_j(t), \tag{3.19}$$

$$\dot{\hat{z}}_j = K_j(\tilde{y}_j - \sqrt{w}\hat{z}_j), \tag{3.20}$$

$$R_{vj}^{-1}(t) = \frac{k_j^4}{((x(t)-a_j)^2+(y(t)-b_j)^2)^2}, \tag{3.21}$$

$$K_j = P_j(t)\sqrt{w}R_{vj}^{-1}(t), \tag{3.22}$$

assuming that $H_j = 0, C_j = \sqrt{w}$ and $R_{wj} = 0, 1 \leq j \leq m$. We have chosen $C_j = \sqrt{w}$ to have similarity with Shannon's channel capacity equation.

The exploration problem does not specify a state to be found, only that a specified amount of information be collected about the probability distribution of that state. The estimated state itself is independent of the optimization problem. A Kalman filter expressing

these system dynamics is as follows:

$$\dot{x} = V\cos\psi, \tag{3.23}$$

$$\dot{y} = V\sin\psi, \tag{3.24}$$

$$\dot{P}_j(t) = -P_j(t)\sqrt{w}R_{vj}^{-1}(t)\sqrt{w}P_j(t), \tag{3.25}$$

$$R_{vj}^{-1}(t) = \frac{k_j^4}{((x(t)-a_j)^2+(y(t)-b_j)^2)^2}, \tag{3.26}$$

An equivalent form of the Kalman filter is the Information Filter, derived in (5). The Kalman filter from (3.11) can be reformed as:

$$\dot{P}_j = H_jP_j + P_jH_j^T - P_jC_j^TR_{vj}^{-1}C_jP_j + R_{wj}, \tag{3.27}$$

$$\zeta_j = P_j^{-1}, \tag{3.28}$$

$$\zeta_jP_j = I, \tag{3.29}$$

$$0 = \dot{\zeta}_jP_j + \zeta_j\dot{P}_j, \tag{3.30}$$

$$\dot{\zeta}_j = -P_j^{-1}\dot{P}_jP_j^{-1}, \tag{3.31}$$

$$= -P_j^{-1}(H_jP_j + P_jH_j^T - P_jC_j^TR_{vj}^{-1}(t)C_jP_j + R_{wj})P_j^{-1}, \tag{3.32}$$

$$= -\zeta_jH_j - H_j^TP_j^{-1} + C_j^TR_{vj}^{-1}(t)C_j - P_j^{-1}R_{wj}P_j^{-1}, \tag{3.33}$$

$$= -\zeta_jH_j - H_j^T\zeta_j + C_J^TR_{vj}^{-1}(t)C_j - \zeta_jR_{wj}\zeta_j \tag{3.34}$$

Referring back to (3.23)-(3.26), we can simplify (3.34) as:

$$\dot{\zeta}_j = \sqrt{w}R_{vj}^{-1}(t)\sqrt{w}, \tag{3.35}$$

$$= \frac{wk_j^4}{((x(t)-a_j)^2+(y(t)-b_j)^2)^2} \tag{3.36}$$

Therefore our final simplified model is:

$$\dot{x} = V\cos\psi, \tag{3.37}$$

$$\dot{y} = V\sin\psi, \tag{3.38}$$

$$\dot{\zeta}_j = \frac{wk_j^4}{((x(t)-a_j)^2+(y(t)-b_j)^2)^2}. \tag{3.39}$$

which is similar to the information collection model formulated from Shannon's channel capacity equation assuming the *SNR* is small. This similarity of the Kalman filter and the Shannon formulation shows that information collection is the same as the reduction of covariance. Knowledge of the covariance (or information collected) can now be used to estimate the final state as:

$$\dot{\hat{z}}_j = K(\tilde{y} - \sqrt{w}\hat{z}_j), \tag{3.40}$$

$$\tilde{y} = \sqrt{w}z_j + v, \tag{3.41}$$

$$K = \zeta_j^{-1}\sqrt{w}R_{vj}^{-1} \tag{3.42}$$

Thus the Kalman filter with a range dependent covariance approximates Shannon's channel capacity equation for the information state. We use this new model with the estimated state throughout this work.

This subsection provides one method (Kalman filters) to determine meaning from information collected. In the real-world, Kalman filters are often used to estimate the state of a system from sensor measurements but add complexity to a system due to their computational requirements and subsequent required power usage. Thus meaning can be obtained from an autonomous explorer at a cost to the system design. But meaning can be useful to an explorer as it can affect the choice of path taken. In some situations, meaning obtained during exploration can also change the mission objectives. Automatic target recognition systems and artificial intelligence systems attempt to interpret meaning from information

collected, but their current use remains limited. To date it is only human explorers that can take advantage of real-time information interpretation to affect their course of exploration and the finding of informative paths, but in many cases it is difficult to send humans to explore.

In this dissertation we recognize the difficulty of information interpretation and meaning and so focus on the collection of information. By explicitly defining information collection and detection with an abstract mathematical model (as compared to the real-world) we are able to distill general properties of exploration while understanding that specific implementations could be greatly aided by online interpretation. These general properties will still aid exploration when appropriate interpretation is available.

Energy Collection Model

In this work, an aircraft is used to illustrate the coupling between kinematics and energetics. Other vehicles can be substituted with similar results. The aircraft is equipped with solar cells, mounted on the top side of the wings, and gains solar energy from the star shining on the cells.

During a time interval $[t_o, t_f]$, the energy collected by the aircraft is:

$$E_{in}(\phi(\cdot), t_f) = \int_{t_o}^{t_f} P_{in}(\vartheta(\phi(t), \psi(t)))dt, \tag{3.43}$$

where $P_{in}(\vartheta(\phi(t), \psi(t)))$ is the power collected by the aircraft and assuming that the solar cells are mounted on a flat plate, let $\vartheta(\phi(t), \psi(t))$ be the incidence angle of the star rays upon the solar cells. The power collected by the solar cells is given by:

$$P_{in}(\phi, \psi) = \eta_{sol} P_{sd} S \cos(\vartheta(\phi, \psi)), \qquad \text{if } \cos(\vartheta(\phi, \psi)) \geq 0, \tag{3.44}$$

$$= 0 \qquad \text{if } \cos(\vartheta(\phi, \psi)) < 0, \tag{3.45}$$

where η_{sol} is the efficiency of the solar cell, P_{sd} is the solar spectral density, and S is the total area of the wing. If less than a full wing is covered by solar cells or there is obscurement due to clouds, η_{sol} can be adjusted to account for this.

The incidence angle, $\vartheta(\phi,\psi)$ can be evaluated as follows. Define $[g] = [\hat{x}_g, \hat{y}_g, \hat{z}_g]^T$ as a vectrix (62) fixed to the ground with $\hat{z}_g$ vertical ascending and $\hat{x}_g$ along the local x-axis. If $\tilde{a}$ and e are the azimuth and elevation of the star, then $\hat{s}$, the unit vector to the star, is given as

$$\hat{s} = [g]^T \begin{bmatrix} \cos(e)\cos(\tilde{a}) \\ \cos(e)\sin(\tilde{a}) \\ \sin(e) \end{bmatrix}. \tag{3.46}$$

Define $[a] = [\hat{x}_a, \hat{y}_a, \hat{z}_a]^T$ as a vectrix fixed to the aircraft. In terms of $[g]$,

$$[a] = R_1(\phi)R_3(\psi)[g], \tag{3.47}$$

where,

$$R_1(\phi) = \begin{bmatrix} 1 & 0 & 0 \\ 0 & \cos(\phi) & \sin(\phi) \\ 0 & -\sin(\phi) & \cos(\phi) \end{bmatrix}, \tag{3.48}$$

$$R_3(\psi) = \begin{bmatrix} \cos(\psi) & \sin(\psi) & 0 \\ -\sin(\psi) & \cos(\psi) & 0 \\ 0 & 0 & 1 \end{bmatrix}, \tag{3.49}$$

represent rotation matrices about the first and third axis, respectively. By inverting this relationship, we obtain

$$[g] = R_3(\psi)^T R_1(\phi)^T [a]. \tag{3.50}$$

Hence, $\hat{s}(\phi,\psi)$ can be expressed, in the aircraft-fixed vectrix, as

$$\hat{s}(\phi,\psi) = \begin{bmatrix} \cos(e)\cos(\tilde{a}) \\ \cos(e)\sin(\tilde{a}) \\ \sin(e) \end{bmatrix} R_3(\psi)^T R_1(\phi)^T [a]. \tag{3.51}$$

Define the incidence angle $\vartheta(\phi,\psi)$ as the angle between the line-of-sight to the star and the $\hat{z}$-axis of the aircraft-fixed vectrix. Then $\vartheta(\phi,\psi) = \arccos(\hat{s}(\phi,\psi)\cdot\hat{z}_a)$. Hence, (3.51) yields:

$$\cos(\vartheta(\phi,\psi)) = \cos(e)\cos(\tilde{a})\sin(\psi)\sin(\phi) - \cos(e)\sin(\tilde{a})\cos(\psi)\sin(\phi) + \sin(e)\cos(\phi), \tag{3.52}$$

or,

$$\cos(\vartheta(\phi,\psi)) = \sin(e)\cos(\phi) - \cos(e)\sin(\phi)\sin(\tilde{a}-\psi). \tag{3.53}$$

The discussion on assumptions for the energy-collection model will be provided in the next subsection.

Energy Loss Model

Energy lost by the aircraft is derived from standard lift, drag and propulsion models (6). During a time interval $[t_o, t_f]$, the energy lost by the aircraft is:

$$E_{out}(\phi(\cdot), V(\cdot), t_f) = \int_{t_o}^{t_f} P_{out}(V,\phi)dt. \tag{3.54}$$

The constant altitude assumption requires $L\cos(\phi) = W$ where L is the lift and W is the weight of the aircraft. The equations governing the power lost driving the propeller,

$P_{out}(\phi,V)$, are:

$$P_{out}(\phi,V) = \frac{T(\phi,V)V}{\eta_{prop}}, \tag{3.55}$$

where,

$$T(\phi,V) = D(\phi,V), \tag{3.56}$$

$$D(\phi,V) = \frac{1}{2}\rho V^2 S C_D(\phi,V), \tag{3.57}$$

$$C_D = C_{D_O} + K_a C_L^2(\phi,V), \tag{3.58}$$

$$C_L(\phi,V) = \frac{2W}{\rho V^2 S\cos\phi}, \tag{3.59}$$

and $T(\phi,V)$ is the thrust of the aircraft, η_{prop} is the efficiency of the propeller, $D(\phi,V)$ is the drag of the aircraft, $C_D(\phi,V)$ is the coefficient of drag, ρ is the atmospheric density, C_{D_O} is the parasitic drag, the aerodynamic coefficient $K_a = \frac{1}{\varepsilon\pi AR}$ represents the amount whereby the induced drag exceeds that of an elliptical lift distribution, ε is the Oswald efficiency factor, $AR = b^2/S$ is the aspect ratio of the wing, b is the wingspan and $C_L(\phi,V)$ is the coefficient of lift.

Many of the assumptions provided in the energetics model are simplifications from a real-world aircraft. The top-surface of a wing is often curved (even if a reflex airfoil is used) forcing the solar-cells to be curved (inducing material stesses) or for a faceted wing to be used (inducing additional drag). Power collection efficiency is often affected by much of the power management system including the maximum power-point tracker, battery chargers and onboard energy storage. Onboard energy storage is limited and charging efficiencies can vary depending on level of current charge and the number of charge cycles already undertaken as well as battery chemistry and battery depth-of-discharge. On average, however, these parameters can be accounted for in the solar cell efficiency parameter,

η_{sol}.

The power provided by the star, modeled by the constant P_{sd}, is not typically constant. Cloud cover, varying thicknesses of atmosphere (such as when the sun is at the horizon rather than overhead) and other disturbances can change P_{sd}. But this parameter does not vary greatly and the power collected by a solar cell still follows a nearly sinusoidal path over the course of a solar-day.

The energy lost by an aircraft must also include the fixed-cost to run onboard electronics and payload. Typically this cost is far less than what is required to fly and so is not included in this study. Certain payloads, however, could make this a non-negligible cost. Additional parameters can also be added to the energy-loss model including the higher-order terms of drag and lift coefficients.

Overall, this model is a simplification of the true energy collection and loss model as compared to the real-world. It has been shown to be an effective one, however, as described in the literature review. We make use of this model to show the coupling between kinematics and energetics while understanding that a more precise model could perhaps be needed in implementation.

3.2.2 Environmental Model

The aircraft explores an area within an environment containing several components that interact with the exploration mission. A star is present that provides energy and objects of interest are located in the exploration area. In this subsection, models are detailed to define each of these components for use in this dissertation.

Solar Position Model

Assume that the aircraft flies in the atmosphere of a planet that (1) is in a circular orbit around the star, and (2) has a spin axis that is inclined with respect to its orbital plane. De-

fine $[I] = [\hat{x}_I, \hat{y}_I, \hat{z}_I]^T$ as an inertial orthonormal vectrix fixed in the orbital plane, where $\hat{x}_I$ is a unit vector along the line of spring equinox, $\hat{y}_I$ is in the orbital plane and $\hat{z}_I$ is defined so that the orbital angular motion is along $+\hat{z}_I$. If Ω is the angular velocity of orbital motion and $\bar{s}$ is a unit vector from the planet to the star, then we have

$$\begin{aligned} \bar{s} &= -[\hat{x}_I \cos\Omega t + \hat{y}_I \sin\Omega t] \\ &= -(\cos\Omega t, \sin\Omega t, 0)[I]. \end{aligned} \tag{3.60}$$

Define $[P] = [\hat{x}_P, \hat{y}_P, \hat{z}_P]^T$ as a planet-fixed vectrix where $\hat{x}_P$ at $t = 0$ is a unit vector pointing along the line of spring equinox, $\hat{y}_P$ is in the equatorial plane and $\hat{z}_P$ is defined so that the planet's spin axis is along $+\hat{z}_P$. If ω is the spin rate of the planet and i is the constant inclination of its spin axis, then

$$[P] = R_3(\omega t) R_1(i)[I]. \tag{3.61}$$

Now, define $[l] = [\hat{x}_l, \hat{y}_l, \hat{z}_l]^T$ as a vectrix fixed at the aircraft's location, where $\hat{x}_l$ is along the unit vector toward the local north, $\hat{y}_l$ is along the unit vector toward the local west and $\hat{z}_l$ is along the ascending vertical. Then, the vectrices $[P]$ and $[l]$ are related by

$$[l] = R_3(\pi) R_2(\frac{\pi}{2} - \lambda) R_3(\gamma)[P], \tag{3.62}$$

where λ is the latitude, γ is the longitude and the elementary rotation matrix R_2 is defined as

$$R_2(\kappa) = \begin{bmatrix} \cos\kappa & 0 & -\sin\kappa \\ 0 & 1 & 0 \\ \sin\kappa & 0 & \cos\kappa \end{bmatrix}. \tag{3.63}$$

The elevation of the star is defined as

$$e = \arcsin(\bar{s} \cdot \hat{z}_l). \tag{3.64}$$

From (3.61),

$$[I] = R_1(-i)R_3(-\omega t)[P], \tag{3.65}$$

and from (3.62),

$$[P] = R_3(-\gamma)R_2(\lambda - \frac{\pi}{2})R_3(-\pi)[l]. \tag{3.66}$$

Therefore, an expansion of (3.60) gives

$$\begin{aligned}
\bar{s} = &-(\cos(\Omega t), \sin(\Omega t), 0)R_1(-i)R_3(-\omega t)R_3(-\gamma) \\
&R_2(\lambda - \frac{\pi}{2})R_3(\pi)[l] \\
&= -(\cos(\Omega t), \sin(\Omega t), 0)R_1(-i)R_3(-\omega t - \gamma) \\
&R_2(\lambda - \frac{\pi}{2})R_3(\pi)[l].
\end{aligned} \tag{3.67}$$

Finally, from (3.64) and (3.67), the elevation of the star at the location of the aircraft is

$$\begin{aligned}
e = &\arcsin(-(\cos(\Omega t), \sin(\Omega t), 0)R_1(-i)R_3(-\omega t - \gamma) \\
&R_2(\lambda - \frac{\pi}{2})R_3(\pi)[0\ 0\ 1]^T) \qquad (3.68) \\
&= \arcsin(\sin(i)\sin(\lambda)\sin(\Omega t) - \cos(\lambda)[\cos(\Omega t)\cos(\gamma + \omega t) \\
&+ \cos(i)\sin(\Omega t)\sin(\gamma + \omega t)]). \qquad (3.69)
\end{aligned}$$

Similarly, the azimuth of the star is defined as

$$\tilde{a} = \arctan(\frac{\bar{s}\cdot\hat{y}_l}{\bar{s}\cdot\hat{x}_l}). \tag{3.70}$$

From, (3.70) and (3.67), the azimuth of the star at the location of the aircraft is

$$\begin{aligned}\tilde{a} &= \arctan(\frac{-(\cos(\Omega t),\sin(\Omega t),0)R_1(-i)R_3(-\omega t-\gamma)R_2(\lambda-\frac{\pi}{2})R_3(\pi)[0\ 1\ 0]^T}{-(\cos(\Omega t),\sin(\Omega t),0)R_1(-i)R_3(-\omega t-\gamma)R_2(\lambda-\frac{\pi}{2})R_3(\pi)[1\ 0\ 0]^T})\\ &= \arctan(\frac{\cos(i)\cos(\gamma+\omega t)\sin(\Omega t)-\cos(\Omega t)\sin(\gamma+\omega t)}{\cos(\Omega t)\cos(\gamma+\omega t)\sin(\lambda)+\sin(\Omega t)[\cos(\lambda)\sin(i)+\cos(i)\sin(\lambda)\sin(\gamma+\omega t)]}),\end{aligned} \tag{3.71}$$

where the inverse tangent must be defined in the correct quadrant.

By definition, *sunrise* is a time t_r such that $e(t_r)=0$ and $\dot{e}(t_r)>0$. *Sunset* is a time t_s such that $e(t_s)=0$ and $\dot{e}(t_s)<0$. *Daylight* is the duration between a sunrise and the next sunset, i.e., t_s-t_r. The *solar day*, t_{sd}, is the interval between two consecutive sunrises. The *daylight duty cycle* is the ratio between daylight and solar day, i.e., $\frac{t_s-t_r}{t_{sd}}$.

Other parameters, such as the Earth's oblateness or nutation, may also affect this model but to a negligible degree. For the purposes of path planning and analyzing the interation between kinematics and energetics, this model provides the needed couplings.

Objects of Interest

The m objects of interest are located at Cartesian positions $(a_j,b_j), 1\leq j\leq m$. Each object of interest has a certain emissivity, reflectivity and absorption which we collectively assume to be represented by a known scalar value $k_j\in\Re$ with units of meters known as the visibility parameter.

Each object of interest can be viewed as a transmitter in a communication process where the transmitted signal contains knowledge about a state of the object of interest. We assume

each state, $z \in \mathfrak{R}$ to be time-invariant such that:

$$\dot{z} = 0 \tag{3.72}$$

where, for example, z can represent the size of an object.

Realistically, objects of interest may not have time-invariant states and different state values may be seen from different angles. Indeed, there may even be interference from different objects of interest if viewed close together. These effects have not been modeled here but remain an opportunity for future work.

3.3 Approach

Throughout this work, we pose optimal control problems with $V(t)$ and $\psi(t)$ serving as the control functions. Data in these problems are based on the complete model of this chapter. See Appendix A for a general statement of an optimal control problem together with its necessary conditions. The necessary conditions take the form of two-point boundary-value problems (TPBVP) involving the minimization of a Hamiltonian function.

In each chapter, the general conditions of Appendix A are specified for the problem at hand. We then study solutions of the resulting TPBVPs to find characteristics of optimal paths and the aircraft that travel on them. Specifically, we are interested in properties that define families of paths or regimes of flight that characterize different aspects of the optimal exploration problem. In addition to exploiting the necessary conditions for various purposes, optimal control inputs are computed for various example problems. See Appendix B for the discretization approach that is used.

In Chapters 4 and 5, a problem is posed based on a restricted form of the complete model where several simplifying assumptions are made. These assumptions are removed in Chapter 6 where the full model is considered.

The proceeding approach is based on the definitions given in Chapter 1 and the com-

plete model constructed in Chapter 3. Additionally, properties from the solutions of the TPBVPs are utilized in Chapter 7 to find characteristics of vehicles and sensors.

Chapter 4

Time-Optimal Exploration

4.1 Introduction and Problem Formulation

This chapter is devoted to the problem of exploring an area in a time-optimal manner. The objective of the mission is to collect information about m objects of interest with known locations $(a_j, b_j), 1 \leq j \leq m$. Although the information collected can be used to detect the state of an object, this chapter focuses on information collection rather than classification. Information is collected by an active onboard isotropic sensor (e.g., radar, sonar), with a signal-to-noise ratio that decays as the reciprocal of the fourth power of the range (3.7). Hence, the problem of time-optimal exploration features the coupling between aircraft kinematics and information collection, which occurs through the signal-to-noise ratio of the sensor.

Based on the integrated system model, the problem of exploration for autonomous vehicles is formulated as an optimal path planning problem where the states are the Cartesian coordinates of the vehicle and the amount of information collected about each object of interest, the objective function is the total mission time, and the boundary conditions are subject to inequality constraints that reflect the requirements of information collection.

We use the model presented in Chapter 3 with the following assumptions: 1) the aircraft has enough on-board energy stored to complete its mission, 2) the aircraft can perform instantaneous turns, 3) the sensor is isotropic and 4) V is constant. Therefore in this chapter

we neglect equations (3.43), (3.54) and (3.3) from the general model and allow $\alpha = 2\pi$, i.e., $\Gamma_j = 1$.

We further assume that 5) that at least one bit of information about each object of interest is required to accomplish the mission. Finally it is assumed that $\dot{I}_j(t)$ is given by (3.7).

Here the mission is to fly from a given initial location (x_o, y_o) with free heading and collect information, $I_j \geq 1$, from each object of interest. The aircraft departs at a given initial time t_o and flies for at most the maximum mission duration, T_M. The terminal position $(x(t_f), y(t_f))$ is free. The Optimal Path Planning Problem is then to find a flight path that accomplishes the mission in a time-optimal manner, i.e., while minimizing the final mission duration.

4.2 Optimal Path Planning

In this section, we derive the necessary conditions for time-optimal flight. The dynamic optimization problem is to minimize, with respect to the time-history of the heading angle, the time to accomplish the mission, i.e.,

$$\min_{\psi(\cdot)} t_f, \tag{4.1}$$

subject to (3.1)-(3.7) and boundary conditions.

4.2.1 Necessary Conditions for Optimality

The necessary conditions for optimality for the minimization problem (4.1) are derived in Appendix A. Here, these necessary conditions are applied to the current problem. With

state $[x, y, I_1, I_2, ..., I_m]^T$ and control input ψ, the Hamiltonian is:

$$H = \sum_{j=1}^{m} \lambda_{I_j} w \log_2(1 + \frac{k_j^4}{[(x-a_j)^2 + (y-b_j)^2]^2}) + \lambda_x V \cos(\psi) + \lambda_y V \sin(\psi) + 1, \tag{4.2}$$

where λ_x, λ_y and $\lambda_{I_j}, 1 \leq j \leq m$ are costate variables.

In this problem formulation, we have no control constraints.

The state equations, consistent with (4.2), are:

$$\dot{x} = V \cos(\psi), \tag{4.3}$$

$$\dot{y} = V \sin(\psi), \tag{4.4}$$

$$\dot{I_j} = w \log_2(1 + \frac{k_j^4}{((x(t)-a_j)^2 + (y(t)-b_j)^2)^2}), 1 \leq j \leq m. \tag{4.5}$$

The costate equations are:

$$\dot{\lambda_x} = \sum_{j=1}^{m} \frac{4k_j^4 w(x(t)-a_j)\lambda_{I_j}}{((x(t)-a_j)^2 + (y(t)-b_j)^2)^3 \Delta_j}, \tag{4.6}$$

$$\dot{\lambda_y} = \sum_{j=1}^{m} \frac{4k_j^4 w(y(t)-b_j)\lambda_{I_j}}{((x(t)-a_j)^2 + (y(t)-b_j)^2)^3 \Delta_j}, \tag{4.7}$$

$$\dot{\lambda_{I_j}} = 0, 1 \leq j \leq m, \tag{4.8}$$

where $\Delta_j = (1 + \frac{k_j^4}{((x(t)-a_j)^2 + (y(t)-b_j)^2)^2}), 1 \leq j \leq m.$

The first-order optimality condition for the minimization of the Hamiltonian with respect to ψ is:

$$0 = v\lambda_y \cos(\psi) - v\lambda_x \sin(\psi). \tag{4.9}$$

The boundary conditions for this problem are:

$$x(0) \text{ given}, \tag{4.10}$$

$$y(0) \text{ given}, \tag{4.11}$$

$$I_j(0) = 0, 1 \leq j \leq m, \tag{4.12}$$

$$x(t_f) \text{ free}, \tag{4.13}$$

$$y(t_f) \text{ free}, \tag{4.14}$$

$$I_j(t_f) \geq 1, 1 \leq j \leq m, \tag{4.15}$$

$$\lambda_{I_j}(t_f) = \text{free if } I_j = 1, 1 \leq j \leq m, \tag{4.16}$$

$$\lambda_{I_j}(t_f) = 0 \text{ if } I_j > 1, 1 \leq j \leq m, \tag{4.17}$$

$$\lambda_x(t_f) = 0 \tag{4.18}$$

$$\lambda_y(t_f) = 0. \tag{4.19}$$

Equations (4.3) - (4.19) provide necessary conditions for optimality in the form of a two-point boundary value problem.

The simplified Hamiltonian relying on (3.8) is:

$$H = \sum_{j=1}^{m} \lambda_{I_j} \frac{wk_j^4}{[(x(t)-a_j)^2 + (y(t)-b_j)^2]^2} + \lambda_x v\cos(\psi) + \lambda_y v\sin(\psi) + 1 \tag{4.20}$$

The simplified necessary conditions for the minimization of the Hamiltonian with re-

spect to ψ become:

$$0 = v\lambda_y \cos(\psi) - v\lambda_x \sin(\psi), \tag{4.21}$$

$$\dot{x} = v\cos(\psi), \tag{4.22}$$

$$\dot{y} = v\sin(\psi), \tag{4.23}$$

$$\dot{I}_j = \frac{wk_j^4}{((x(t)-a_j)^2+(y(t)-b_j)^2)^2}, 1 \leq j \leq m, \tag{4.24}$$

$$\dot{\lambda_{I_j}} = 0, 1 \leq j \leq m, \tag{4.25}$$

$$\begin{aligned} \dot{\lambda_x} &= \sum_{j=1}^{m} \frac{4k_j^4 w(x(t)-a_j)\lambda_{I_j}}{((x(t)-a_j)^2+(y(t)-b_j)^2)^3}, \\ \dot{\lambda_y} &= \sum_{j=1}^{m} \frac{4k_j^4 w(y(t)-b_j)\lambda_{I_j}}{((x(t)-a_j)^2+(y(t)-b_j)^2)^3}, \end{aligned} \tag{4.26}$$

and the boundary conditions remain the same as in (4.10) - (4.19).

4.3 Properties of Extremal Flight Paths

In terms of the complete model, visibility and isolation are quantified by the parameters k_j and w respectively. Specifically, the distance r_j can be defined by the relationship:

$$I_f = w\log_2\left(1+\frac{k_j^4}{r_j^4}\right), \tag{4.27}$$

where after solving for r_j,

$$r_j = \frac{k_j}{\sqrt[4]{2^{\frac{I_f}{w}}-1}}, \tag{4.28}$$

and is such that a radar located at distance r_j from the jth object of interest collects information about that object at a rate of I_f bits per unit of time. The set of objects of interest is isolated if the m disks, centered at Cartesian coordinates (a_j, b_j) and with radii

$r_j, 1 \leq j \leq m$, respectively, do not intersect. Define each of these m disks D_j, where D_j is the isotropic visibility disk centered on the jth object of interest. When the vehicle is within the visibility disk of the jth object, i.e., $(x,y) \in D_j$, the object is considered visible. Otherwise the object is invisible to the vehicle. Define D to be the union of all visibility disks $D_j, 1 \leq j \leq m$, i.e., $D = \cup_{j=1}^{m} D_j$. When an object is considered visible an appreciable rate of information is collected.

Further definitions simplify the remaining analysis. Objects are said to be clustered if their visibility discs are pathwise connected. Furthermore, clusters are said to be isolated if they are not pathwise connected. Finally, an isolated object has the property of not being in any cluster.

4.3.1 Properties of Time-Optimal Exploration

We can use the necessary conditions that minimize the Hamiltonian with respect to ψ to prove the following properties of extremals.

Proposition 4.3.1. *If the objects of interest are isolated, then the optimal flight paths are approximated by sequences of straight lines (far from the objects of interest) connected by short turns (near the objects of interest).*

By far, we mean locations outside of the visibility disks for the objects of interest and by near we mean locations within the visibility disks.

Proof of Proposition 4.3.1

Assume that the objects of interest are isolated. Whenever all objects of interest are invisible, i.e., $(x,y) \notin D$, the right hand sides of (4.6) and (4.7) are negligible, implying that the costates correponding to the Cartesian coordinates of the aircraft are approximately constant. Then (4.9) implies that the heading angle of the aircraft is also approximately constant, implying that its path approximates a straight line.

When a vehicle approaches one of the objects of interest (and the object is visible), the above argument no longer applies and the vehicle may turn. However, the turn is relatively short because it is predicated upon closeness to the object of interest. Once the vehicle leaves the vicinity of that object, it resumes an approximately straight path, as per the above argument.

Corollary 4.3.2. *If in addition to being isolated, the objects of interest are poorly visible, then the problem becomes a traveling salesman problem (TSP) (44).*

Proof of Corollary 4.3.2

In the TSP case, the information rate of each object approaches zero, through a low w or k_j or high separation distance between the object of interest and the aircraft. If we assume that $\frac{wk_j^4}{((x(t)-a_j)^2+(y(t)-b_j)^2)^2} = 0$, then λ_x and λ_y are constant and equal to zero as is required by their final conditions. The optimality condition relates the ratio of λ_x and λ_y to the heading angle, ψ. Thus, the heading angle remains constant and the aircraft travels straight.

It is optimal in this case for the aircraft to visit each object of interest individually before switching to another target.

Proposition 4.3.1 implies that, in the isolated case, each aircraft essentially "visits" a sequence of objects of interest, flying straight paths between them.

Proposition 4.3.3. *When the visibility of all the objects of interest approaches infinity, t_f approaches zero and the length of path traveled by the aircraft approaches zero.*

We call the situation described by Proposition 4.3.3 the Watchtower case.

Proof of Proposition 4.3.3

In the Watchtower case, each object's information transmission rate approaches infinity, either through a high bandwidth, w, or visibility parameter, k_j, or low separation distance between the object of interest and the aircraft. We assume that the denominator of (3.7) is

never zero, that is, the aircraft is always away from any object of interest. As k_j approaches infinity, the right hand side of (3.7) also approaches infinity. For any final time of flight, no matter how short, a k_j can always be found that is large enough that, within the alloted time, enough information can be collected to satisfy the boundary conditions. This means that the aircraft does not need to move to collect information in the Watchtower case. This argument is valid for all headings.

4.3.2 Control Rate

Although the problem stated in Section 4.2 has no constraint on the magnitude of the control, ψ, in the real-world, one should be concerned with the time rate of change of the control. Real-world actuators are limited in control rate they can achieve and this must be accounted for in the system design. The gentle rate of turn defined in Proposition 4.3.1 also suggests a magnitude constraint. This magnitude can be evaluated as follows. Consider the optimality condition, (4.9). A derivative with respect to time gives:

$$0 = V\cos(\psi)\dot{\lambda}_y - \lambda_x V\cos(\psi)\dot{\psi} - V\dot{\lambda}_x\sin\psi - \lambda_y\dot{\psi}\sin\psi. \tag{4.29}$$

Substitution of (4.6) and (4.7) into (4.29) gives:

$$\begin{aligned} 0 = {} & V\cos(\psi)\frac{4k^4\lambda_I(y(t)-b)}{((x(t)-a)^2+(y(t)-b)^2)^3} - \lambda_x V\cos(\psi)\dot{\psi} \\ & - \lambda_y V\dot{\psi}\sin\psi - V\frac{4k^4\lambda_I(x(t)-a)}{((x(t)-a)^2+(y(t)-b)^2)^3}\sin\psi. \end{aligned} \tag{4.30}$$

After rearranging, (4.30) becomes:

$$\dot{\psi} = \frac{V\cos(\psi)\frac{4k^4\lambda_I(y(t)-b)}{((x(t)-a)^2+(y(t)-b)^2)^3} - V\frac{4k^4\lambda_I(x(t)-a)}{((x(t)-a)^2+(y(t)-b)^2)^3}\sin\psi - \lambda_y\dot{\psi}\sin\psi}{\lambda_x V\cos(\psi)+\lambda_y V\sin\psi} \tag{4.31}$$

When $(x,y) \notin D$, $((x-a)^2+(y-b)^2)^3$ becomes large. This drives λ_x and λ_y to zero which, together with (4.31), indicates that ψ is approximately constant. Otherwise, the rate of change of ψ depends on the rates at which information is collected about visible objects.

4.4 Characteristics of Optimal Paths

Figure 4.1 presents an optimal flight path for an aircraft exploring an area with three objects of interest computed with the method presented in Appendix B. Each object is designated by an "x" on the Figure. The small circles have radii r_j defined in Equation (4.28). The lengths on this and many of the following plots have been scaled by a characteristic length l_c, where l_c in this dissertation is the visibility parameter of the first object of interest, k_1. In this example, the aircraft does not fly over the objects of interest, but only approaches each of them and then turns away towards the next. Thus, the total optimal path consists of straight flights and short turns.

In the TSP limiting case, all of the objects of interest have a very low visibility. Figure 4.1 presents the same objects of interest as in Figure 4.1, but each object is barely visible. Here the aircraft must virtually reach the target before enough information is collected and similarities to typical TSPs exist.

Figure 4.2 demonstrates a hybrid example: one object of interest is relatively visible while two others are barely visible. The resulting optimal path is a gentle curve near the visible object and a typical TSP touring path towards the other two objects.

4.4.1 Radius of Closest Approach

Consider a single vehicle approaching an isolated object with a second object far away. To satisfy the information boundary conditions (4.16), the vehicle must enter the visibility disk of the first object of interest for at least a short duration. The object itself, at the center of the visibility disk, need not be encountered. The minimum range from the explorer to

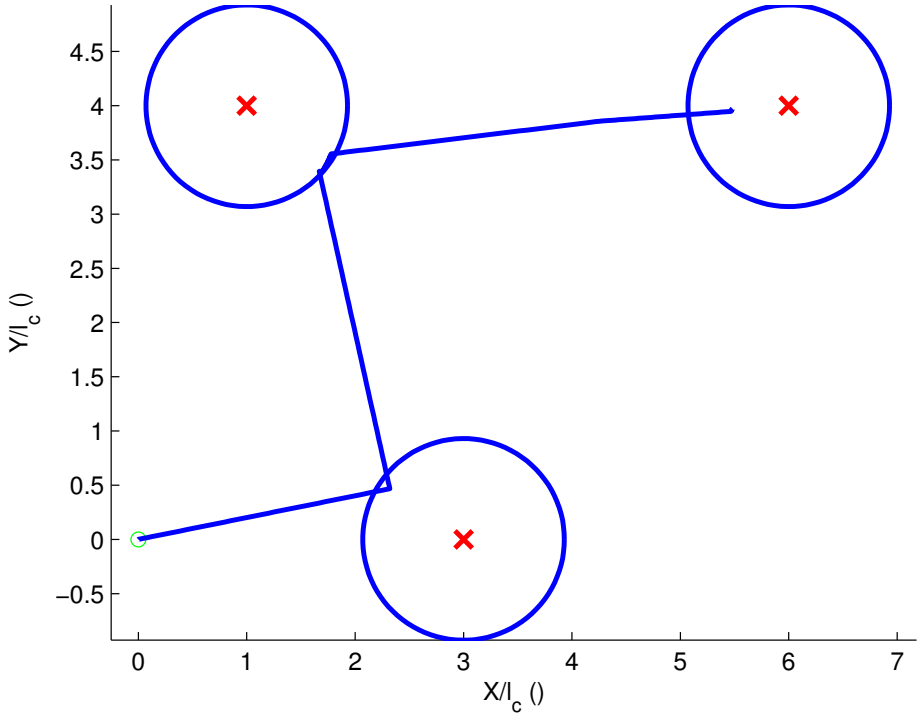

Figure 4.1 Optimal flight path for an aircraft with two objects of interest. The objects of interest have equal visibility discs of radius r_j and are centered at locations designated by an "x".

the object of interest is the radius of closest approach.

This radius can be found as follows. Integrating (4.5) over a path satisfying the optimality condition yields the amount of information collected. Over a short time period, the rate at which information is collected can be approximated by a constant. Similarly, a path entering and leaving a visibility disk, on which a vehicle collects exactly one bit of information, can be approximated by a parabola. The midpoint of the parabola is the point at which exactly one half of the required amount of information is collected. This point is also the smallest range from the explorer to the object of interest, the so-called radius of closest approach.

The disk around the object defined by this radius of closest approach is the disk of influence for an object. Any path that penetrates this disk is guaranteed to collect at least the specified amount of information by definition.

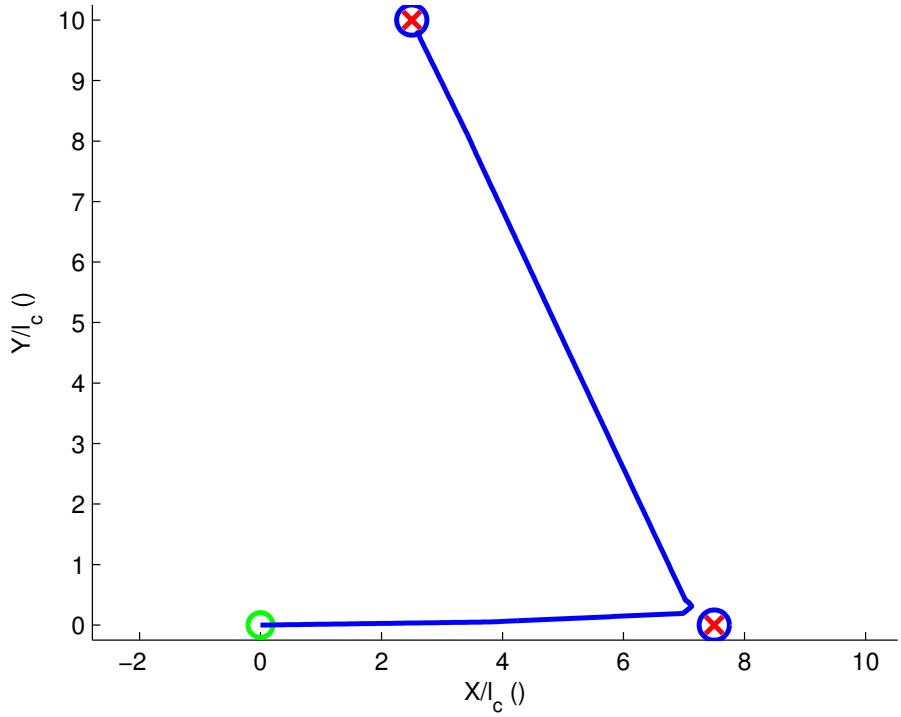

Figure 4.2 Optimal flight path in a TSP limiting case with two objects of interest. The objects have low visibility (as indicated by small visibility disks)

Although the radius of closest approach can be expected to vary as a function of the relative location of the objects of interest, we have observed that, in practice, this variation is small. Figure 4.4 illustrates a typical parametric study of the radius of closest approach as a function of the angle σ between the line-of-sight to the closest object of interest and the line between the two objects.

4.5 Information Constraints

During the vehicle mission, information is collected from each object of interest. Because of the inequality information boundary conditions, more than the specified amount information can be collected during a time-optimal flight. At the end of flight, an object j has an active information constraint if $I_j(t_f) = 1$. These objects are called critical ob-

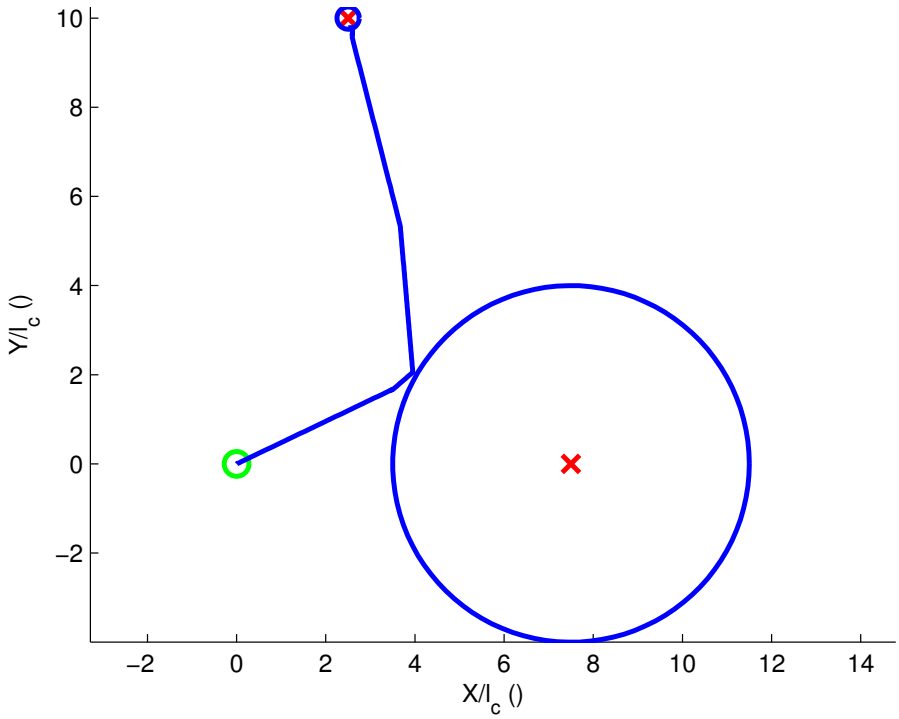

Figure 4.3 Optimal flight path for a vehicle exploring an area with objects of interest with different visibility parameters

jects. Alternatively, object j has an inactive information constraint if, at the end of flight, $I_j(t_f) > 1$.

4.5.1 Isolated Objects

In the case of isolated objects, active and inactive information constraints can be illustrated by an example.

Using the aircraft model, consider a case with two isolated objects as in Figure 4.5.

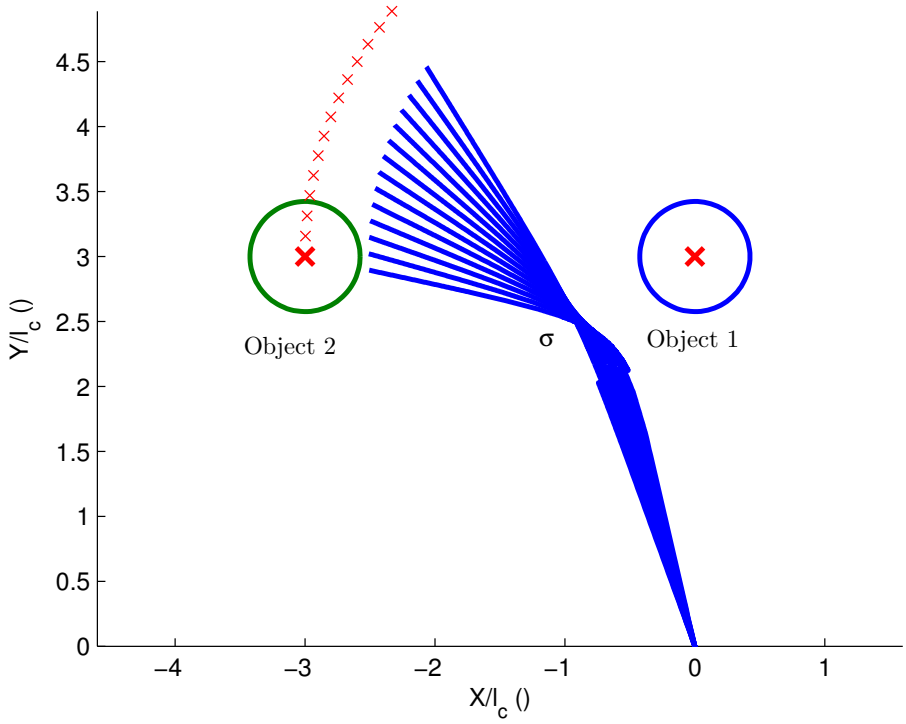

Figure 4.4 Optimal flight paths for a single aircraft when approaching an object of interest at different bearings. σ is the angle between the line-of-sight from the aircraft to the closest object of interest and the line between the two objects. The visibility discs have been removed for a majority of the second objects of interest for clarity.

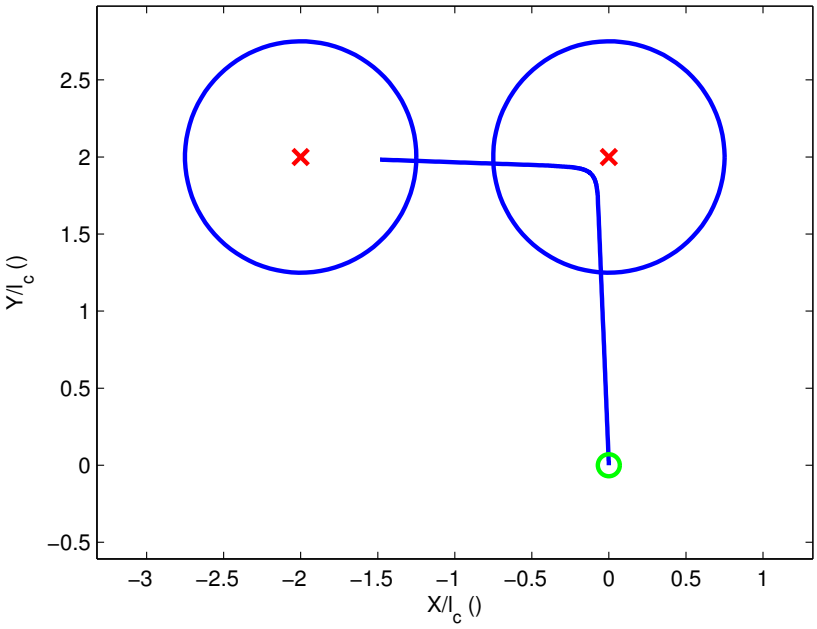

(a) Flight Path

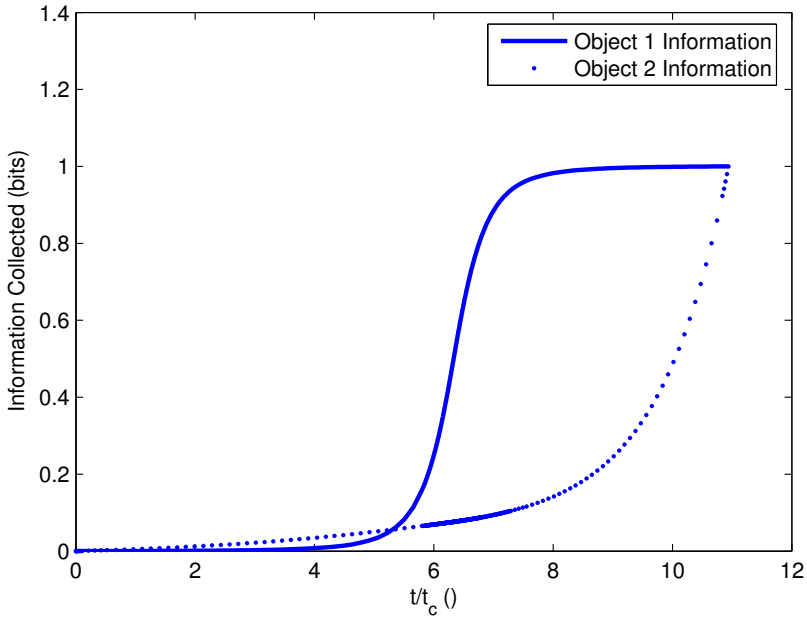

(b) Information Collection

Figure 4.5 Optimal flight path for a single aircraft with two critical objects. The critical objects of interest have exactly one bit of information collected at the end of flight.

At the end of flight, there is exactly 1 bit of information collected about each of the two objects of interest. If the objects were aligned with the original flight path of the aircraft, as in Figure 4.6, one bit is collected about the second object while more than one bit of information is collected about the first. Though other paths can be found collecting exactly one bit of information about each object, they are not time-optimal. Indeed if Object 1 was not present, or had no information constraint, the time-optimal path would lead directly to Object 2. Now add the information constraint on Object 1. By the relaxation principle (101), an extremal path satisfying the boundary conditions can do no better, i.e., complete the mission in less time, than the path that is constrained by boundary conditions. Since the original time-optimal path and the second extremal path are identical, the extremal path must be time-optimal as well.

4.5.2 Clustered Objects

We illustrate active and inactive information constraints by example. In a simple clustered case, as in Figure 4.7, the aircraft collects greater than one bit of information about the first object and exactly one bit about the second.

In a more complicated clustered case, as in Figure 4.8, the aircraft must find a time-optimal path that is constrained by information state boundary inequalities. Rather than plan for each object of interest, however, our astute planner only needs to plan between the critical objects. Thus the problem can be reduced in size from one with m objects to one with only critical objects.

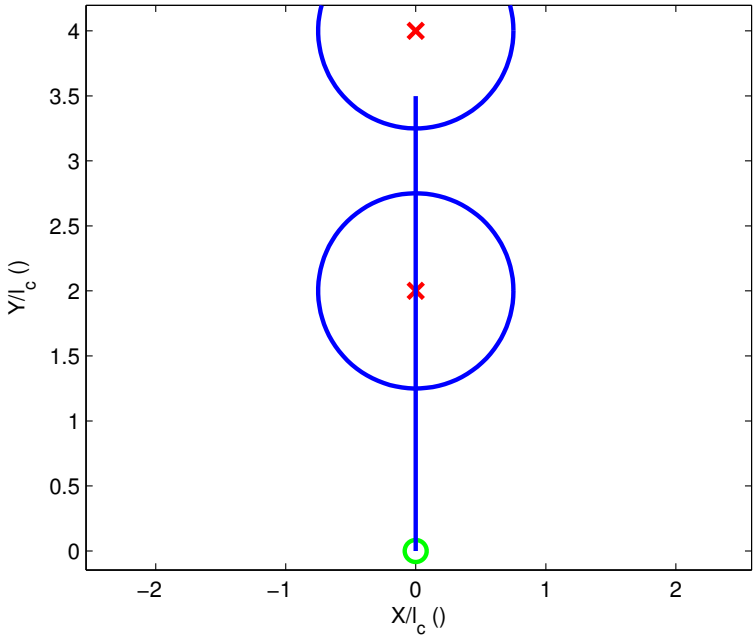

(a) Flight Path

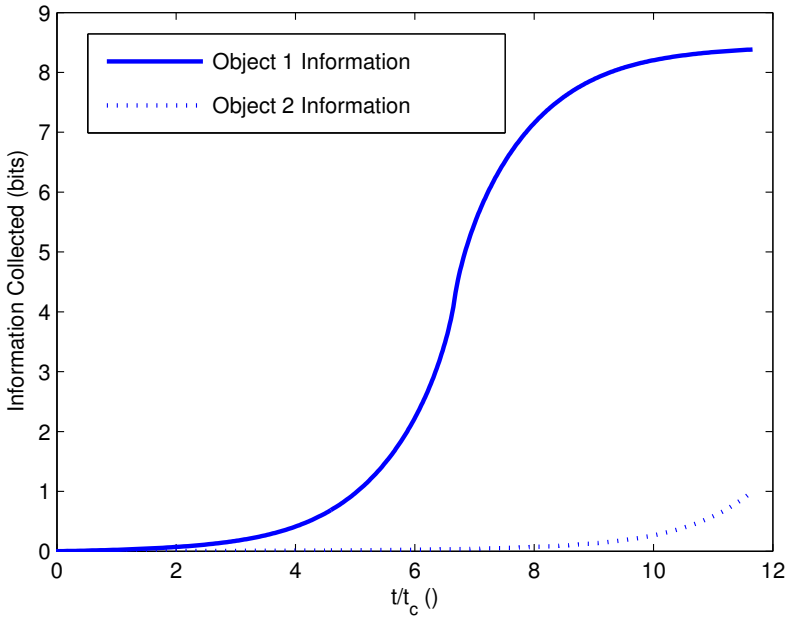

(b) Information Collection

Figure 4.6 Optimal flight path for a single aircraft with one critical object

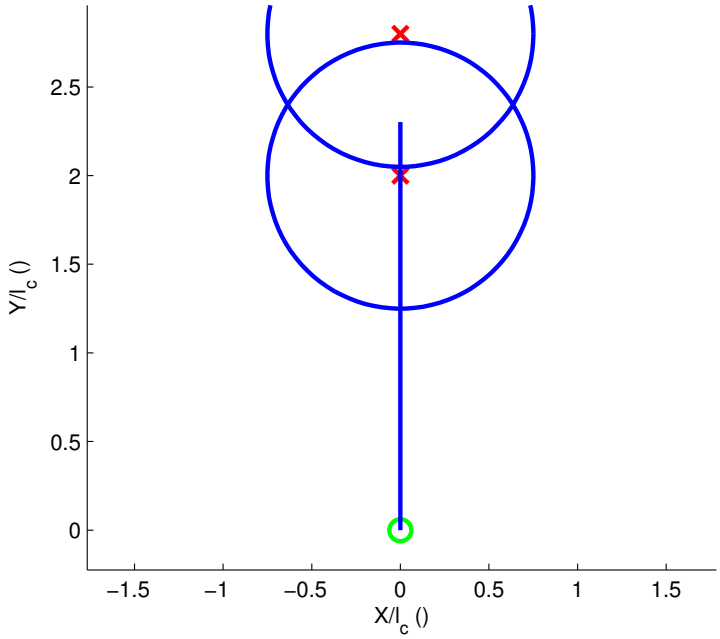

(a) Flight Path

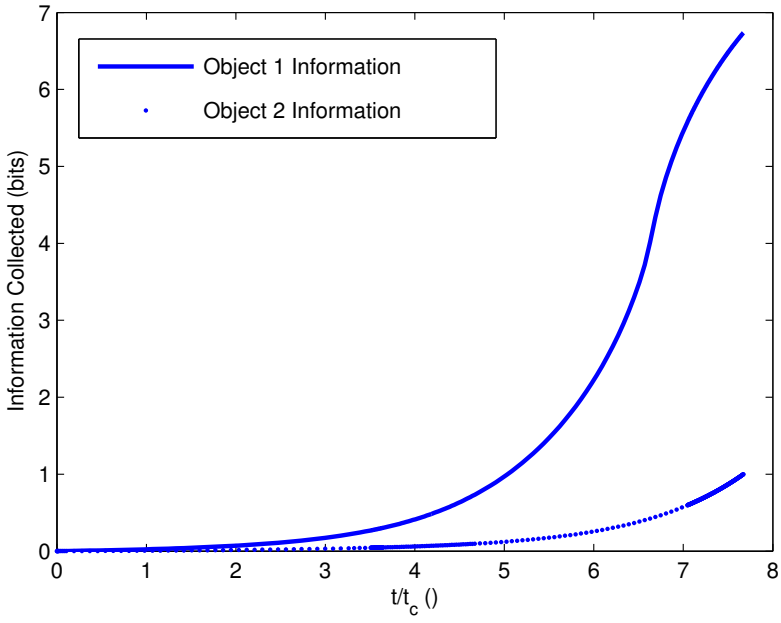

(b) Information Collection

Figure 4.7 Optimal flight path for a single aircraft with two non-isolated objects - one of which is critical

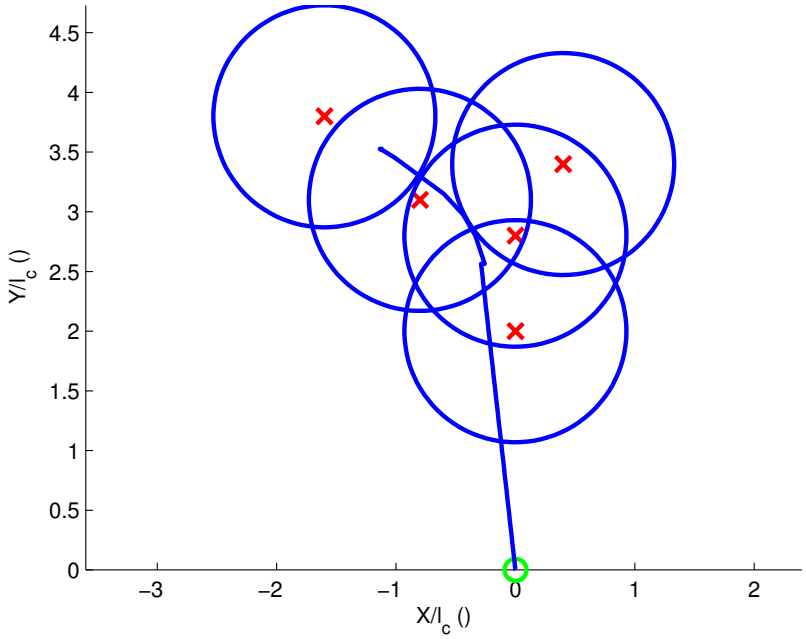

(a) Flight Path

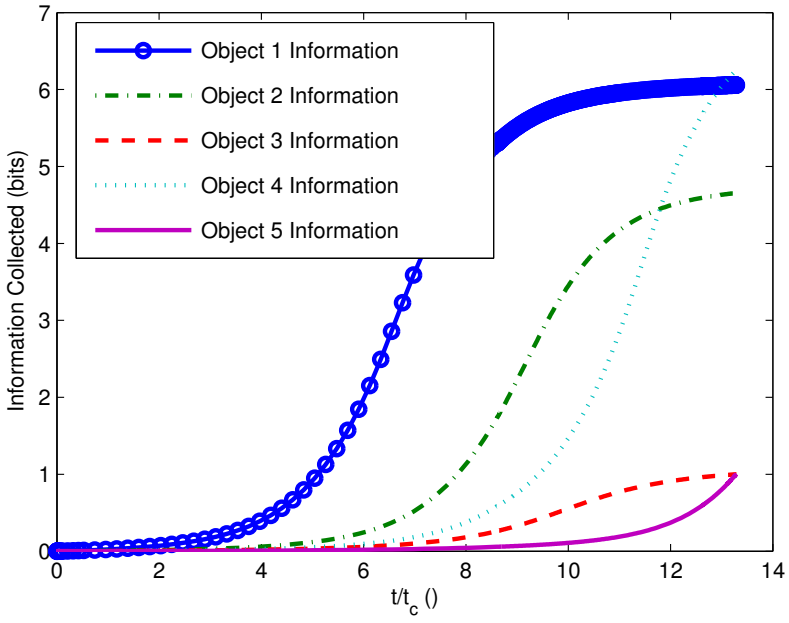

(b) Information Collection

Figure 4.8 Optimal flight path for a single aircraft with many non-isolated objects

4.6 Time-Optimal Exploration Heuristics

Several heuristics have been created to simplify or solve the problem of time-optimal exploration. While the optimal path can be found from solutions of the two-point boundary-value problem, it is often difficult to solve this problem or even to initialize it correctly. The heuristics in this section have been constructed from observed and analytical properties of optimal solutions and can be used to find near-optimal paths or to initialize a TPBVP solver.

4.6.1 Critical Objects Heuristic

Here we identify a heuristic that can be used for a class of problems with clustered objects. Consider a set of objects whose Cartesian coordinates form a straight line. If a path is formed by connecting the objects in a greedy fashion, the amount of information collected about each object can be evaluated. Those objects whose final information state is exactly one bit are declared to be critical objects. The flight path planned, at the end of the problem, is optimized based only on the critical objects and their information boundary conditions.

If the objects are shifted slightly from their straight line configuration, the path is also altered. While the optimal path can shift dramatically, even discontinuously, with these small alterations, the optimum, or total mission time, shifts only slightly.

An example of this heuristic is shown in Figures 4.8 and 4.9. In the first, a greedy path is optimized upon. The resulting flight path and information collection is shown. In the second figure, only a path connecting the critical objects is optimized upon. The flight path and final information collected about each object of interest is also shown.

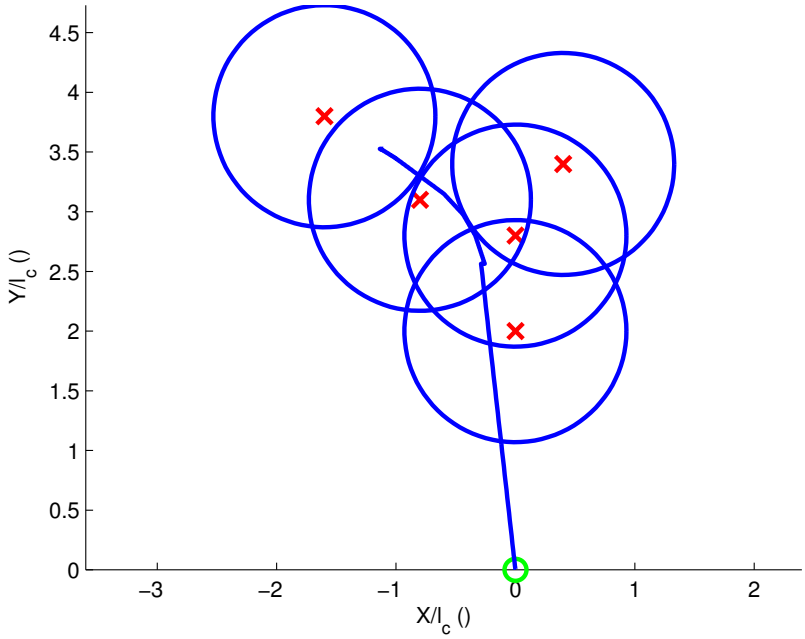

(a) Flight Path

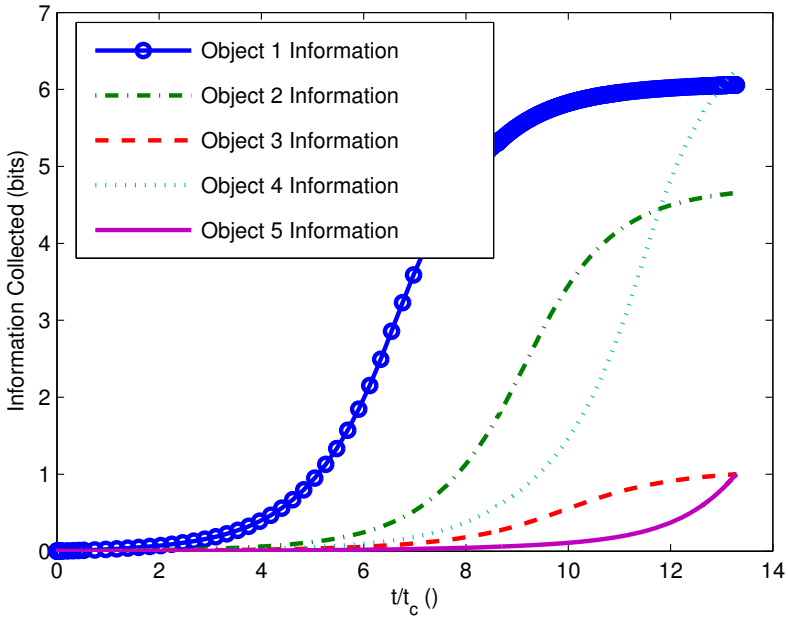

(b) Information Collection

Figure 4.9 Optimal flight path for a single aircraft with a path planned only for the two critical objects

This heuristic can be used to simplify the computational requirements of solving the TPBVP. Rather than plan for m objects of interest with $2m$ information constraints (initial and final constraints), the path planner only must plan for critical objects of interest, a subset of the m objects.

4.6.2 Rubberband Heuristic

A simplified model of the exploration problem can be illustrated on a wooden board. Here, each object of interest is represented by a screw, the radius of closest approach by a rubberband and the optimal path by a string. At constant speed, the length of the string is proportional to the mission duration.

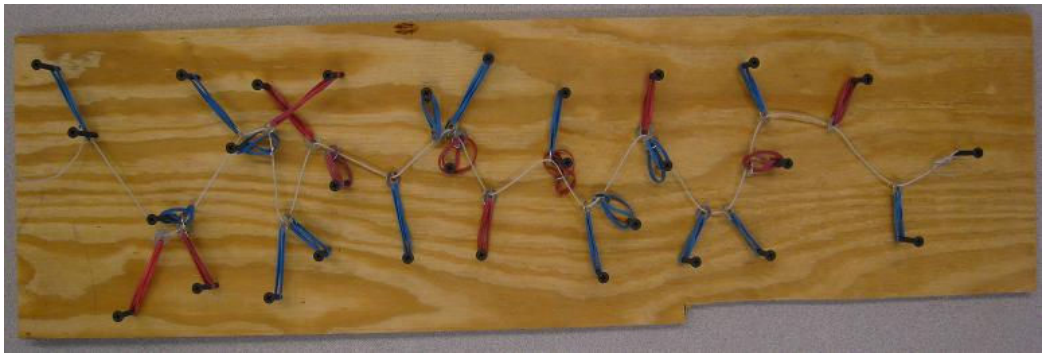

Figure 4.10 Wooden board demonstrating the RubberBand Heuristic

One property is the connection between vehicle speed and object visibility. As the aircraft slows, it spends more time within the visibilitydisk and more information is collected. Thus, the slower the speed of the aircraft, the larger the visibility disk. With knowledge of the visibility parameter for each object of interest, we can find the speed a vehicle can travel on a constant heading that assures all information requirements are met. Furthermore, we can find the heading at which this speed is maximized. This property is shown in Figure 4.11

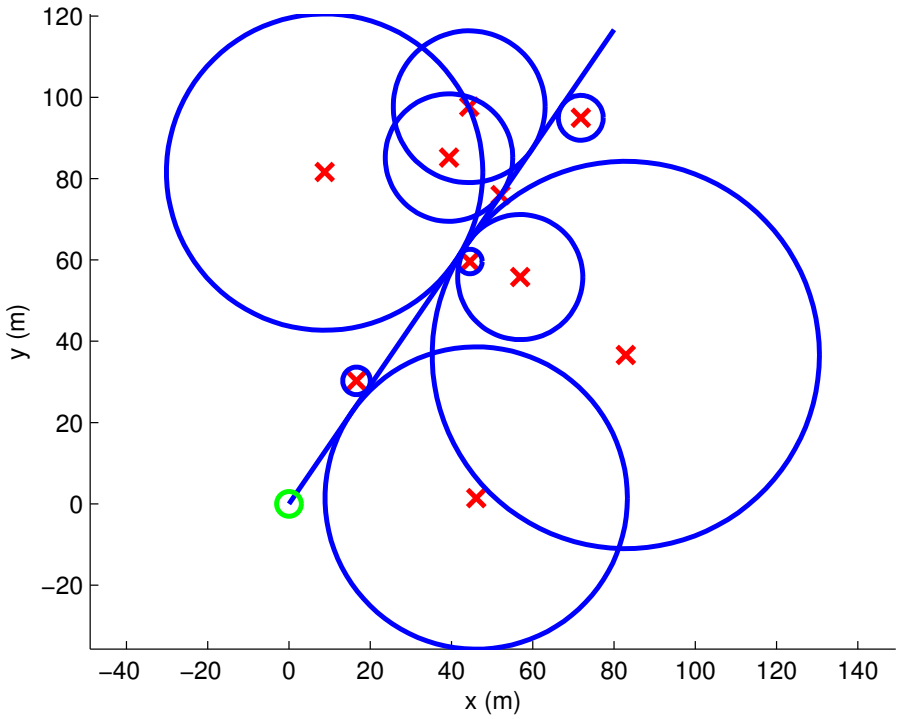

Figure 4.11 Constant heading flight satisfying information boundary conditions

4.6.3 Generalized Traveling Salesman Problem

While useful, the critical objects heuristic and rubberband heuristic suffer from a need to know the sequence of objects to visit. Each object is centered in a disk of influence, and only one point within this disk needs to be visited to achieve mission objectives. Thus the problem is similar to the TSP shown in Figure 4.13 and described earlier.

A generalized form of this problem, in which a salesman must visit one city within each state, is appropriately called the Generalized Traveling Salesman Problem or GTSP(60).

GTSP Exploration considers a set of sets, $\hat{S}$ where $s_j \in \hat{S}, 1 \leq j \leq m$ contains elements. These elements are the Cartesian positions within the disk of influence around object j. Each set s_j must have one element visited, i.e., the vehicle path must include an element in each set, in a minimal time fashion. There is no requirement as to which element in a set s_j is visited. This transforms the exploration problem into one of object sequencing and

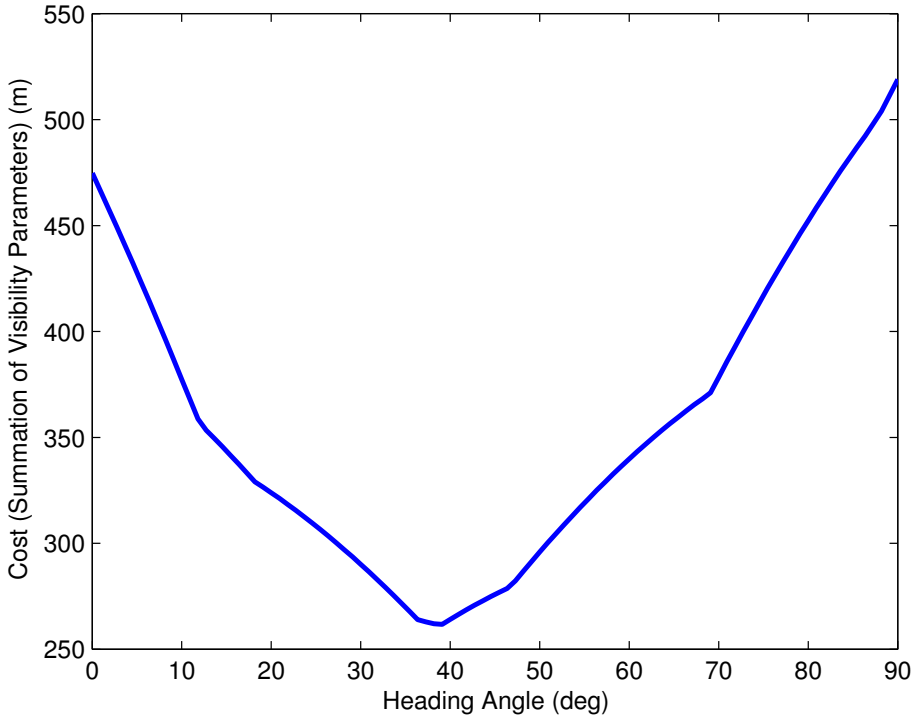

Figure 4.12 Constant heading flight cost as a function of heading

element selection. Similar to the critical objects heuristic, if a set s is visited exactly once, the information constraint associated with that set is active, otherwise it is inactive.

4.6.4 GTSP Solver

The GTSP solution is a path connecting each set s_j where the sum of all the path lengths is minimized. There are two things to consider when optimizing this path: 1) the distance between subsequent objects of interest (the positions of which are elements of each set s_j) and 2) the cardinality of s_j.

A TSP can be considered a GTSP with each set s_j of cardinality one. The sequence of elements visited determines the total path length. In the GTSP, the selection of the optimal element in the set s_j influences the total path length and can change which sequence of sets to visit is optimal.

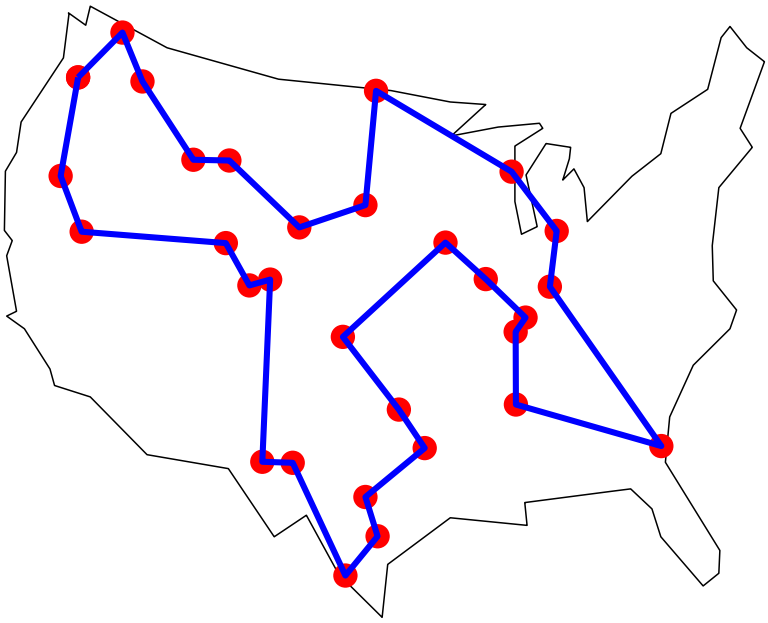

Figure 4.13 An example of a Traveling Salesman Problem solution taken from *travel.m* in Matlab.

An algorithm is created to attempt to optimize both the sequence of sets and selection of visited elements in each set. Consider a set of 15 objects of interest as in Figure 4.14.

A random path can be generated beginning at the aircraft initial position and continuing through elements of each set s_j. At each iteration of the algorithm, two subsets of $\hat{S}$ of size two are chosen. If elements s_j of these subsets can be swapped in the path sequence resulting in a reduction of the total path length, the swap is kept. This method is often known as a 2-opt swap (135) and is a member of a family of similar swapping algorithms known as k-opt (28).

If the swap is successful, a search algorithm, e.g., in Matlab, *fminsearch*, is used to find the element of each $s_j, 1 \leq j \leq m$ that provides the minimum total path length for a given

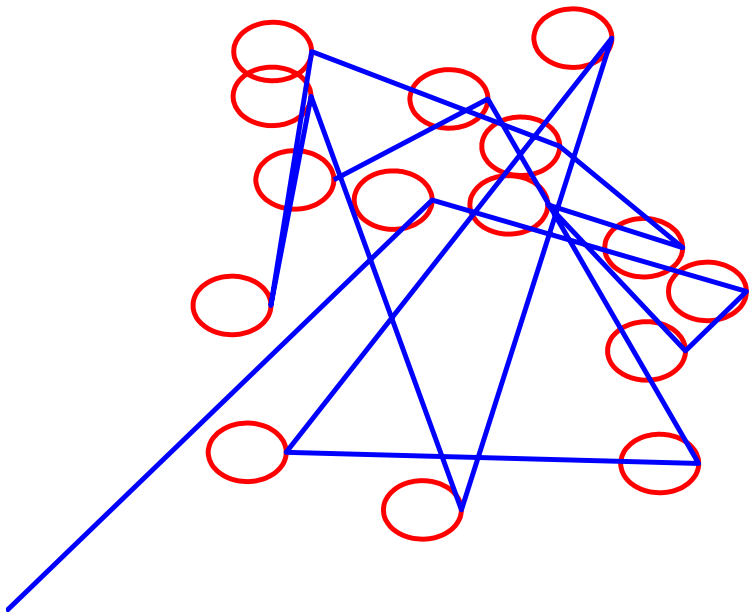

Figure 4.14 GTSP solver start condition with 15 objects of interest

sequence. Each resulting iteration either successfully reduces the total path length or does not change the path. The algorithm ends after a preset number of subsequent iterations fails to reduce the total path length. One solution (though possibly not the optimal solution) is presented in Figure 4.15 where the computation time is a a function of iterations. In this example, the computation time was approximately 5 minutes on a Windows XP laptop running at 2 GHz with 2 GB RAM.

This algorithm can be supplemented by the use of other GTSP solvers (54). The applicability of GTSP and TSP algorithms to time-optimal exploration problems allows a wide range of literature to be leveraged (15), (57).

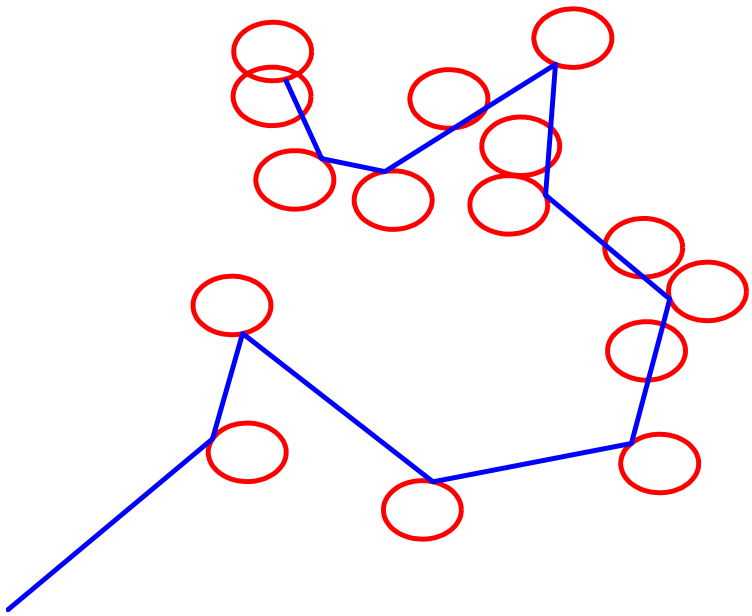

Figure 4.15 GTSP solver end condition with 15 objects of interest

4.7 Summary of Time-Optimal Exploration

This chapter has presented an information-based formulation for time-optimal exploration. The problem of optimal path planning is formulated by noting the similarity between information and exploration. This formulation exploits the coupling of kinematics with informatics. We have presented necessary conditions for optimality with multiple objects of interest and a single vehicle. These necessary conditions have been solved using a discretization technique, which highlights the qualitative nature of extremals. This nature has been characterized in several propositions. Several heuristics including the critical object heuristic, rubber band heuristic and GTSP heuristic have been developed utilizing these propositions to allow for quick solving of near-optimal flight paths when exploring in a time-optimal manner.

Chapter 5

Energy-Optimal Exploration

5.1 Introduction and Problem Formulation

Future exploration of Mars, laid out by the Vision for Space Exploration (91), requires long endurance unmanned aerial vehicles that use resources that are plentiful on Mars. One possible way of achieving this is to use a solar-powered aircraft that flies perpetually, which motivates the problems solved in this chapter. The aircraft considered in this chapter is distinguished from the majority of aircraft by its power source: it is equipped with solar cells on the upper surface of the wings as well as onboard energy storage. These solar cells collect energy that is used to drive a propeller.

This chapter considers the problem of energy-optimal path planning for solar-powered aircraft in level flight and quantifies the requirement for perpetual endurance in solar-powered flight. Perpetual endurance is the ability of an aircraft to collect more energy from the star than it loses in flying during a solar day. These problems feature the interaction between three subsystems: aircraft kinematics, energy collection, and energy loss. While the current literature discusses methods to optimize aircraft aerodynamic design for energy usage, there is no approach that examines the coupling of solar energy collection and energy loss with the aircraft kinematics nor is there a specific quantification of the requirement for perpetual endurance of solar-powered flight in terms of aircraft and environmental parameters. Consequently, the purpose of this chapter is twofold: (1) to investigate the coupling

between energy collection, energy loss and kinematics and account for it in optimal path planning and (2) to identify the requirement for perpetual endurance.

In summary, the integrated model considered in this chapter is as follows. The bank angle and speed determine the heading and the position of the aircraft through (3.1)-(3.3). The bank angle, together with the star's position from (3.69) and (3.71) determines the incidence angle through (3.53). The incidence angle of the star together with the bank angle and speed determine the energy collected and lost by the aircraft during flight through (3.44)-(3.43) and (3.59)-(3.54), respectively.

The most significant limitations of the model (3.1)-(3.54) are the assumptions of quasi-static equilibrium flight at constant altitude. Since these assumptions can be satisfied in practice, but are restrictive, the energy optimization results presented in this chapter provide conservative bounds on what can be achieved when these assumptions are violated. Removing these assumptions is the subject of future work.

5.2 Problem Formulation

This chapter considers the following two types of missions with associated problems:

5.2.1 Energy-Optimal Flight

Here the mission is to fly from a given initial location and heading (x_o, y_o, ψ_o) to a given final location and heading (x_f, y_f, ψ_f) departing at a given initial time t_o and taking at most a given mission time T_M. We assume that T_M is very short compared to daylight, hence the star is fixed in the sky during the mission. To accomplish extended flight, we stitch several missions together, where the final conditions of one mission become the initial conditions for the next. The star is assumed to move between these missions. The Optimal Path Planning Problem is then to find a flight path that accomplishes the mission in an energy-optimal manner, i.e., while maximizing the final value of aircraft energy.

5.2.2 Perpetual Loiter

Here the mission is to fly from a given initial location and time (x_o, y_o, t_o) so that, over the time interval $[t_o, t_o + t_{sd}]$, the aircraft collects more energy from the star than it spends flying. We assume that the aircraft speed is suficiently small so that its longitude and latitude do not change significantly over the duration of a solar day, hence the longitude and latitude of the aircraft are fixed during the mission. The Perpetual Loiter Problem is then to derive conditions on the aircraft and environment parameters introduced in Chapter 3 that make the mission possible.

5.3 Optimal Path Planning

In this section, we derive the necessary conditions for energy-optimal flight. The dynamic optimization problem is to maximize, with respect to the time histories of the bank angle and speed, the final energy of the solar-powered aircraft, i.e.,

$$\max_{\phi(\cdot),V(\cdot)} E_{Total} \triangleq (E_{in} - E_{out}), \tag{5.1}$$

subject to (3.1)-(3.69) and boundary conditions.

5.3.1 Necessary Conditions for Optimality

The necessary conditions for optimality for the maximization problem (5.1) are derived in Appendix A. Here, these necessary conditions are applied to the current problem. With state $[x, y, \psi]^T$ and control input $(\phi, V)^T$ the Hamiltonian is:

$$H(x, y, \psi, \lambda_x, \lambda_y, \lambda_\psi, \phi, V) = P_{in}(\vartheta(\phi, \psi)) - P_{out}(\phi, V) + \lambda_x V \cos\psi + \lambda_y V \sin\psi + \lambda_\psi \frac{g \tan\phi}{V}, \tag{5.2}$$

where ϑ depends on ϕ and ψ through (3.53) and λ_x, λ_y, and λ_ψ are the costates. Here, the only control constraints are that $V > 0$ and $|\phi| < \frac{\pi}{2}$.

Remark 5.3.1. It is not necessary to impose a tight constraint on the magnitude of the bank angle. Indeed, banking requires lifting (See (3.59)), lifting induces drag (See (3.57)), drag requires thrust (See (3.56)), which implies power loss (See (3.55)). Since the path planning aims at achieving optimal final energy, the magnitude of the bank angle is naturally limited by these phenomena. Figure 5.1 provides a visualization of this phenomena.

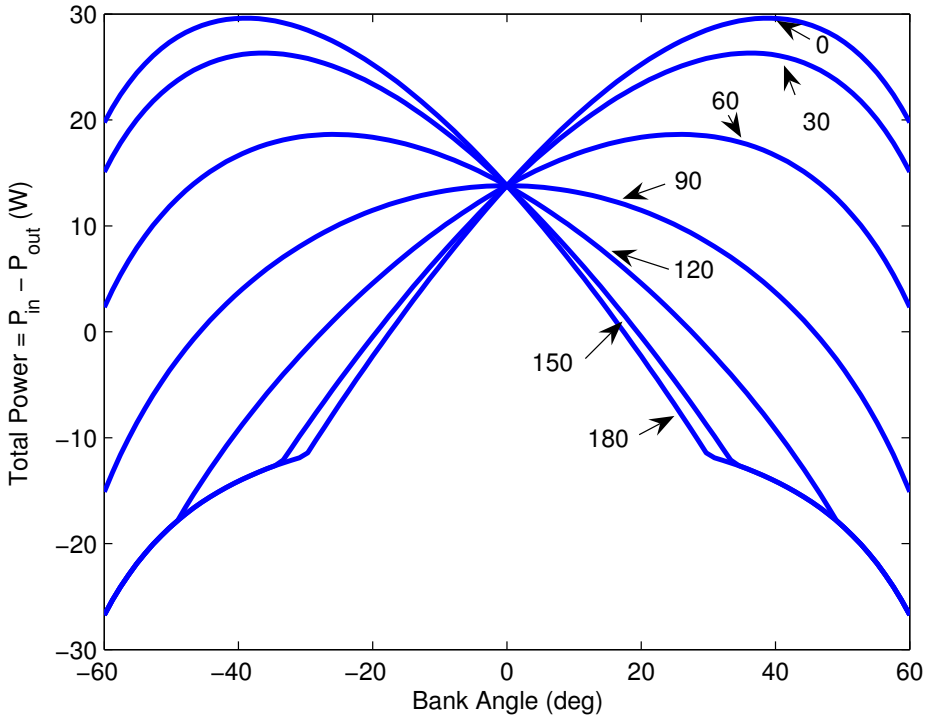

Figure 5.1 Total $P_{in} - P_{out}$ for an aircraft heading east with the star at azimuth 90 degrees and for various star elevations and bank angles.

The state equations, consistent with (5.1), are:

$$\dot{x} = \frac{\partial H}{\partial \lambda_x} = V\cos(\psi), \tag{5.3}$$

$$\dot{y} = \frac{\partial H}{\partial \lambda_y} = V\sin(\psi), \tag{5.4}$$

$$\dot{\psi} = \frac{\partial H}{\partial \lambda_\psi} = \frac{g\tan(\phi)}{V}. \tag{5.5}$$

The costate equations are:

$$\dot{\lambda_x} = \frac{-\partial H}{\partial x} = 0, \tag{5.6}$$

$$\dot{\lambda_y} = \frac{-\partial H}{\partial y} = 0, \tag{5.7}$$

$$\dot{\lambda_\psi} = \frac{-\partial H}{\partial \psi} = -\lambda_y V\cos\psi + \lambda_x V\sin\psi - \eta_{sol}P_{sd}S\cos e\cos(\tilde{a}-\psi)\sin\phi. \tag{5.8}$$

The first-order optimality conditions for the minimization of the Hamiltonian with respect to ϕ and V are:

$$\begin{aligned}\frac{\partial H}{\partial \phi} &= -\eta_{sol}P_{sd}S(\cos(e)\cos(\phi)\sin(\tilde{a}-\psi)+\sin(e)\sin(\phi)) \\ &\quad - \frac{4K(mg)^2\sin(\phi)}{\eta_{prop}\rho SV\cos^3(\phi)} + \frac{g\lambda_\psi}{V\cos^2(\phi)} = 0,\end{aligned} \tag{5.9}$$

$$\begin{aligned}\frac{\partial H}{\partial V} &= \lambda_x\cos(\psi) + \frac{8K(mg)^2\sec(\phi)^2}{\eta_{prop}\rho SV^2} - \frac{3\rho SV^2(C_{D_o}+\frac{4K(mg)^2\sec(\phi)^2}{\rho^2S^2V^4}}{2\eta_{prop}} \\ &\quad + \lambda_y\sin(\psi) - \frac{g\lambda_\psi\tan(\phi)}{V^2} = 0.\end{aligned} \tag{5.10}$$

The second order Legrendre-Clebsch condition is that the Hessian of the Hamiltonian be negative semi-definite, i.e.:

$$\frac{\partial^2 H}{\partial(\phi,V)^2} \leq 0, \tag{5.11}$$

where, if

$$\frac{\partial^2 H}{\partial(\phi,V)^2} = \begin{bmatrix} H_{\phi\phi} & H_{\phi V} \\ H_{\phi V} & H_{VV} \end{bmatrix}, \tag{5.12}$$

(5.13)

$$\begin{aligned}
H_{\phi\phi} &= \frac{\eta_{prop}\eta_{sol}\rho P_{sd} S^2 V(-(\cos(\phi)\sin(e)) + \cos(e)\sin(\tilde{a}-\psi)\sin(\phi))}{\eta_{prop}\rho SV} \\
&\quad + \frac{-4K(mg)^2\sec(\phi)^4 + 2\sec(\phi)^3(g\lambda_\psi\eta_{prop}\rho S\cos(\phi) - 4K(mg)^2\sin(\phi))\tan(\phi)}{\eta_{prop}\rho SV}, \\
H_{\phi V} &= -\frac{g\lambda_\psi\sec(\phi)^2}{V^2} + \frac{4K(mg)^2\sec(\phi)^2\tan(\phi)}{\eta_{prop}\rho SV^2}, \\
H_{VV} &= \frac{8K(mg)^2\sec(\phi)^2}{\eta_{prop}\rho SV^3} - \frac{3\rho SV(C_{D_o} + \frac{4K(mg)^2\sec(\phi)^2}{\rho^2 S^2 V^4})}{\eta_{prop}} + \frac{2g\lambda_\psi\tan(\phi)}{V^3}.
\end{aligned} \tag{5.14}$$

The boundary conditions for point-to-point flight are:

$$x(t_o) = x_o, \tag{5.15}$$

$$y(t_o) = y_o, \tag{5.16}$$

$$\psi(t_o) = \psi_o, \tag{5.17}$$

$$x(t_f) = x_f, \tag{5.18}$$

$$y(t_f) = y_f, \tag{5.19}$$

$$\psi(t_f) = \psi_f. \tag{5.20}$$

Since the final time is free, then we must also satisfy:

$$H(x,y,\psi,\lambda_x,\lambda_y,\lambda_\psi,\phi,V)|_{t_f} = 0,$$
$$t_f < t_o + T_M. \tag{5.21}$$

However, if $t_f = t_o + T_M$, Eq. (5.21) does not necessarily hold.

Equations (5.3)-(5.21) provide necessary conditions for optimality in the form of a two-point boundary value problem.

We will also define here the minimum power velocity, $V_{Power_{min}}$ as:

$$V_{Power_{min}} = \sqrt[4]{\frac{4KW^2}{3C_{D_o}\rho^2 S^2\cos^2(\phi)}}. \tag{5.22}$$

It is important to note the distinction between $V_{Power_{min}}$ and $V_{Energy_{min}}$ where $V_{Energy_{min}} = \sqrt[4]{\frac{4KW^2}{C_{D_o}\rho^2 S^2\cos^2(\phi)}} = 1.31V_{Power_{min}}$.

5.4 The Power Ratio

If $E_{Total} < 0$ in (5.1) we have that $P_{in} < P_{out}$ on average. Conversely, if $E_{Total} > 0$ we have $P_{in} > P_{out}$ on average. These conditions may be expressed on average as $\frac{P_{in}}{P_{out}} < 1$ or $\frac{P_{in}}{P_{out}} > 1$, respectively. When considering a straight unbanked flight path between an initial location and a final location this ratio is:

$$P_R(e) = \frac{2\eta_{prop}\eta_{sol}\rho P_{sd} S^2 V_{Power_{min}}\sin(e)}{C_{D_O}\rho^2 S^2 V_{Power_{min}}^4 + 4K(mg)^2}. \tag{5.23}$$

where

$$V_{Power_{min}} = \sqrt[4]{\frac{4KW^2}{3C_{D_o}\rho^2 S^2}}. \tag{5.24}$$

We refer to the non-dimensional parameter P_R as the Power Ratio.

On an energy-optimal flight, we can evaluate the energy collected and energy lost, and compute another nondimensional quantity, the energy ratio, E_R, as:

$$E_R = \frac{\int_{t_o}^{t_f} P_{in}(\vartheta(\phi,\psi))dt}{\int_{t_o}^{t_f} P_{out}(\phi,V)dt}. \tag{5.25}$$

E_R defines two flight regimes, which we call the Drag Regime and the Solar Regime, corresponding to $E_R < 1$ and $E_R \geq 1$, respectively.

Table 5.1 Comparison of P_R and E_R on Energy-Optimal Paths

P_R	E_R	Error $((P_R - E_R)/E_R)$
2.3492	2.3511	-0.08%
2.2016	2.2125	-0.49%
2.0771	2.0745	0.13%
1.9112	1.9307	-1.01%
1.7704	1.7822	-0.66%
1.6304	1.6226	0.48%
1.4810	1.4548	1.80%
1.3149	1.2983	1.28%
1.1526	1.1551	-0.22%
1.0068	1.0041	0.27%
0.9385	0.9496	-1.17%
0.7861	0.8180	-3.9%
0.6315	0.6864	-8.00%
0.4751	0.5470	-13.14%

Although P_R does not depend on $(\phi,\psi,\tilde{a})$ with the assumptions made about the atmosphere, it turns out that it closely approximates E_R, as can be seen in Table 5.1. Table 5.1 is given for typical energy-optimal flight paths, with each entry generated with conditions similar to those described in Table 5.2. These conditions were chosen as a representative sample of the many more sets of conditions examined in our numerical investigations. Thus, we have the following:

Remark 5.4.1. P_R is usually a good enough approximation of E_R to determine the regime

of the optimal flight.

5.5 Properties of Extremal Flight Paths

From the necessary conditions, we formulate the following propositions with proofs found in Appendix C.

Proposition 5.5.1. *If P_{sd} is sufficiently small, then $\phi(t) = 0$ and $V = V_{Energy_{min}}$ generate a path that satisfies the necessary conditions for optimal flight, and $t_f \leq t_o + T_M$.*

Note that, in practice, P_{sd} small implies $P_R < 1$. However, Proposition 5.5.1 does not mean that $P_R < 1$ implies $\phi(t) = 0$ and $V = V_{Energy_{min}}$ generate the only path that satisfies the necessary conditions of optimality. It is possible to find additional paths (69) satisfying the necessary conditions where $P_R < 1$ and $\phi(t) \neq 0$.

Proposition 5.5.2. *If $P_R > 1$, and T_M and P_R are sufficiently large, then the optimal path must satisfy $t_f = t_o + T_M$ and $V = V_{Power_{min}}$.*

Proposition 5.5.2 implies that when $P_R > 1$ and large enough, and T_M is large enough, the optimal path takes as much time as allowed, flying at the most advantageous speed. Propositions 5.5.1 and 5.5.2 are proven in Appendix C, D and E, based on Remark 5.4.1.

5.5.1 Characteristics of Optimal Paths

The same set of simulation conditions was used for each result presented in this section. These conditions are shown in Table 5.2. The method to find these trajectories is discussed in Appendix B.

Figures 5.2 and 5.3 are representative samples of optimal flight paths. Each flight path was then evaluated based upon flight duration and total energy at the end of flight. A summary of the conditions and results for figure 5.2 is presented in table 5.3.

Table 5.2 Simulation Conditions

Initial Position	(x_o, y_o)	(0,0)	m
Initial Energy	E_o	0	J
Initial Heading	ψ_o	127	deg
Final Position	(x_f, y_f)	(700,1300)	m
Maximum Mission Time	T_M	300	s
Velocity of Minimum Power	$V_{Power_{min}}$	15	m/s
Vehicle Parameters	*Metis Aircraft*	Appendix F	

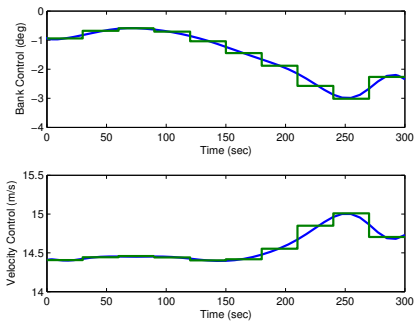

(a) Bank Angle and Velocity

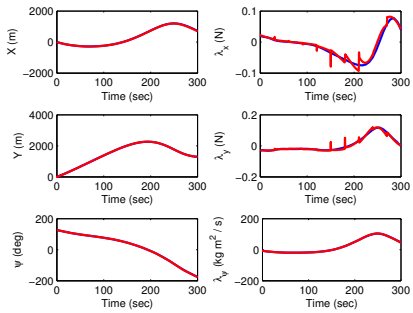

(b) States and Costates

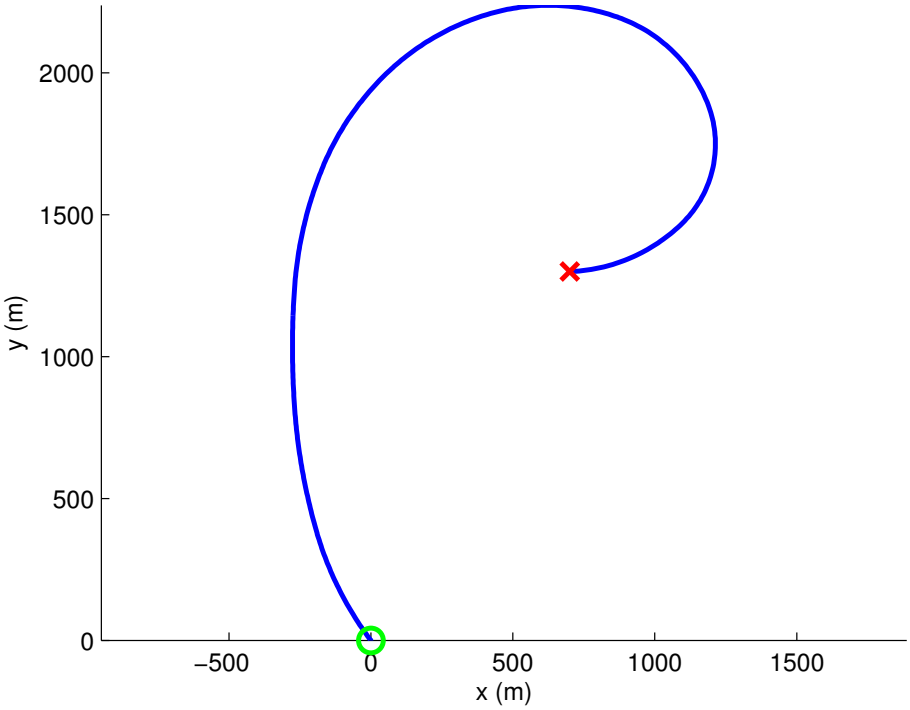

(c) Flight Path

Figure 5.2 Example of an energy optimal flight path based on table 5.3.

Table 5.3 Figure 5.2 Simulation Conditions and Results

Star Position	$(\tilde{a}, e)$	(0,45)	deg
Solar Spectral Density	P_{sd}	380	W/m^2
Final Heading	ψ_f	180	deg
Flight Duration	$t_f - t_o$	300	s
Total Final Energy	E_T	6764	J
Energy In	E_{in}	12646	J

Of particular note, in Figure 5.2, is the positive value of E_{Total} at the end of flight, indicating a net gain of energy. The flight duration is equal to T_M. The final time, t_f, is free in this problem subject to $t_f \leq t_o + T_M$. The aircraft also only made a slow, sweeping turn with $|\phi(t)| << 1$ at all times. Throughout the flight, the speed remained at a constant 15 m/s. The results from this flight are in accordance with Proposition 5.5.2.

A summary of the conditions and results for Figure 5.3 is presented in Table 5.4. The major difference with the previous case is that the star has set. During this flight, the bank angle is close to zero degrees, indicating almost no turning. The only turn was at the beginning of flight to obtain a direct heading towards the destination. The control inputs during this turn indicate a high bank angle for a short duration. The flight duration was only 80 s, much less than T_M. In this case, the total energy at the end of the flight was negative, indicating more energy was lost than collected. The speed throughout the flight remained at a constant 19 m/s. The results from this flight are in accordance with Proposition 5.5.1.

Table 5.4 Figure 5.3 Simulation Conditions and Results

Star Position	$(\tilde{a}, e)$	(0,0)	deg
Solar Spectral Density	P_{sd}	380	W/m^2
Final Heading	ψ_f	61	deg
Flight Duration	$t_f - t_o$	80	s
Total Final Energy	E_T	-1776.1	J
Energy In	E_{in}	0	J

As shown in Figures 5.2 and 5.3, the flight path characteristics vary widely as the star elevation is changed. Figure 5.4 is obtained by varying the elevation of the star (with $\tilde{a} = 0$) and recording the total energy of the resulting optimal flight path while the remaining aircraft, environmental and mission parameters are fixed. The elevation of the star is varied

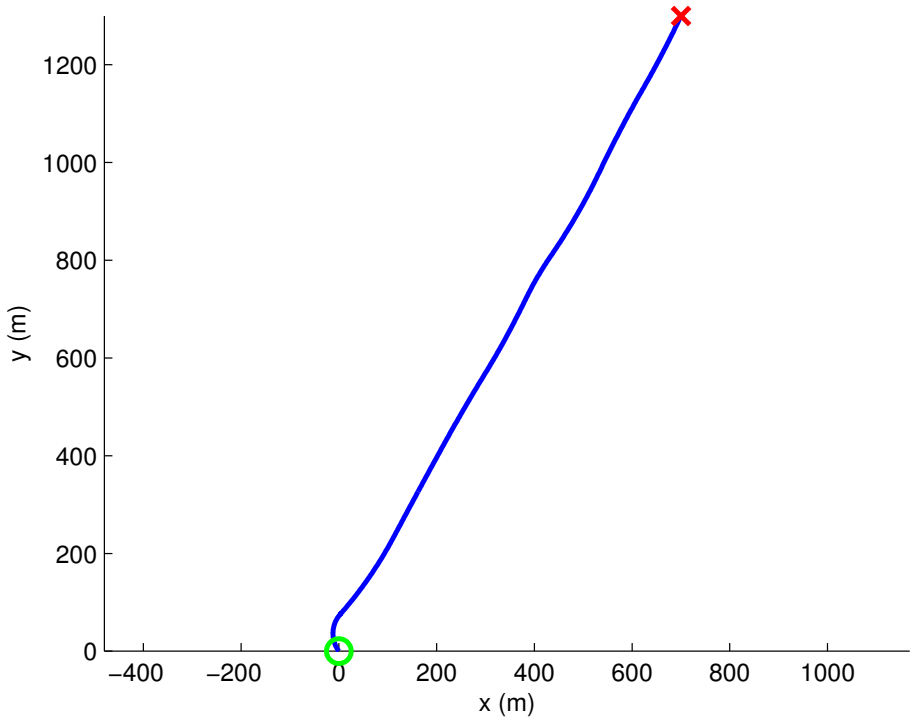

Figure 5.3 Example of an energy optimal flight path based on table 5.4.

from 0 to 90 degrees. While the total energy of the aircraft at the end of flight remains positive, a nearly sinusoidal relationship between elevation of the star and energy emerges. This relationship persists until the total energy becomes negative. At this transition point, the trend departs from a nearly sinusoidal function, which suggests a change in regime. The transition exhibited in Figure 5.4 supports the use of the Power Ratio as a predictor of the optimal regime.

Disturbances such as wind can affect the flight path of the aircraft. These disturbances are considered in (69).

5.5.2 Extremal Path Summary

In summary, extremal flight paths can be obtained as follows. When $P_R < 1$, extremal flight paths are best described by Proposition 5.5.1. When $P_R > 1$, extremal flight paths satisfy

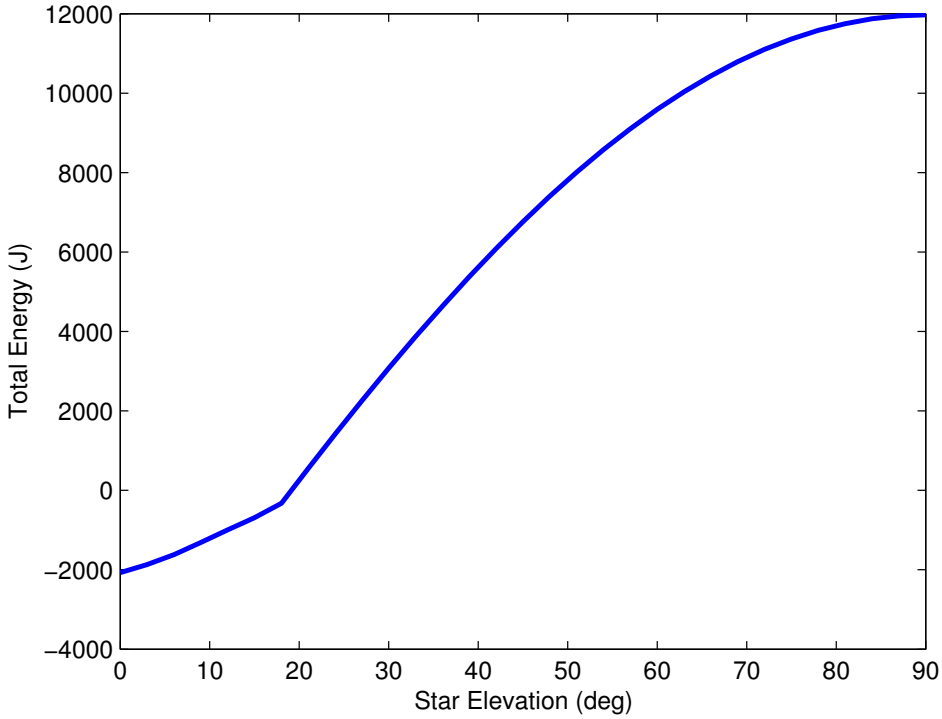

Figure 5.4 Total energy at end of flight as a function of solar elevation

Proposition 5.5.2. From Proposition 5.5.1 and 5.5.2, the velocity in both regimes is not an independent control but is instead dependent upon the regime and the bank angle.

5.6 Perpetuity Threshold

5.6.1 Derivation of the Perpetuity Threshold

For perpetual endurance, including the case of the loiter problem, it is required that, over the duration of a solar day, the energy collected by the aircraft exceed or be equal to the energy lost, i.e.,

$$\frac{E_{in}}{E_{out}} \geq 1. \tag{5.26}$$

From (3.43) and (3.54), this is equivalent to:

$$\frac{\int_{t_{r_1}}^{t_s} P_{in}(\vartheta(\phi,\psi))dt}{\int_{t_{r_1}}^{t_{r_2}} P_{out}(\phi,V)dt} \geq 1, \tag{5.27}$$

where we need only consider the daylight hours for the power collected. Here, t_{r_1} is the time of sunrise on a solar day, t_s is the next time of sunset, and t_{r_2} is the time of sunrise on the next solar day.

Since the final conditions for loiter are free and banking requires energy, energy-optimal loitering paths have zero bank angle and a speed equal to $V_{Power_{min}}$. We use (3.44) and the time-invariance of P_{out} to show that (5.27) is equivalent to

$$\frac{\eta_{sol} P_{sd} S \int_{t_r}^{t_s} \sin(e(t))dt}{P_{out} t_{sd}} \geq 1. \tag{5.28}$$

Let $\bar{e}$ be the average elevation of the star, i.e., let $\bar{e}$ satisfy:

$$\sin(\bar{e}) = \frac{1}{t_s - t_r} \int_{t_r}^{t_s} \sin(e(t))dt \tag{5.29}$$

We can simplify (5.28) as

$$\frac{\eta_{sol} P_{sd} S \sin(\bar{e})(t_s - t_r)}{P_{out} t_{sd}} \geq 1. \tag{5.30}$$

Comparing this to (5.23), this inequality is equivalent to:

$$P_R(\bar{e}) \geq \frac{t_{sd}}{t_s - t_r}. \tag{5.31}$$

Hence (5.31) solves the perpetuity problem by establishing the following:

Remark 5.6.1. Perpetual endurance is possible if and only if the Power Ratio, evaluated at

the average star elevation, exceeds the reciprocal of the daylight duty cycle.

Remark 5.6.2. Note that the right hand side of (5.31) is always greater than or equal to 1. Therefore, perpetual endurance always requires that the Power Ratio, evaluated at the average star elevation, be greater than or equal to 1.

5.6.2 Comparative Analysis of the Perpetuity Thresholds on Earth and Mars

The results of Section 5.6.1 provide a threshold, dependent upon location and time, that must be exceeded by the Power Ratio for perpetual endurance. Note that design parameters and environmental parameters affect the Power Ratio and this will be studied in Chapter 7. However, if we fix the design of the aircraft, we can examine the effect of environmental parameters on the Power Ratio. Furthermore, we can compare the design requirements for perpetual endurance between Earth and Mars.

The Perpetuity Threshold has been shown to be the ratio, $\frac{t_{sd}}{t_s - t_r}$. We can compare this ratio, as a function of mean anomaly Ωt and latitude, between Earth and Mars, as shown in Figures 5.5 and 5.6. Note that the Perpetuity Threshold approaches infinity when the daylight duty cycle approaches zero and we have limited the plot to thresholds smaller than six. The arctic regions are those latitudes above $90^\circ - i$ and below $-90^\circ + i$. During part of the year, these regions can have extended periods of total darkness or total light, that is, there are no local sunrises or sunsets for multiple rotations of the planet. For areas of total light (i.e., arctic summer), the Power Ratio need only exceed 1 for perpetual endurance. We have not considered regions of total darkness (i.e., arctic winter) in this dissertation because requirements on battery size put this case outside the scope of practical solar-powered aircraft.

Table 5.5 compares the planetary characteristics of Earth and Mars.

The maximum deviation between the thresholds on Earth and Mars is 6.3% with a mean deviation of $-5 \times 10^{-2}\%$. The Perpetuity Thresholds between Earth and Mars are therefore

Table 5.5 Planetary Characteristics of Earth and Mars

		Earth	Mars	
Duration of Solar Day	t_{sd}	23.93	24.62	hours
Days in Year		365.25	687	days
Inclination of Axis	i	23.5	25	deg

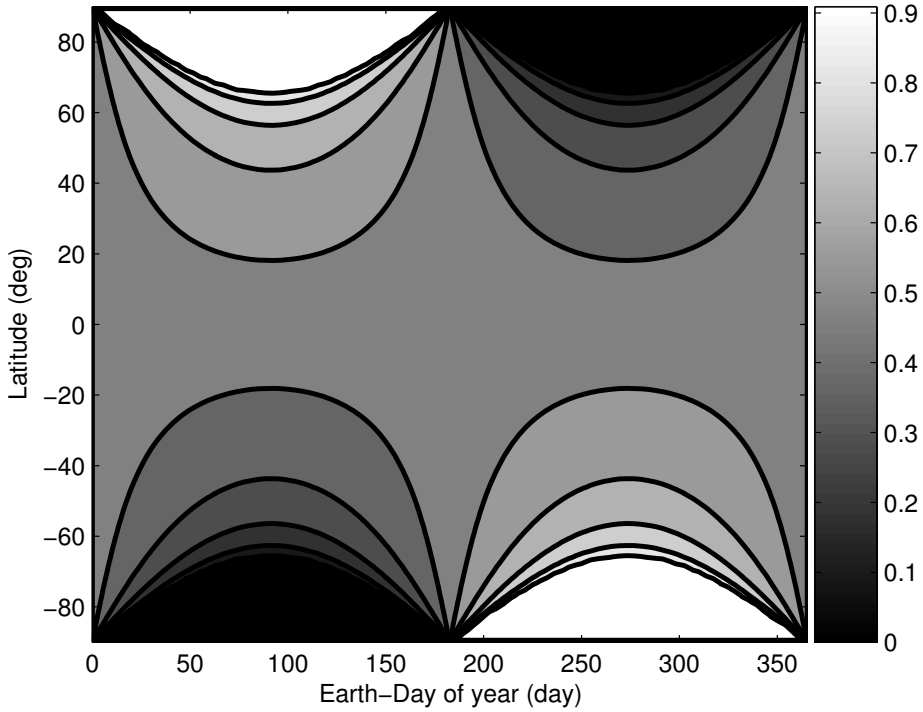

Figure 5.5 Map of Daylight Duty Cycle on Earth

similar since the maximum and average deviations are small.

5.7 Summary of Energy-Optimal Exploration

Path-planning for solar-powered aircraft can be improved if a model that couples the kinematics with the energetics through the bank angle of the aircraft is used. By identifying and predicting the regime of optimal flight through use of the Power Ratio, significant energy savings can be made.

During perpetual flight, a positive total energy balance must be achieved over a solar

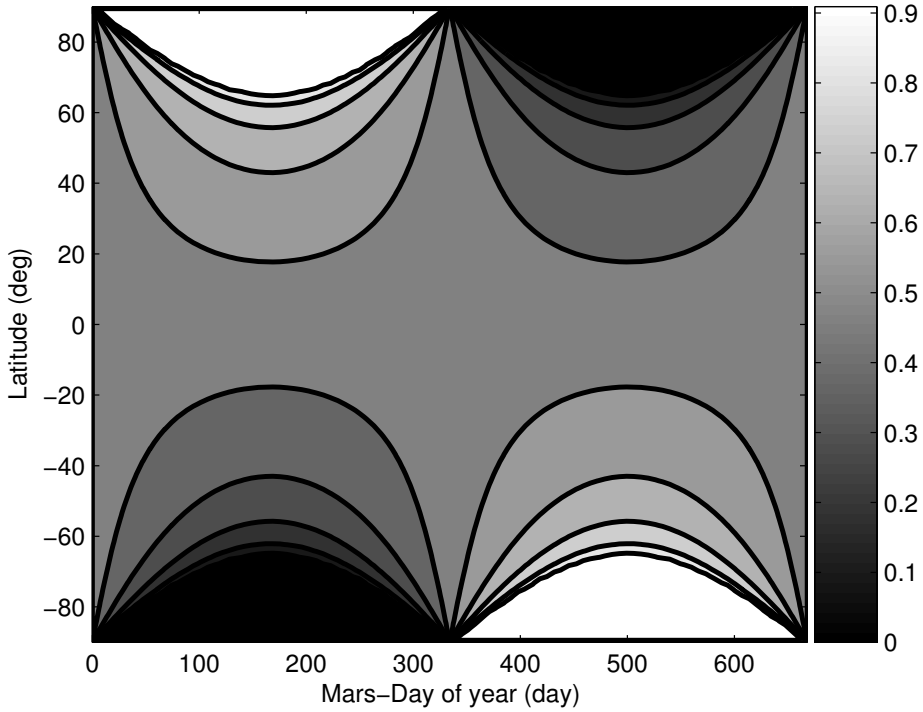

Figure 5.6 Map of Daylight Duty Cycle on Mars

day. By translating this requirement on the Power Ratio, we obtain that perpetual solar-powered flight is achievable if and only if the Power Ratio, evaluated at the average star elevation, is greater than or equal to the reciprocal of the daylight duty cycle.

These requirements and regimes of flight enable a solar-powered aircraft to extend its endurance (and thus loiter time) to collect the required amounts of information to complete the exploration mission. In the following chapter we will consider a combination of time-optimal and energy-optimal path planning for exploration missions.

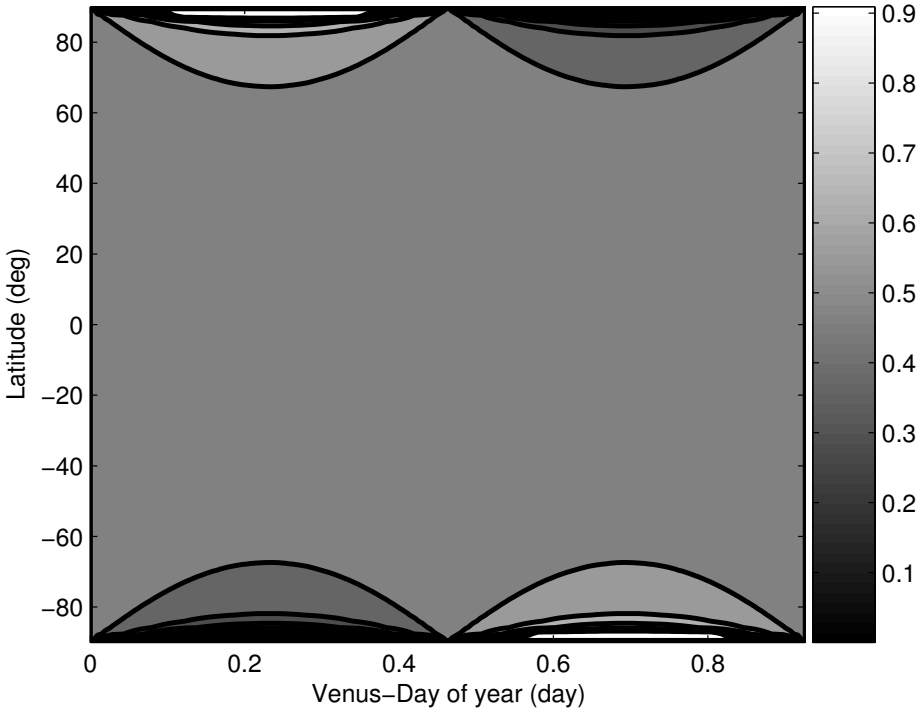

Figure 5.7 Map of Daylight Duty Cycle on Venus

Chapter 6

Energy and Time Optimal Exploration

6.1 Introduction and Problem Formulation

The challenges of exploring an area while attempting to optimize a combination of the total energy at the end of the mission and the overall mission duration are considerable. To maintain a positive total energy, a solar-powered aircraft must trade off the characteristics of energy-optimal paths with those of time-optimal paths. Intuitively, if a solar-powered vehicle is able to loiter, the total energy of the vehicle is likely to increase at the cost of mission duration. Similarly, a vehicle flying along a time-optimal path should likely reduce the number of its energy-saving maneuvers to achieve the mission objectives in a minimal amount of time. In this chapter, we consider the problem of a combination of time-optimal and energy-optimal path planning. The optimal path planning problem is formulated where cost function is dependent upon both total energy at the end of the mission and the final mission time to complete the mission and the boundary conditions subject to inequality constraints that reflect the requirements of information collection.

We consider the full model presented in Chapter 3. The sensor used is isotropic and, because the missions are short, the star is assumed fixed in the sky.

The mission is to fly from a given initial location and heading (x_o, y_o, ψ_o) so that, over the time interval $[t_o, t_o + T_M]$, the aircraft collects a specified amount of information about objects of interest. We assume that the aircraft kinematics follow (3.1) - (3.3) and that T_M is

very short compared to daylight, hence the star is fixed in the sky during the mission. The Optimal Exploration Problem is then to find a flight path that accomplishes the mission in a time-optimal and energy-optimal manner where the cost of time and energy are scaled by $\bar{T}_o$ and $\bar{E}_o$ respectively and weighted by a parameter $\zeta, 0 \leq \zeta \leq 1$.

6.2 Optimal Path Planning

In this section, we derive the necessary conditions for time-optimal and energy-optimal flight. The optimization problem is to maximize, with respect to the time-history of the bank angle, a convex combination of the scaled final energy, $E_{Total}/\bar{E}_o$, of the solar-powered aircraft and the negative of the scaled mission duration, $T_M/\bar{T}_o$, i.e.,

$$\max_{\phi(\cdot)} \left[\zeta \frac{E_{Total}}{\bar{E}_o} - (1-\zeta) \frac{T_M}{\bar{T}_o} \right], 0 \leq \zeta \leq 1, \tag{6.1}$$

subject to (3.1)-(3.69) and boundary conditions.

6.2.1 Necessary Conditions for Optimality

The necessary conditions for optimality for the maximization problem (6.1) are derived in Appendix A. Here these necessary conditions are applied to the current problem. It is interesting to note that since a linear combination of the costs from Chapter 4 and Chapter 5 are used in (6.1), the necessary conditions can be obtained as a linear combination of the necessary conditions from those respective problems. With states $[x, y, \psi, I_1, I_2, ..., I_m]$ and control input ϕ, the Hamiltonian is:

$$H(x,y,\psi,I_1,...,I_m,\lambda_x,\lambda_y,\lambda_\psi,\lambda_{I_1},...,\lambda_{I_m},\phi) = \zeta(P_{in}-P_{out})/\bar{E}_o - (1-\zeta)1/\bar{T}_o + \lambda_x V\cos\psi$$
$$+\lambda_y V\sin\psi + \lambda_\psi \frac{g\tan\phi}{V} + \sum_{j=1}^{m} \lambda_{I_j} w\log_2(1+\frac{k_j^4}{[(x(t)-a_j)^2+(y(t)-b_j)^2]^2}), \tag{6.2}$$

where λ_x, λ_y, λ_ψ and $\lambda_{I_j}, 1 \le j \le m$ are the costates. Here, the only control constraint is that $V > 0$. While the velocity is constrained by performance of the engine and altitude, it is assumed that the aircraft can at least fly at the minimum-power velocity $V_{Power_{min}}$ given in (5.22). As discussed in Chapter 5, ϕ is limited by the nature of the problem.

The state equations, consistent with (6.1), are:

$$\dot{x} = \frac{\partial H}{\partial \lambda_x} = V\cos(\psi), \tag{6.3}$$
$$\dot{y} = \frac{\partial H}{\partial \lambda_y} = V\sin(\psi), \tag{6.4}$$
$$\dot{\psi} = \frac{\partial H}{\partial \lambda_\psi} = \frac{g\tan(\phi)}{V}, \tag{6.5}$$
$$\dot{I}_j = \frac{\partial H}{\partial \lambda_{I_j}} = w\log_2(1+\frac{k_j^4}{((x(t)-a_j)^2+(y(t)-b_j)^2)^2}), 1 \le j \le m. \tag{6.6}$$

The costate equations are:

$$\dot{\lambda_x} = \frac{-\partial H}{\partial x} = \sum_{j=1}^{m} \frac{4k_j^4 w(x(t)-a_j)\lambda_{I_j}}{((x(t)-a_j)^2+(y(t)-b_j)^2)^3\Delta_j}, \tag{6.7}$$
$$\dot{\lambda_y} = \frac{-\partial H}{\partial y} = \sum_{j=1}^{m} \frac{4k_j^4 w(y(t)-b_j)\lambda_{I_j}}{((x(t)-a_j)^2+(y(t)-b_j)^2)^3\Delta_j}, \tag{6.8}$$
$$\dot{\lambda_\psi} = \frac{-\partial H}{\partial \psi} = -\lambda_y V\cos\psi + \lambda_x V\sin\psi - \eta_{sol}P_{sd}S\cos e\cos(a-\psi)\sin\phi,$$
$$\dot{\lambda_{I_j}} = 0, 1 \le j \le m, \tag{6.9}$$

where $\Delta_j = (1 + \frac{k_j^4}{((x(t)-a_j)^2+(y(t)-b_j)^2)^2}), 1 \leq j \leq m$.

The first-order optimality condition for the maximization of the Hamiltonian with respect to ϕ is:

$$\frac{\partial H}{\partial \phi} = -\eta_{sol} P_{sd} S_c (\cos(e)\cos(\phi)\sin(\tilde{a}-\psi) + \sin(e)\sin(\phi)) - \frac{4KW^2\sin(\phi)}{\eta_{prop}\rho SV\cos^3(\phi)} + \frac{g\lambda_\psi}{V\cos^2(\phi)} = 0. \tag{6.10}$$

The boundary conditions for exploration flight are:

$$x(t_o) = x_o, \tag{6.11}$$

$$y(t_o) = y_o, \tag{6.12}$$

$$\psi(t_o) = \psi_o, \tag{6.13}$$

$$I_j(t_o) = 0, 1 \leq j \leq m, \tag{6.14}$$

$$x(t_f) \text{ free}, \tag{6.15}$$

$$y(t_f) \text{ free}, \tag{6.16}$$

$$\psi(t_f) \text{ free}, \tag{6.17}$$

$$I_j(t_f) \geq 1, 1 \leq j \leq m, \tag{6.18}$$

$$\lambda_x(t_f) = 0, \tag{6.19}$$

$$\lambda_y(t_f) = 0, \tag{6.20}$$

$$\lambda_\psi(t_f) = 0, \tag{6.21}$$

$$\lambda_{I_j}(t_f) = \text{ free if } I_j(t_f) = 1, 1 \leq j \leq m, \tag{6.22}$$

$$\lambda_{I_j}(t_f) = 0 \text{ if } I_j(t_f) > 1, 1 \leq j \leq m. \tag{6.23}$$

Equations (6.3) - (6.23) provide necessary conditions for optimality in the form of a

two-point boundary value problem.

6.3 Properties of Extremal Flight Paths

6.3.1 Properties from the Necessary Conditions

From the necessary conditions, we formulate the following propositions.

Proposition 6.3.1. *If P_{sd} is sufficiently small, Proposition 4.3.1 can be used to generate a path that satisfies the necessary conditions for optimal flight, i.e., the time-optimal solution may be used.*

Proof of Proposition 6.3.1:

The aircraft is flying in the Drag Regime. Thus (6.9) and (6.10) simplify with $\phi = 0$ as:

$$0 = -\eta_{sol} P_{sd} S_c \cos(e) \sin(\tilde{a} - \psi) + \frac{g\lambda_\psi}{V}, \tag{6.24}$$

$$\dot{\lambda_\psi} = -\lambda_y V \cos\psi + \lambda_x V \sin\psi. \tag{6.25}$$

If $\phi = 0$, (6.24) implies that λ_ψ is constant. Therefore $\dot{\lambda}_\psi = 0$ and (6.25) equals zero. Then, (6.25) is equivalent to (4.9). Thus the necessary conditions for the minimization of the Hamiltonian (4.2) with respect to ψ are reconstructed under the conditions of Proposition 4.3.1 and in the context of time-optimal and energy-optimal paths.

Corollary 6.3.2. *If P_{sd} is small and the vehicle is outside of all visibility disks, a constant heading path is optimal for exploration.*

Proof of Corollary 6.3.2:

From Proposition 5.5.1, a straight flight path when operating in the Drag Regime is optimal. From Proposition 4.3.1, a time-optimal explorer travels straight when outside the visibility disk of all objects.

In summary, when P_{sd} is small, a vehicle should fly along time-optimal paths (as established in Chapter 4) to satisfy mission objectives while remaining time-optimal and energy-optimal.

6.3.2 Characteristics of Optimal Paths

Here we consider simulation results for the full problem, i.e., the time-optimal and energy-optimal path planning. The same set of simulation conditions was used for each result presented in this section. These conditions are shown in Table 6.1.

Table 6.1 Simulation Conditions

Initial Position	(x_o, y_o)	(0,0)	m
Initial Energy	E_o	0	J
Initial Heading	ψ_o	45	deg
Velocity of Minimum Power	$V_{Power_{min}}$	15	m/s
Vehicle Parameters	Appendix F		
Star Azimuth	$\tilde{a}$	180	deg
Star Elevation	e	45	deg
Solar Spectral Density	P_{sd}	150	W/m^2

Consider the cost function (6.1). We can compare the solution of the optimal control problem produced for this cost function and that of a similar cost function:

$$\max_{\phi(\cdot)} \left[\zeta E_{in}/(E_{out}\bar{E}_o) - (1-\zeta)T_M/\bar{T}_o\right]. \tag{6.26}$$

These cost functions are not equivalent. However, here we consider solutions to the optimal control problem. Figures 6.1 and 6.2 compare the flight paths produced by optimizing each of these cost functions. In each case, the final time and control forming the optimal paths are within 1.5% of each other while a comparison of E_R and P_R shows a difference of 0.56%. Each path is similar to the time-optimal path for a single aircraft flying between two visible objects of interest.

If the mission ends when enough information is collected from both objects of interest, we can evaluate the cost as follows. Figures 6.1 and 6.2 indicate that maximizing E_{Total}

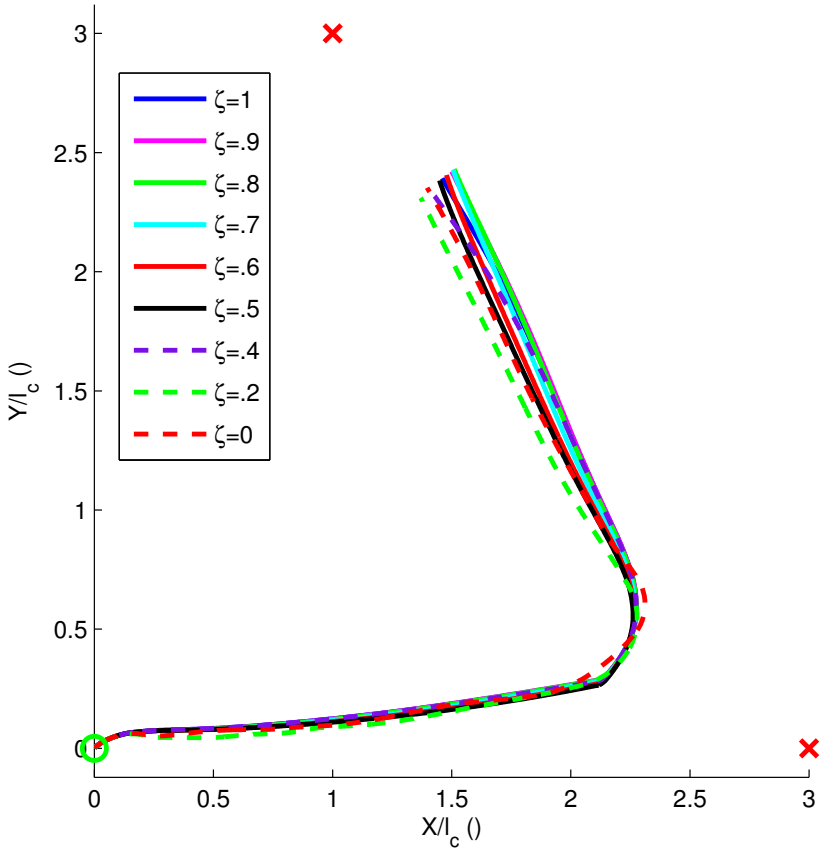

Figure 6.1 Example of time-optimal and energy-optimal flight paths as $0 \leq \zeta \leq 1$ with star position $(180, 45)$ deg with a cost function including E_{Total}

produces the same control within 1.5% as maximizing E_R for all ζ and thus the results of the optimal control problems are indistinguishable. We therefore use E_R in our cost function for the following analysis:

$$\max_{\phi(\cdot)} \left[\zeta E_{in}/(E_{out}\bar{E}_o) - (1-\zeta)T_M/\bar{T}_o\right], \tag{6.27}$$

$$= \max_{\phi(\cdot)} \left[\zeta P_R/E_o - (1-\zeta)T_M/T_o\right], \tag{6.28}$$

where E_R has been shown to be approximately equal to P_R by 5.4.1. As the star remains at position $(180, 45)$ deg and neither the aircraft nor the environment changes between flight

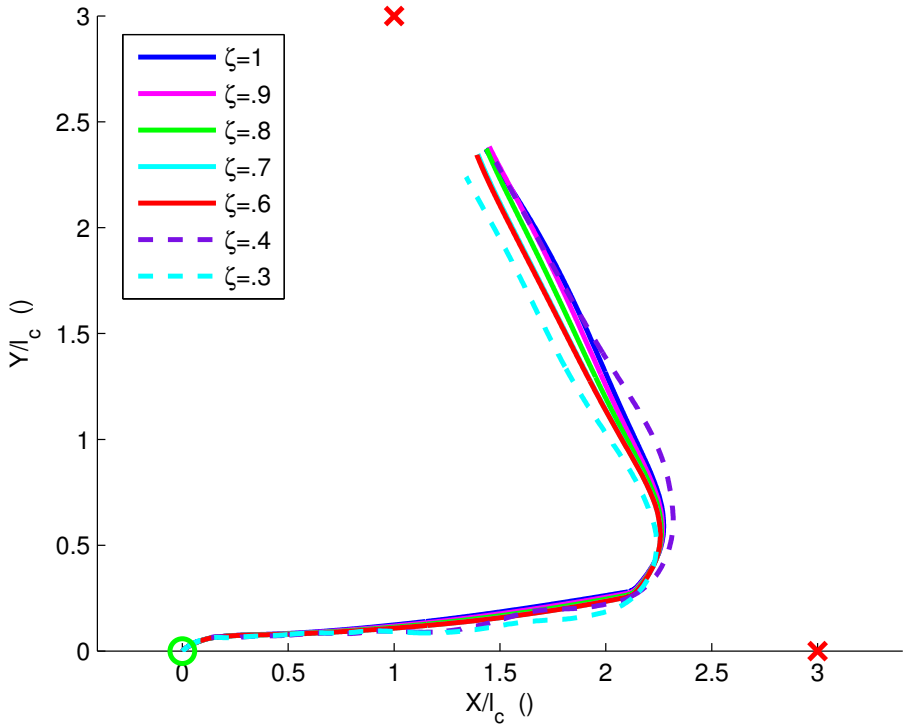

Figure 6.2 Example of time-optimal and energy-optimal flight paths as $0 \leq \zeta \leq 1$ with star position $(180, 45)$ deg with a cost function including E_R

examples, P_R remains fixed. Thus, to maximize (6.28), the time should be minimized. We can then state that:

Proposition 6.3.3. *When attempting to both minimize the time of flight and maximize the total energy at the end of flight, a time-optimal flight path is optimal for all values of* $\zeta, 0 \leq \zeta \leq 1$.

and

Remark 6.3.4. Exploration is driven by time rather than energy.

6.4 Summary of Time-Optimal and Energy-Optimal Exploration

Path planning for solar-powered aircraft performing exploration missions can be improved if we examine properties of the combination time-optimal and energy-optimal flight paths. When Proposition 5.5.1 holds, the vehicle should fly in a time-optimal manner at $V_{Power_{min}}$. When Proposition 5.5.2 holds, the extremal paths roughly follow the time-optimal path but loiter after the mission objectives have been met. For solar-powered aircraft, a time-optimal path is the best way to complete an exploration mission. The vehicle, however, must be capable of remaining in flight, i.e., $P_R \geq 1$. We examine the vehicle characteristics that allow this and the impacts this has on vehicle payloads in the next chapter.

Chapter 7

Exploration Agents

7.1 Introduction and Problem Formulation

Here we consider the third component of the exploration problem: the agent. Often the performance of the exploration depends upon the agent capabilities. Both payload mass and aircraft cost can limit this performance. More specifically for a solar-powered aircraft, additional mass decreases the Power Ratio and increase the challenges of perpetual flight (see Appendix G). Thus mass is a aircraft design driver and can restrict the ability of onboard sensors. In fact, isotropic sensors are often the exception rather than the rule for autonomous aircraft. In this chapter, we consider realistic restrictions upon the sensor model.

This chapter considers the problem of time-optimal path planning with non-isotropic sensors. The onboard sensors can only collect information when an object of interest is positioned within an active sensing cone with respect to the aircraft's orientation. The aperture of this sensor cone affects the solution to the optimal path planning problem. In fact, the aperture diameter of non-isotropic sensors is often very small to achieve high resolution at a far distance. This tunnel vision approach limits the ability of an area-coverage attempt to solve this problem.

Again we use the model presented in Chapter 3 with the following assumptions: 1) the aircraft has enough on-board energy stored to complete its mission, 2) the aircraft can

perform instantaneous turns and 3) we assume that only one bit of information about each object of interest is required to accomplish the mission.

Here the mission is to travel from a given initial location (x_o, y_0) with free heading and collect at least one bit of information from each object of interest. The aircraft departs at a given initial time t_o and flies for at most the maximum mission duration T_M. The Optimal Path Planning Problem is then to find a flight path that accomplishes the mission in a time-optimal manner while accounting for non-isotropic sensors.

7.2 Optimal Path Planning

In this section, we derive the necessary conditions for optimality. While similar necessary conditions have been developed in earlier chapters, here we account for non-isotropic sensors, which affects the derivation. The dynamic optimization problem is to minimize, with respect to the time-history of the heading angle, the time to accomplish the mission, i.e.,

$$\min_{\psi(\cdot)} t_f, \tag{7.1}$$

subject to (3.1)-(3.7) and boundary conditions.

7.2.1 Necessary Conditions for Optimality

The necessary conditions for optimality for the minimization problem (7.1) are derived in Appendix A. Here, these necessary conditions are applied to the current problem. With states $[x, y, I_1, I_2, ..., I_m]^T$ and control input ψ, the Hamiltonian is:

$$H = \sum_{j=1}^{m} \lambda_{I_j} \Gamma(\Theta) w \log_2(1 + \frac{k_j^4}{[(x(t)-a_j)^2 + (y(t)-b_j)^2]^2}) + \lambda_x v \cos(\psi) + \lambda_y v \sin(\psi) + 1, \tag{7.2}$$

where λ_x, λ_y and $\lambda_{I_j}, 1 \leq j \leq m$ are costate variables.

In this problem formulation, we have no control constraints.

The state equations, consistent with (7.2), are:

$$\dot{x} = v\cos(\psi), \tag{7.3}$$

$$\dot{y} = v\sin(\psi), \tag{7.4}$$

$$\dot{I_j} = \Gamma(\Theta) w \log_2(1 + \frac{k_j^4}{((x(t)-a_j)^2 + (y(t)-b_j)^2)^2}), 1 \leq j \leq m. \tag{7.5}$$

The costate equations are:

$$\dot{\lambda_{I_j}} = 0, 1 \leq j \leq m, \tag{7.6}$$

$$\begin{aligned}\dot{\lambda_x} = &\sum_{j=1}^{m} \frac{4k_j^4 w \Gamma(\Theta)(x(t)-a_j)\lambda_{I_j}}{((x(t)-a_j)^2 + (y(t)-b_j)^2)^3} \\ &- \frac{4k_j^4 w \frac{\delta\Gamma(\Theta)}{\delta x}\lambda_{I_j}}{((x(t)-a_j)^2 + (y(t)-b_j)^2)^2},\end{aligned} \tag{7.7}$$

$$\begin{aligned}\dot{\lambda_y} = &\sum_{j=1}^{m} \frac{4k_j^4 w \Gamma(\Theta)(y(t)-b_j)\lambda_{I_j}}{((x(t)-a_j)^2 + (y(t)-b_j)^2)^3} \\ &- \frac{4k_j^4 w \frac{\delta\Gamma(\Theta)}{\delta y}\lambda_{I_j}}{((x(t)-a_j)^2 + (y(t)-b_j)^2)^2}.\end{aligned} \tag{7.8}$$

The first-order optimality condition for the minimization of the Hamiltonian with respect to ψ is:

$$\begin{aligned}0 = &v\lambda_y\cos(\psi) - v\lambda_x\sin(\psi) \\ &- \sum_{j=1}^{m} \frac{4k_j^4 w \frac{\delta\Gamma(\Theta)_j}{\delta\psi}\lambda_{I_j}}{((x(t)-a_j)^2 + (y(t)-b_j)^2)^2}.\end{aligned} \tag{7.9}$$

The boundary conditions for this problem are:

$$x(0) = x_o, \tag{7.10}$$

$$y(0) = y_o, \tag{7.11}$$

$$I_j(0) = 0, 1 \leq j \leq m, \tag{7.12}$$

$$x(t_f) \text{ free}, \tag{7.13}$$

$$y(t_f) \text{ free}, \tag{7.14}$$

$$I_j(t_f) \geq 1, 1 \leq j \leq m, \tag{7.15}$$

$$\lambda_{I_j}(t_f) = \text{free if } I_j = 1, 1 \leq j \leq m, \tag{7.16}$$

$$\lambda_{I_j}(t_f) = 0 \text{ if } I_j > 1, 1 \leq j \leq m, \tag{7.17}$$

$$\lambda_x(t_f) = 0, \tag{7.18}$$

$$\lambda_y(t_f) = 0. \tag{7.19}$$

7.2.2 Sensitivity to Sensor Aperture

In this subsection we will analyze the effect of a non-isotropic sensor on the necessary conditions.

The sensitivity of the necessary conditions to a non-isotropic sensor appears in three areas: the optimality condition and the two costates for position. If $\frac{d\Gamma(\Theta)}{d\Theta} = 0$, the $\frac{\delta\Gamma(\Theta)}{\delta\Theta}$ term would reduce to zero and eliminate the fractional component of the optimality condition. This term includes a kind of 'map', turning the heading towards unvisited objects of interest. If instead, $\Gamma(\Theta)$ were not dependent upon Θ, as in Chapter 4, any objects outside of the vehicle's initial sensor cone would never be visited.

7.3 Properties of Path Planning with Non-Isotropic Sensors

The objective of exploration is to collect information about states of specific objects in the exploration area. Often, this information is used to classify or identify a particular object of interest. While visiting an object directly will ensure classification, we have shown it is usually only needed to approach an object and classify it from a distance. Here we use the theory and information collection model developed in the previous chapters to predict where the location of classification can occur. Knowledge of this point or set of points can be used to find paths between multiple objects of interest.

When an object is to be classified, a certain amount of information needs to have been collected about it. In this dissertation, we consider information to be additive. Roughly, the inverse of information is variance, or uncertainty about the state of an object. An alternative way of looking at the location of classification is that it is the point where uncertainty has been reduced to a given threshold. This threshold is predetermined as a given level of confidence. Rather than increasing information collection, we seek to reduce uncertainty to a predefined level so as to make a confident decision.

The model of information collection defined earlier provides the maximum rate of information that can be achieved with the onboard sensor and a particular object of interest. By integrating forward in time along a predefined path, we can predict the amount of information accrued at a given time instant. If we examine all the straight paths passing near an object of interest from an initial vehicle location, we can predict every point where the information boundary conditions are met. This is illustrated in Figure 7.1. Because of the non-isotropic nature of the sensors in this chapter, information is only collected upon approach to the object of interest. Isotropic sensors allow for a prediction curve that can encircle an object of interest.

From analysis of the necessary conditions as well as examination of example cases, several properties of optimal paths with a non-isotropic sensor can be stated.

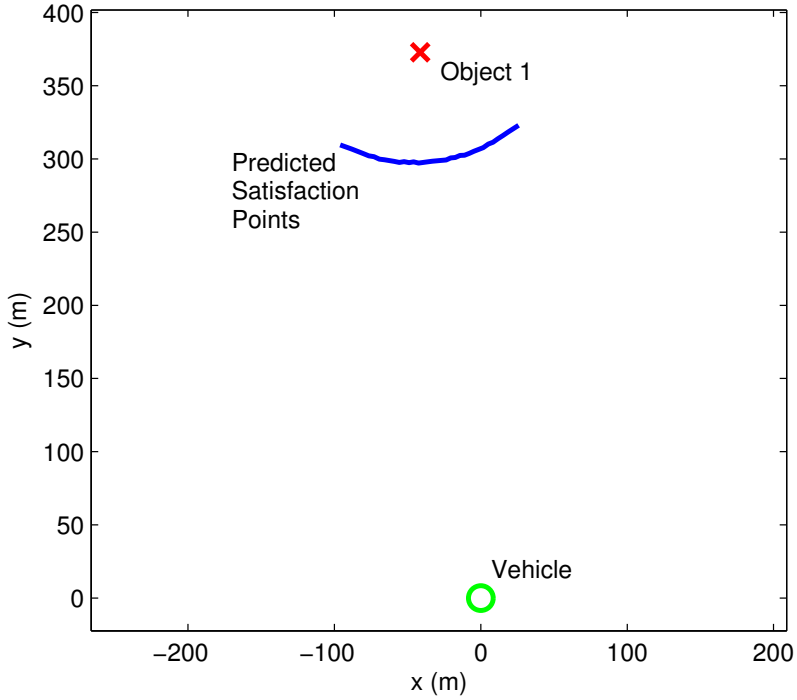

Figure 7.1 Non-Isotropic Information Boundary Condition Satisfaction Prediction

Proposition 7.3.1. *When traveling between several objects of interest, if the objects of interest are isolated, then the optimal flight paths consist of sequences of straight lines (far from the objects of interest) connected by instantaneous turns (near the objects of interest).*

Proposition 7.3.1 is illustrated in Figure 7.4.

Proposition 7.3.2. *When positioned at either endpoint of the prediction curve, the angle between the vehicle's heading and the line of sight to the object of interest will equal half of the width of the sensor cone.*

Proposition 7.3.2 is illustrated in Figure 7.2.

Proposition 7.3.3. *When a line from the vehicle's initial position to the second object of interest passes through the prediction curve, the vehicle will travel straight to the second object of interest and collect more than the specified amount of information from the first*

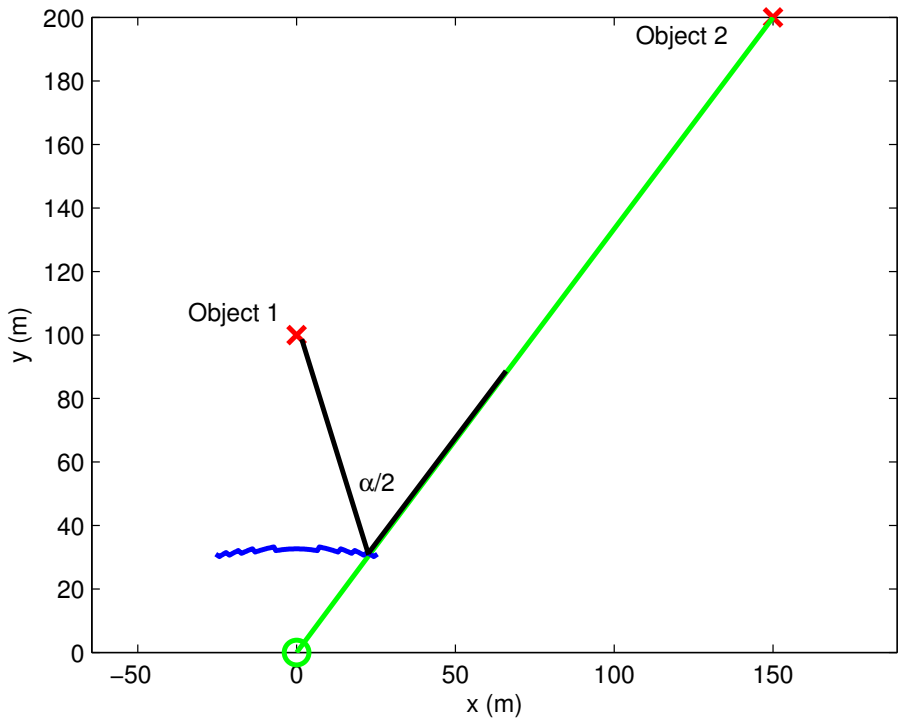

Figure 7.2 Illustration of Proposition 7.3.2 when $\alpha = \frac{2\pi}{3}$

object of interest. When the line travels through the endpoints of the prediction curve, the vehicle will travel straight to the second object of interest and collect exactly the specified amount of information from the first object of interest.

Proposition 7.3.3 is illustrated in Figures 7.5 and 7.6.

Proposition 7.3.4. *If Proposition 7.3.2 does not hold, the vehicle will travel to the a point on the first object of interest's prediction curve closest to the next sequential object of interest and make an instantaneous turn to travel straight to the second object.*

Proposition 7.3.4 is illustrated in Figure 7.4.

These propositions can be utilized to create an algorithm to travel between multiple objects of interest. The key point in satisfying the boundary conditions is to predict the location where constraint satisfaction occurs.

```
Initialization;
Determine next object in sequence;
while Not all objects are identified do
    while θ_Prediction < α do
        Integrate along straight path on ψ_Prediction;
        if Path satisfies boundary conditions then
            Add path to possibilities;
        else
            Ignore path;
        end
        Increment θ_Prediction;
    end
    Determine next object in sequence;
    From possibilities, find closest path to next object;
end
```

Figure 7.3 Method to travel through a sequence of objects of interest

A real-world implementation of this algorithm is more complicated. While in this dissertation we have assumed that information accrues according to (3.7), often this is not the case. Additionally, we have assumed information is received at the maximum rate possible. Implementation is still possible, however, if the prediction curve is continuously updated (at a rate faster than the travel time of the vehicle to the turning point).

Most Automatic Target Recognition (ATR) systems return a value for uncertainty along with a state estimate (for example, a Kalman filter used in this way continuously updates the covariance matrix). While the information rate shown in (3.7) is the maximum value, it does set an upper limit on the distance from the object of interest that the vehicle must travel. By satisfying the boundary conditions set by the true covariance (from the ATR), we can account for the probable nonlinearity of uncertainty reduction. At each timestep, an estimate for the prediction curve is generated based on (3.7). As the vehicle travels, information is collected, uncertainty is reduced and the initial value for information needed is no longer zero but depends upon the remaining uncertainty from the ATR. Thus a feedback loop is formed where the input is the desired uncertainty value, the plant is an estimate

based upon the maximum rate of information achievable and the error is the difference between this maximum and the information actually collected by the ATR.

A better solution would be to use an estimator to examine the true rate of information collection by the ATR and estimate the true value of k_j. This would correct the information model for environmental conditions and give a better prediction of the curve for constraint satisfaction.

It should be noted that this algorithm can be implemented with any sequencing method. This offers the flexibility of improving an optimal TSP type path that visits each object to one that takes advantage of the prediction curve (a generalized TSP problem).

7.3.1 Characteristics of Optimal Paths

An example optimal path between two objects of interest with a vehicle equipped with a non-isotropic sensor is shown in Figure 7.4. Here conditions for Proposition 7.3.4 are satisfied.

Proposition 7.3.3 is illustrated in both figures 7.5 and 7.6.

An implementation of Algorithm 1 is shown in Figure 7.7. The sequence of objects was chosen using a greedy algorithm. Other methods, such as a TSP solver may also be utilized. An optimal solution would need to utilize a Generalized TSP solver or directly solve the necessary conditions.

7.4 Empirical Results

The previously described algorithm using a non-isotropic sensor was implemented in a laboratory setting using a ground-based vehicle equipped with non-isotropic ultrasonic sensors with a total aperture of 12 degrees. The vehicle was tasked with estimating the correct radius of a cylindrical object of interest which was obscured through the use of acoustically translucent material. A second object of interest was used in the path planning process with

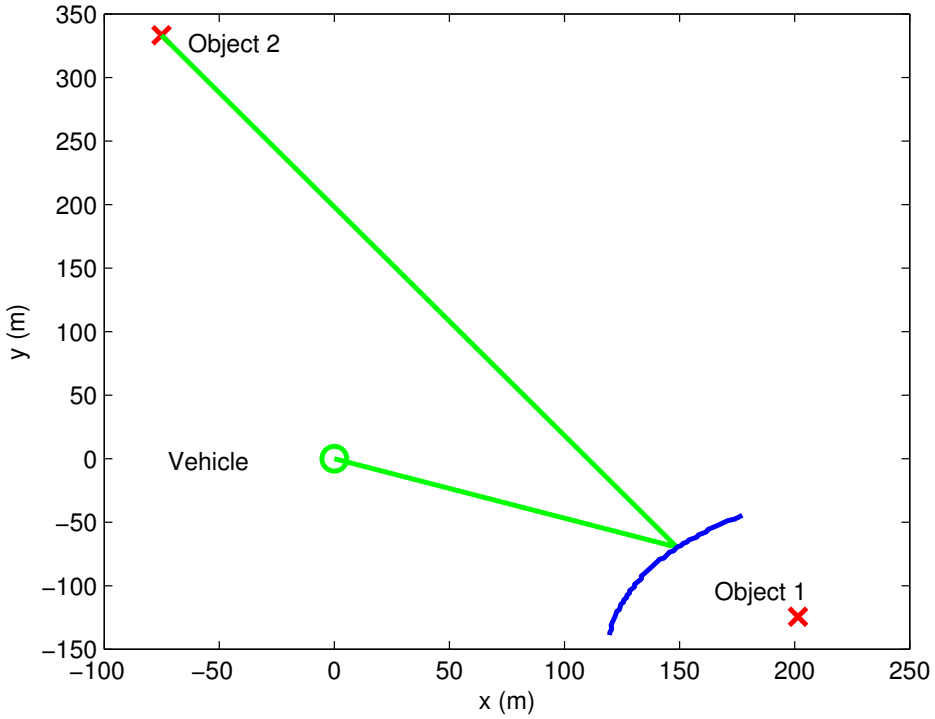

Figure 7.4 Illustration of Proposition 7.3.4

no obscuring material.

The results of this study are presented in Figures 7.8 and 7.9. The vehicle was able to correctly reduce the uncertainty about the radii of the objects of interest without directly visiting the objects of interest. Furthermore, the rate of decay of uncertainty was similar to the inverse of the information collection model used in this dissertation.

7.5 Summary of Exploration with Non-Isotropic Sensors

While the capabilities of the vehicle can decrease the sensor performance, it is still possible to complete exploration mission objectives and collect information about objects of interest, even in the presence of uncertainty. By accounting for the couplings between the components of exploration, we can successfully design, test and deploy optimal exploration agents capable of accounting for trade-offs on all levels of exploration.

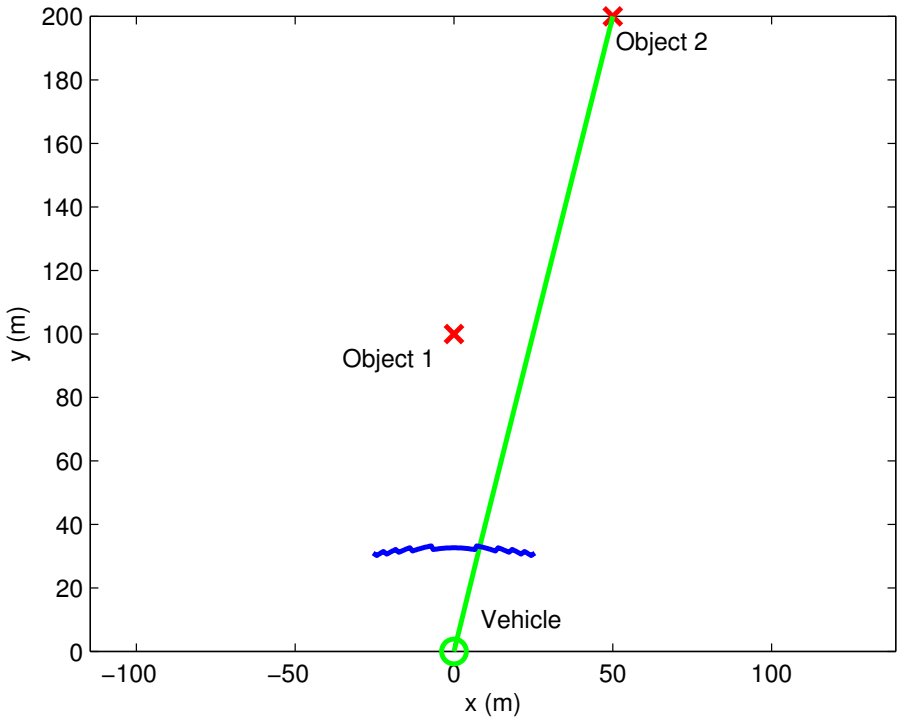

Figure 7.5 Illustration of Proposition 7.3.2 when more than the required amount of information is collected about object one

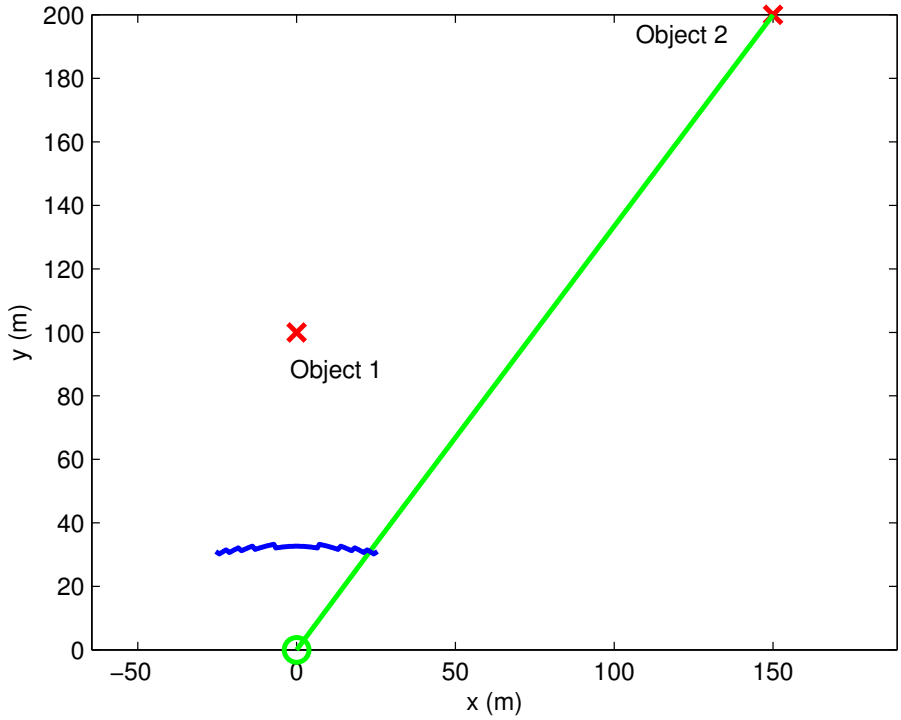

Figure 7.6 Illustration of Proposition 7.3.3 when the boundary condition is exactly satisfied for object one

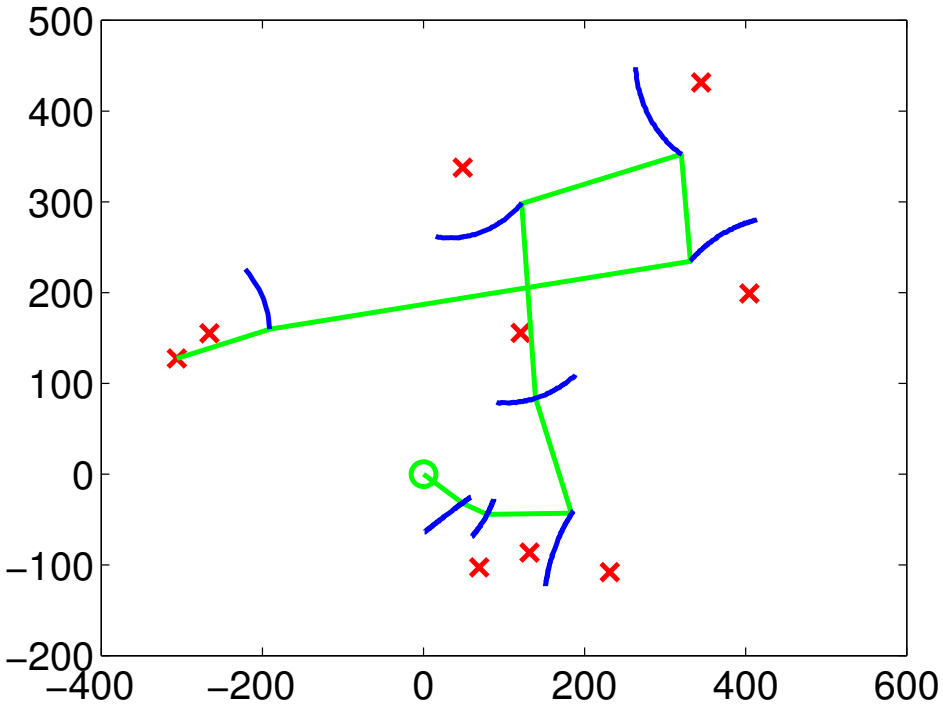

Figure 7.7 Implementation of Algorithm 1. X's are objects of interest, the O is the vehicle, the dashed line is the path and the curves are predicted points of constraint satisfaction.

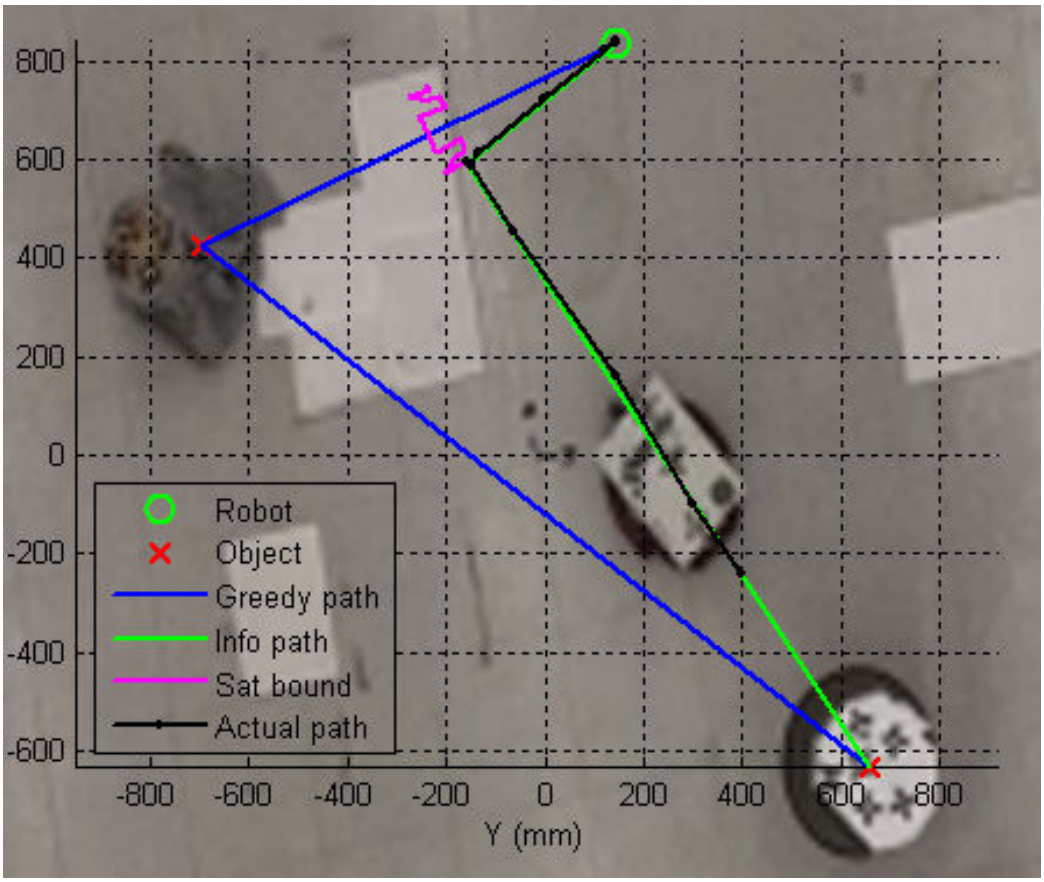

Figure 7.8 A plot of several different paths for the explorer overlaid on the video of the explorer finishing the exploration mission. A clear plot is presented in Figure 7.9

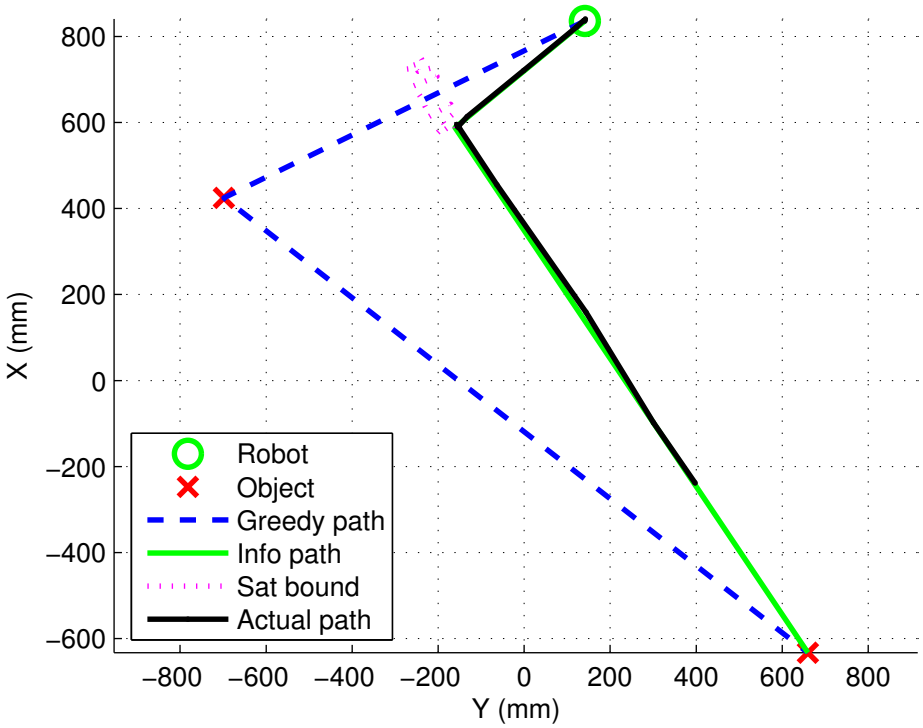

Figure 7.9 A plot of several different paths for the explorer. Shown are the greedy (TSP) path, the predicted, information-optimal, path and the actual ground track of the vehicle. Also shown is the point where 1 bit of information is collected.

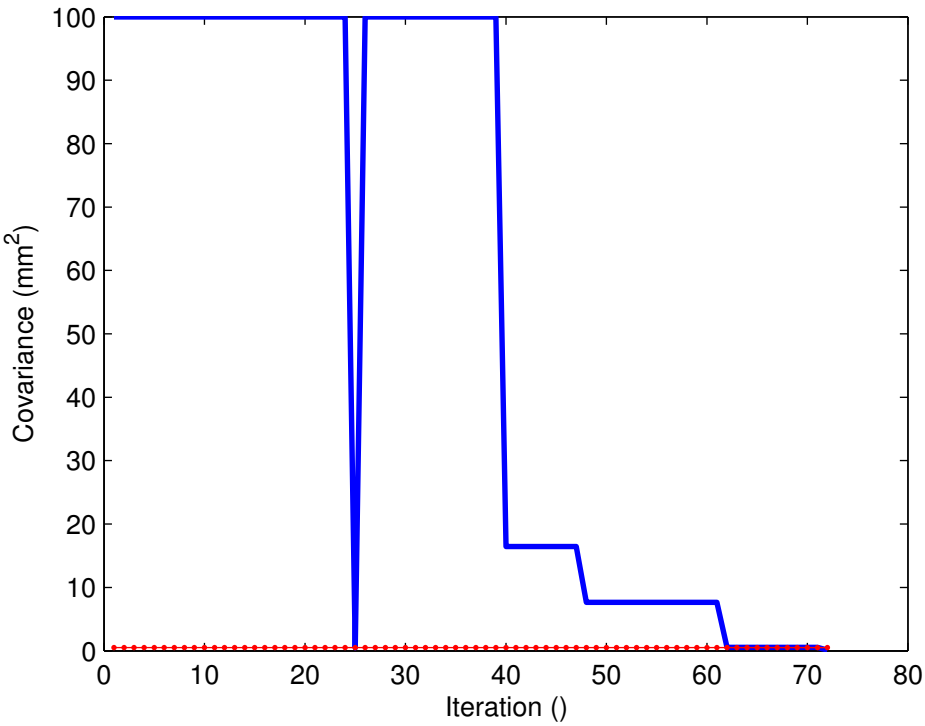

Figure 7.10 A plot of the decay of covariance as a function of iteration. Note that after the covariance is reduced to the appropriate threshold for the first object of interest it is reset for the second object of interest.

Chapter 8

Conclusions

8.1 Summary and Contributions

Today we send autonomous explorers far across the cosmos, deep under the sea and high into the air. These explorers are often limited, by capabilities and by constraints, which makes satisfying mission objectives difficult. Challenges are present in all of the components of exploration: the mission, the path and the agent, and their link to information. When we design any of these components of exploration, we must be cognizant of the trade-offs that exist within them. A priori knowledge with a posteriori knowledge, time with energy and cost with performance. Little work has been done to recognize these trade-offs let alone exploit them to ease the exploration problem.

This dissertation was undertaken to identify properties of optimal exploration missions that recognize and exploit the interactions between the components of exploration. As a motivating example, the specific case of a solar-powered aircraft flying on Mars is considered.

Exploration is formulated as an optimal control problem with the steering decisions of the vehicle serving as the input. Inherent in the problem is the recognition of existing parallels between communication and exploration. Specifically, an agent may collect information in a manner similar to that of a communication receiver, but has the additional benefit of mobility. This mobility allows the agent to choose a path that is optimally

informative. The full model presented combines kinematics, informatics, estimation and energetics to form an integrated system from which the properties of exploration can be distilled.

This work first examines time-optimal exploration paths where the mission objective, to collect information about objects of interest, is expressed as inequality boundary conditions. Several regimes of flight are identified, including the preference to fly straight while objects of interest are not visible and to gently turn when they are visible. Heuristics are presented that take advantage of these properties to improve path planning in the cases of isolated and clustered objects. Furthermore, a connection is drawn between the Generalized Traveling Salesman Problem and time-optimal exploration, allowing a large literature to be leveraged to find time-optimal flight paths.

Time, however, is not the only cost of an optimal exploration mission. Real-world vehicles require energy to travel, and, to emphasize this point, we analyze path planning for a solar-powered aircraft. Several regimes of flight are identified, each of which has different energy-optimal path characteristics.

Though individual properties for time-optimal and energy-optimal paths are presented, we are interested in an exploration mission that requires a combination of the total energy at the end of the mission and the mission duration to be optimized. Through simulation and analysis, general properties of path planning for exploration are derived.

Finally, constraints upon the agent are considered within the context of the exploration problem. Paths are planned for a vehicle with an onboard non-isotropic sensor. A heuristic algorithm, based upon properties derived from simulation examples, is presented that allows for path planning even in the presence of many objects and uncertainty. This algorithm is implemented empirically with a single exploration agent.

8.2 Conclusions

The challenges of exploration are inextricably linked to the interactions of its components, but these challenges can be mitigated through an understanding of the trade-offs. In this dissertation, we provide a new, coupled model for exploration systems. By concentrating on information collection rather than classification, we have decoupled the problem of exploration from that of detection.

Throughout this work, we have considered several optimal path planning problems. We have shown that when flying in a time-optimal manner, an aircraft should fly straight when far from the objects of interest and gently turn when close. The sequence of objects to be visited can be determined through the use of a GTSP heuristic and a sample is provided.

When using solar-powered aircraft, the Power Ratio, a non-dimensional parameter that can be computed at design time, is shown to correctly predict the regime of optimal flight. The Power Ratio is also shown to be important in evaluating the ability of a solar-powered aircraft to fly perpetually. If the Power Ratio is larger than the so-called Perpetuity Threshold, perpetual flight is possible. Both the Power Ratio and Perpetuity Threshold were previously undefined.

Most exploration missions require both energy and time to be optimized. We have found that an exploration vehicle should fly along straight paths no matter what the regime of flight. In fact, a study of this problem reveals time is a driver for exploration missions while energy is not.

Extended endurance flight requires a Power Ratio that is greater than one, or that more energy be collected than lost over the course of the mission. This requirement can be used to specify the capabilities of the vehicle and its payload. Even with degraded capabilities, we empirically show an exploration agent successfully completing a mission in an optimal manner. Specifically we have found properties of flight when using a non-isotropic sensor.

8.3 Future Work

In this work, we have treated information as a measure of uncertainty in knowledge of the state and the rate of information collection as a channel capacity. We have also decoupled exploration and classification (in this work we considered information collection rather than classification). Additional work should be completed to develop flight paths that take the stochastic nature of information into account, for instance, treating the problem in a Bayesian manner. An understanding must also be provided of the additive nature of information, most likely through the use of Fisher's definition.

Furthermore, we assume an object of interest transmits the same information at all relative azimuths, i.e., each object of interest is an isotropic transmitter. Typically this assumption does not hold. One method to address this issue is to consider non-isotropic objects of interest rather than only non-isotropic sensors. In this dissertation, we define a non-isotropic sensor that has a sensitivity that depends on the location of the object of interest relative to that of the vehicle. Many other types of sensors exist and further analysis should be completed to examine properties of optimal exploration paths when these sensors are utilized.

Efforts should continue to develop and analyze solar-powered aircraft. Due to their short history, their capabilities are only now being realized in the form of several advanced programs at the government, academic and industry levels. In this dissertation, we consider solar-powered aircraft in level flight. Further work should continue to examine solar-powered aircraft capable of non-level flight and accelerated flight. As the Power Ratio has proven to be useful in determining many capabilities of these vehicles, additional studies should be undertaken to investigate its relevance (or perhaps that of an equivalent parameter) in non-level and accelerated flight.

This work is naturally extensible to cooperative exploration systems. Indeed, distributed explorers can ease the difficulty of exploration. The exploration area may be divided between cooperative vehicles, or vehicles can collaborate, in which case knowledge

is shared. However, considerations must be given to the type of multi-vehicle interactions that occur. These interactions require a deeper understanding of the nature of information and its relationship to state estimation. For instance, cooperative exploration can be viewed as a distributed sensing problem within which the sensors choose paths that are informative in the global sense though perhaps not locally.

Preliminary work shows that the basic properties discovered in this dissertation are also present in the cooperative exploration case. Thus, further extensions of this work include empirical studies to expand upon the exploration problem and to identify additional constraints and components that affect cooperative exploration. It is expected that these cooperative explorers will be useful for both civilian and military endeavors. Indeed, the US Air Force is now interested in increasing the uses for unmanned vehicles by 2010 (61) including usage of multiple heterogenous vehicles. NASA too employs collaborative exploration techniques in the tasking of its Martian satellites (50) to find areas of interest for the Mars Exploration Rovers.

Finally, it should be noted that exploration problems are and will continue to be prevalent in the foreseeable future. Human existence is characterized by curiosity and exploration missions often provide fundamental results that improve (or dictate) basic scientific understanding. Here on Earth, many exploration missions still exist in a variety of challenging environments, but exploration should continue beyond Earth as well. This dissertation used an example of a solar-powered aircraft exploring Mars. While this mission is not yet feasible, it requires only human ingenuity and political will to complete. But this is only one of many places yet to be explored. Asteroids, moons, planets and deep space all lack even a fundamental understanding of their characteristics. This dissertation has laid some basic groundwork for enhancing exploration missions. It is hoped that these missions will occur and that, someday, the agents are no longer autonomous, but that it is humans, who, once more, explore the unknown.

Appendices

Appendix A

Optimal Control

Optimal control problems can take on many forms. The one considered here involves a general n-order dynamic system with n-dimensional state $x(t)$ (components $x_i(t), i = 1,...,n$) and an m dimensional control function $u(t)$, that for $0 \leq t \leq t_f$, satisfy the conditions

$$\dot{x}(t) = f(x(t), u(t)), \tag{A.1}$$

$$u(t) \in \Omega \subset \Re^m, \tag{A.2}$$

$$x(0) = x_0, x_i(t_f) = x_{if}, i \in I \subset \{1,...,n\}. \tag{A.3}$$

Here, Ω is the constraint set for the control function, x_o is a specified initial state, and $x_{if}, i \in I$ are specified values of the terminal state (for $i \notin I$ the values of $x_i(t_f)$ are unconstrained or "free"). Subject to conditions (A.1) - (A.3) the objective is to find $u(t)$ such that a cost

$$J = \int_0^{t_f} C(x(t), u(t))dt, \tag{A.4}$$

is minimized over a suitable class of $u(t)$ (for example, $u(t)$ is piecewise continuous). The functions $f(x,u)$ and $C(x,u)$ are smooth (at least continuously differentiable).

Suppose an optimal control $u^*(t)$ exists and $x^*(t)$ is the corresponding solution of (A.1)-

(A.3) with $x^*(t) = x(t)$ and $u^*(t) = u(t)$. Then the pair $(x^*(t), u^*(t))$ satisfies a set of necessary conditions. See, for example, (27) and (80). For optimal control problem (A.1) - (A.4), the conditions take the form of a two-point boundary value problem (TPBVP) of order $2n$ with n conditions at $t = 0$ and n conditions at $t = t_f$. The conditions are stated elegantly in terms of a so-called Hamiltonian function:

$$H(x,u,\lambda) = C(x,u) + \sum_{i=1}^{n} \lambda_i f_i(x,u), \tag{A.5}$$

$$x \in \Re^n, u \in \Re^m, \lambda \in \Re^n \tag{A.6}$$

Specifically $\lambda^*(t)$ exists such that the following conditions are satisfied for $0 \leq t \leq t_f$ and $i = 1, ..., n$:

$$\dot{x}_o^*(t) = f_i(x^*(t)u^*(t)\lambda(t)) = \frac{\partial H}{\partial \lambda i}(x^*(t), u^*(t), \lambda(t)), \tag{A.7}$$

$$\dot{\lambda}_i^*(t) = -\sum_{j=1}^{n} \lambda_j(t) \frac{\partial f_j}{\partial x_j}(x^*(t), u^*(t)) - \frac{\partial C}{\partial x_i}(x^*(t), u^*(t)) = -\frac{\partial H}{\partial x_i}(x^*(t), u^*(t), \lambda(t)), \tag{A.8}$$

$$\text{conditions (A.3) are satisfied, } \lambda_i(t_f) = 0 \text{ for } i \notin I, \tag{A.9}$$

$$u^*(t) = \arg\min_{v \in \Omega} H(x^*(t), v, \lambda^*(t)), \tag{A.10}$$

$$\text{if } t_f \text{ is free } H(x^*(t_f), u^*(t_f), \lambda^*(t_f)) = 0. \tag{A.11}$$

In summary, the TPBVP consists of the equations of motion (A.7), the costate equations (A.8), the split boundary conditions (A.9), the minimum principle (A.10) and a special condition (A.11) that applies to the Hamiltonian when t_f is free. It is possible in rare situations that (A.7) - (A.11) are satisfied with $C(x,y)$ deleted.

When $\Omega = \Re^m$ the minimum principle implies

$$\frac{\partial H}{\partial u}(x^*(t), u^*(t), \lambda(t)) = 0, \tag{A.12}$$

$$\frac{\partial^2 H}{\partial u^2}(x^*(t), u^*(t), \lambda(t) \geq 0. \tag{A.13}$$

Here $\frac{\partial H}{\partial u}$ and $\frac{\partial^2 H}{\partial u^2}$ are respectively the gradient vector and Hessian matrix of H with respect to u. Expressions (A.12) can replace (A.10) in the TPBVP, but then the TPBVP is a weaker set of necessary conditions than (A.7) - (A.11).

Appendix B

Discretization Procedure

To obtain numerical approximations of optimal paths, we discretize the optimal control problem as follows. For a chosen integer $n \geq 1$, we subdivide the interval $[t_o, t_f]$ into n subintervals $[t_o, t_1], [t_1, t_2], ..., [t_{n-1}, t_f]$ of equal duration. In each subinterval we assume that the control input is constant, i.e., $(\phi(t), V(t)) = (\phi_j, V_j), t \in [t_j, t_{j+1}]$, where the parameters $(\phi_j, V_j), 0 \leq j \leq n-1$, are unknown.

We treat the parameters (ϕ_j, V_j), $0 \leq j \leq n-1$, and t_f as inputs to a nonlinear optimization problem. As an initial choice, in all subintervals we choose $\phi_j = 0$, $V_j = V_{Power_{min}}$ and $t_f = t_o + T_M$. Constraints upon this problem are imposed from the boundary conditions in the optimal control problem. The objective function is the given by the specific problem formulation. We then numerically solve for optimal flight paths using the MATLAB® Optimization Toolbox function *fmincon* and the ordinary differential equation solver *ode45*.

Appendix C

Proofs of Propositions 5.5.1 and 5.5.2

Propositions 5.5.1 and 5.5.2 were inferred from observed characteristics of numerical approximations of optimal flight paths. We will now prove them through application of the necessary conditions (5.3)-(5.11), using Experimental Fact 5.4.1.

C.1 Proof of Proposition 5.5.1

We first assume that $\phi(t) = 0$, simplify the necessary conditions and solve for the states and costates subject to the constraints (5.15)-(5.21). This results in:

$$\phi = 0, \tag{C.1}$$

$$V = V_{Energy_{min}}, \tag{C.2}$$

$$\psi = \arctan(\frac{y_f - y_o}{x_f - x_o}), \tag{C.3}$$

$$t_f = \frac{x_f - x_o}{\cos\psi V} = \frac{y_f - y_o}{\sin\psi V}, \tag{C.4}$$

$$\lambda_x = 0, \tag{C.5}$$

$$\lambda_y = 0, \tag{C.6}$$

$$\lambda_\psi = \frac{V\eta_{sol}P_{sd}S\cos(e)\sin(\tilde{a} - \psi)}{g}, \tag{C.7}$$

where each of the costates is constant. Here, both V and ψ remain constant at their initial values. A derivation of (C.1)-(C.7) is provided in Appendix D. The flight duration depends on the distance to the final destination and the velocity.

It is shown in Appendix D that the flight conditions (C.1)-(C.7) satisfy the second order condition for optimality. Since $\phi = 0$ yields a path that satisfies the necessary conditions for optimal flight, we have proven Proposition 1.

C.2 Proof of Proposition 5.5.2

Since $E_{Total} > 0$, the optimal path must satisfy $E_{in} - E_{out} > 0$. From Experimental Fact 1, this yields $P_{in} - P_{out} > 0$. For E_{Total} large enough, $P_{in} - P_{out}$ will be large enough to be the dominant term in the right hand side of (5.2). Therefore, $H > 0$ when $P_R > 1$ and large enough.

From Appendix A we may express the transversality conditions as:

$$[\lambda^T \delta x - H \delta t]_{t_o}^{t_f} = 0, \tag{C.8}$$

or, when focusing on the variation of the final time,

$$H(t_f)\delta t_f = 0. \tag{C.9}$$

Since $H > 0$, $\delta t_f = 0$ which implies that the final time is fixed. Therefore $t_f = t_o + T_M$, which proves the first claim.

We must now examine the velocity of the aircraft when $E_{Total} > 0$. Consider an extremal path that satisfies boundary conditions (5.15)-(5.21) with $V > V_{Power_{min}}$. If this same path is flown with $V = V_{Power_{min}}$, E_{Total} will be higher than with $V > V_{Power_{min}}$. Since velocity is constrained to be greater than or equal to $V_{Power_{min}}$, a maximum E_{Total} occurs when $V = V_{Power_{min}}$. Thus $V = V_{Power_{min}}$ is optimal and we have proven the second claim and

Proposition 5.5.2.

Appendix D

Derivation of Drag Regime First Order Necessary Conditions

D.1 Satisfaction of the Drag Regime First Order Necessary Conditions

The first order necessary conditions, evaluated at $\phi = 0$, are:

$$\frac{\partial H}{\partial \phi} = -\eta_{sol} P_{sd} S_c \cos(e) \sin(\tilde{a} - \psi) + \frac{g\lambda_\psi}{V} = 0, \tag{D.1}$$

$$\frac{\partial H}{\partial V} = \lambda_x \cos(\psi) + \frac{8KW^2}{\eta_{prop}\rho SV^2} - \frac{3\rho SV^2(C_{D_o} + \frac{4KW^2}{\rho^2 S^2 V^4})}{2\eta_{prop}} + \lambda_y \sin(\psi) = 0, \tag{D.2}$$

$$\dot{x} = \frac{\partial H}{\partial \lambda_x} = V\cos(\psi), \tag{D.3}$$

$$\dot{y} = \frac{\partial H}{\partial \lambda_y} = V\sin(\psi), \tag{D.4}$$

$$\dot{\psi} = \frac{\partial H}{\partial \lambda_\psi} = 0, \tag{D.5}$$

$$\dot{\lambda_x} = \frac{-\partial H}{\partial x} = 0, \tag{D.6}$$

$$\dot{\lambda_y} = \frac{-\partial H}{\partial y} = 0, \tag{D.7}$$

$$\dot{\lambda_\psi} = \frac{-\partial H}{\partial \psi} = -\lambda_y V\cos\psi + \lambda_x V\sin\psi. \tag{D.8}$$

Since $\dot{\lambda_x}$, $\dot{\lambda_y}$, and $\dot{\psi}$ are all zero, λ_x, λ_y and ψ are all constants. Equation (D.2) becomes a function of constant parameters and V. From this we can see that V must be constant as well. Similarly, (D.1) is now a function of constant parameters and λ_ψ. Accordingly, λ_ψ must also be constant, and:

$$\dot{\lambda_\psi} = -\lambda_y V \cos\psi + \lambda_x V \sin\psi = 0. \tag{D.9}$$

Now (D.1) yields:

$$\lambda_\psi = \frac{\eta_{sol} P_{sd} V S \cos(e) \sin(\tilde{a} - \psi)}{g}. \tag{D.10}$$

We can now solve for λ_x and λ_y using (D.2) and (D.9) as:

$$\lambda_x = -\frac{(-4KW^2 + 3C_{D_O}\rho^2 S^2 V^4)\cos\psi}{2\eta_{prop}\rho S V^2}, \tag{D.11}$$

$$\lambda_y = \frac{(-4KW^2 + 3C_{D_O}\rho^2 S^2 V^4)\sin\psi}{2\eta_{prop}\rho S V^2}. \tag{D.12}$$

which are on average small evaluated with typical aircraft parameters.

Consider a straight and level flight path from point A to point B. If P_{in} is small, the total energy during this flight is:

$$E_{Total} = P_{out}\Delta t, \tag{D.13}$$

where Δt is the duration of the flight. Since a destination is given, Δt can be rewritten as d/V where d is the distance between point A and point B. Hence the minimum energy velocity is:

$$V_{Energy_{min}} = \sqrt[4]{\frac{4KW^2}{C_{D_o}\rho^2 S^2 \cos^2(\phi)}} = 1.31 V_{Power_{min}}, \tag{D.14}$$

which is also the velocity at which the aircraft is most aerodynamically efficient.

D.2 Satisfaction of the Drag Regime Second Order Condition

The second order condition is:

$$\frac{\partial^2 H}{\partial \phi^2} \leq 0, \tag{D.15}$$

where, if

$$\frac{\partial^2 H}{\partial \phi^2} = \begin{bmatrix} \alpha & \beta \\ \beta & \gamma \end{bmatrix}, \tag{D.16}$$

$$\begin{aligned}
\alpha &= \frac{\eta_{prop}\eta_{sol}\rho P_{sd} S^2 V(-(\cos(\phi)\sin(e)) + \cos(e)\sin(\tilde{a}-\psi)\sin(\phi))}{\eta_{prop}\rho SV} \\
&\quad + \frac{-4KW^2\sec(\phi)^4 + 2\sec(\phi)^3(g\lambda_\psi \eta_{prop}\rho S\cos(\phi) - 4KW^2\sin(\phi))\tan(\phi)}{\eta_{prop}\rho SV}, \\
\beta &= -\frac{g\lambda_\psi \sec(\phi)^2}{V^2} + \frac{4KW^2\sec(\phi)^2\tan(\phi)}{\eta_{prop}\rho SV^2}, \\
\gamma &= \frac{8KW^2\sec(\phi)^2}{\eta_{prop}\rho SV^3} - \frac{3\rho SV(C_{D_o} + \frac{4KW^2\sec(\phi)^2}{\rho^2 S^2 V^4})}{\eta_{prop}} + \frac{2g\lambda_\psi\tan(\phi)}{V^3}.
\end{aligned}$$

To check that the second order condition is satisfied, we show that the left hand side of (D.15) is negative definite. This holds by Sylvester's Criterion, if, and only if, the determinant of the first nested principal minor of (D.16) is negative and the determinant of (D.16) is positive.

We will begin with the first nested principal minor as

$$\frac{\eta_{prop}\eta_{sol}\rho P_{sd}S^2V(-(\cos(\phi)\sin(e))+\cos(e)\sin(\tilde{a}-\psi)\sin(\phi))}{\eta_{prop}\rho SV}$$
$$+\frac{-4KW^2\sec(\phi)^4+2\sec(\phi)^3(g\lambda_\psi\eta_{prop}\rho S\cos(\phi)-4KW^2\sin(\phi))\tan(\phi)}{\eta_{prop}\rho SV}. \quad \text{(D.17)}$$

By simplifying and assuming $\phi = 0$ according to Proposition 1, we obtain,

$$-4KW^2-\eta_{prop}\eta_{sol}\rho P_{sd}S^2V\sin(e), \quad \text{(D.18)}$$

which is always negative, and the first criterion is satisfied.

We must next examine the determinant of (D.16) which, if $\phi = 0$, reduces to

$$(-g^2\lambda_\psi\eta_{prop}^2\rho^2S^2+16K^2W^4+12C_{D_o}K\rho^2S^2V^4W^2+3C_{D_o}\eta_{prop}\eta_{sol}\rho^2P_{sd}S^4V^5\sin(e)$$
$$+4K\eta_{prop}\eta_{sol}\rho P_{sd}S^2VW^2\sin(e))/V^4. \quad \text{(D.19)}$$

In (D.19), we substitute expression (D.10) for λ_ψ to obtain

$$(A+D)(3C+D)-B^2, \quad \text{(D.20)}$$

where

$$A = VP_{sd}\rho S^2\eta_{prop}\eta_{sol}\sin(e), \quad \text{(D.21)}$$
$$B = VP_{sd}\rho S^2\eta_{prop}\eta_{sol}\cos(e)\sin(\tilde{a}-\psi), \quad \text{(D.22)}$$
$$C = C_{D_o}\rho^2S^2V^4, \quad \text{(D.23)}$$
$$D = 4KW^2. \quad \text{(D.24)}$$

If P_{sd} is small enough, then expression (D.20) is positive, which completes the proof.

Appendix E

Energy-Optimal Flight Paths with Free Destination

The purpose of this section is to show that $\phi = 0$ yields paths that are extremal (i.e., satisfy the first and second order conditions for optimality) with respect to the problem of energy-optimal flight with free destination.

If $\phi = 0$, the state equations become:

$$\dot{x} = \frac{\partial H}{\partial \lambda_x} = V\cos(\psi), \tag{E.1}$$

$$\dot{y} = \frac{\partial H}{\partial \lambda_y} = V\sin(\psi), \tag{E.2}$$

$$\dot{\psi} = \frac{\partial H}{\partial \lambda_\psi} = 0, \tag{E.3}$$

showing that the heading is constant.

The first two costate equations are:

$$\dot{\lambda_x} = \frac{-\partial H}{\partial x} = 0, \tag{E.4}$$

$$\dot{\lambda_y} = \frac{-\partial H}{\partial y} = 0, \tag{E.5}$$

which, combined with the boundary conditions (5.15)-(5.21) show that $\lambda_x = \lambda_y \equiv 0$. This

simplifies the last costate equation as:

$$\dot{\lambda_\psi} = \frac{-\partial H}{\partial \psi} = 0, \tag{E.6}$$

which, combined with the boundary conditions (5.15)-(5.21) shows that $\lambda_\phi \equiv 0$.

After the above simplifications, (5.9) reduces to:

$$\frac{\partial H}{\partial \phi} = -\eta_{sol} P_{sd} S_c \cos(e) \sin(\tilde{a} - \psi) = 0, \tag{E.7}$$

which is satisfied by letting $\psi = a$, i.e., by letting the aircraft head in the direction of the star.

Similarly, (5.10) reduces to:

$$\frac{\partial H}{\partial V} = \frac{8KW^2}{\eta_{prop}\rho SV^2} - \frac{3\rho SV^2(C_{D_o} + \frac{4KW^2}{\rho^2 S^2 V^4})}{2\eta_{prop}} = 0. \tag{E.8}$$

which is only satisfied if $V = V_{Power_{min}}$.

The second order condition reduces to:

$$\frac{\partial^2 H}{\partial(\phi, V)^2} \leq 0, \tag{E.9}$$

where, if

$$\frac{\partial^2 H}{\partial(\phi, V)^2} = \begin{bmatrix} H_{\phi\phi} & H_{\phi V} \\ H_{\phi V} & H_{VV} \end{bmatrix}, \tag{E.10}$$

(E.11)

$$H_{\phi\phi} = \frac{\eta_{prop}\eta_{sol}\rho P_{sd} S^2 V(-\sin(e))}{\eta_{prop}\rho SV} + \frac{-4KW^2}{\eta_{prop}\rho SV}, \tag{E.12}$$

$$H_{\phi V} = 0, \tag{E.13}$$

$$H_{VV} = \frac{8KW^2}{\eta_{prop}\rho SV^3} - \frac{3\rho SV(C_{D_o} + \frac{4KW^2}{\rho^2 S^2 V^4})}{\eta_{prop}}. \tag{E.14}$$

$$\tag{E.15}$$

It is easily checked that choosing $\phi = 0$ and $V = V_{Power_{min}}$ yields $H_{\phi\phi} < 0$ and $H_{\phi\phi}H_{VV} > 0$, implying that the second order condition is satisfied.

In summary, choosing $\phi = 0$, $\psi = a$ and $V = V_{Power_{min}}$ yields a path that satisfies the first and second order conditions for optimality for the problem of energy-optimal flight with free destination.

Appendix F

Aircraft Model Parameters

F.1 The *Metis* Aircraft

The aircraft model used in all simulations and numerical results in this paper were developed by the University of Michigan SolarBubbles Team (70), (24), and (29). Aerodynamic coefficients were evaluated through the use of Athena Vortex Lattice and Fluent and verified experimentally through full size wind tunnel testing(24).

The flying wing aircraft, pictured in Figure F.1, has the characteristics listed in Table F.1.

Table F.1 Aircraft Model Parameters

Wing Area	S	0.1566	m^2
Mass	m	1.2	kg
Wingspan	b	0.711	m
Oswald Efficiency Factor	ε	0.992	
Parasitic Drag	C_{D_o}	0.011	
Propeller Efficiency	η_{prop}	0.7	
Air Density	ρ	1.29	kg/m^3

F.2 The *Hui* Aircraft

The glider aircraft, pictured in Figure F.2, *Hui*, has the characteristics listed in Table F.2.

Figure F.1 Wind Tunnel Aircraft Model

Table F.2 Hui Model Parameters

Wing Area	S	1.25	m^2	Ref. (24)
Mass	m	1.95	kg	Ref. (24)
Wingspan	b	3.01	m	Ref. (24)
Oswald Eff. Factor	ε	0.9139		Ref. (24)
Parasitic Drag	C_{D_o}	0.0065		Ref. (24)
Propeller Eff.	η_{prop}	0.7		(est)

F.3 The *Gossamer Penguin*

The *Gossamer Penguin* was developed by AeroVironment in 1979 as a manned solar-powered aircraft. Approximate aerodynamic coefficients as found in Refs (85) and (105) are listed in Table F.3 and the aircraft is pictured in Figure F.3.

Figure F.2 The Huitzilopochtli Aircraft

Table F.3 Gossamer Penguin Model Parameters

Wing Area	S	30.85	m^2	Ref. (85)
Mass	m	67.13	kg	Ref. (105)
Wingspan	b	21.6	m	Ref. (105)
Oswald Eff. Factor	ε	0.94		(est)
Parasitic Drag	C_{D_o}	0.01		(est)
Propeller Eff.	η_{prop}	0.7		(est)

Figure F.3 The Gossamer Penguin

Appendix G

Aircraft Design with the Power Ratio

As proven previously, the Power Ratio provides a metric for evaluating the regime of optimal flight for a solar-powered aircraft as well as its ability to maintain perpetual flight. Here we evaluate how characteristics of the aircraft and the environment affect the Power Ratio. To maintain perpetual flight, the value of the Power Ratio must exceed the inverse of the daylight duty cycle. Hence, requirements on the Power Ratio drive vehicle mass (as is shown in the derivation to follow). This mass constraint influences the computational and payload capacity of the aircraft.

G.1 Comparatison of the Power Ratios on Earth and Mars

The Power Ratio, (5.23), can be rewritten as

$$P_R = \left[0.402 P_{sd} \eta_{sol} \sin(e) \sqrt{\rho} g^{\frac{2}{3}}\right] \left[\sqrt[4]{\frac{\eta_{prop}^4 b^6 \varepsilon^3 \pi^3 S^3}{C_{D_o} m^6}}\right], \tag{G.1}$$

highlighting the separate roles of environmental and aircraft parameters, respectively. Furthermore, if a constant loading and thickness are assumed across the wing planform, we can set $m = \rho_w S$ where ρ_w is the mass per unit area of the wing using $AR = b^2/S$. This

simplifies (G.1) as

$$P_R = \left[0.402 P_{sd} \eta_{sol} \sin(e) \sqrt{\rho} g^{\frac{2}{3}}\right] \left[\sqrt[4]{\frac{\eta_{prop}^4 \varepsilon^3 \pi^3 AR^3}{C_{D_o} \rho_w^6}}\right], \tag{G.2}$$

which indicates that to increase the Power Ratio, a low wing density and high aspect ratio should be used. To-date, all successful solar-powered aircraft have low wing density and high aspect ratio (18). The second term in the right hand side of (G.2) elucidates why this is so.

To compare the power ratios of a given aircraft on Earth and Mars, rewrite (G.2) as

$$P_R = 0.402 \eta_{sol} \sin(e) \sqrt[4]{\frac{\eta_{prop}^4 \varepsilon^3 \pi^3 AR^3}{\rho_w^6}} \left(\frac{P_{sd} \sqrt{\rho}}{g^{\frac{3}{2}} \sqrt[4]{C_{D_o}}}\right), \tag{G.3}$$

where P_{sd}, ρ, g and C_{D_o} are all determined by the planet. Note that C_{D_o} depends on the Reynolds number of the aircraft, which itself depends upon viscosity and atmospheric density. The contributions of P_{sd}, ρ, g and C_{D_o} to the Power Ratio (G.3) are summarized in the term

$$\frac{P_{sd} \sqrt{\rho}}{g^{\frac{3}{2}} \sqrt[4]{C_{D_o}}}, \tag{G.4}$$

whose values on Earth and Mars can be compared. Table G.1 compares the constant environmental parameters, P_{sd}, ρ and g, on Earth and Mars.

Table G.1 Environmental Parameters on Earth and Mars

	Earth	Mars	
P_{sd}	1,353	589	W/m^2
g	9.86	3.71	m/sec^2
ρ	1.29	0.015	kg/m^3
$\frac{P_{sd}\sqrt{\rho}}{g^{\frac{3}{2}}}$	49.63	10.10	$(\frac{kg}{m^3})^{\frac{3}{2}}$

Note that the quantity $\frac{P_{sd}\sqrt{\rho}}{g^{\frac{3}{2}}}$ is 4.9 times larger on Earth than on Mars. Reference (94) also compares solar-powered flight on Earth and Mars and reaches a similar conclusion, but

without accounting for parasitic drag. We must indeed consider C_{D_o} in (G.4). Since C_{D_o} depends upon velocity, atmospheric density and viscosity, a comparison of its values on Earth and Mars is not straightforward. Figure G.1 illustrates this comparison over a range of speeds. Note that C_{D_o} is always smaller for Earth than for Mars.

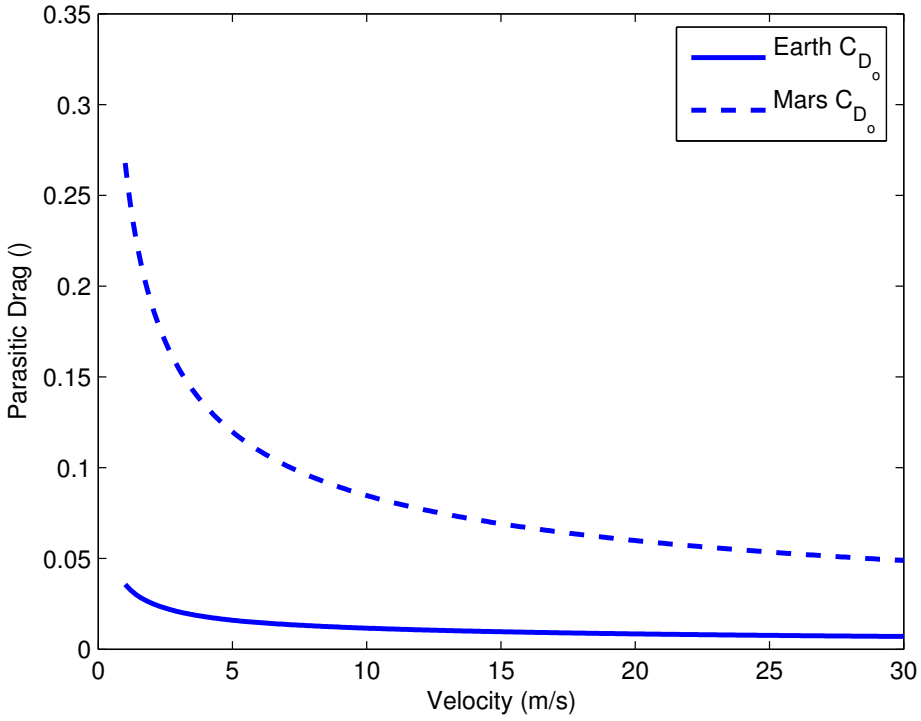

Figure G.1 Comparison of C_{D_o} on Earth and on Mars

With Figure G.1 we can compute the P_{out} as a function of velocity for both Earth and Mars as in Figure G.2.

Combining the results of Table G.1 and Figure G.1 leads to the following conclusion: *The Power Ratio of an aircraft on Earth is always at least 4.9 times larger than the Power Ratio of the same aircraft on Mars.*

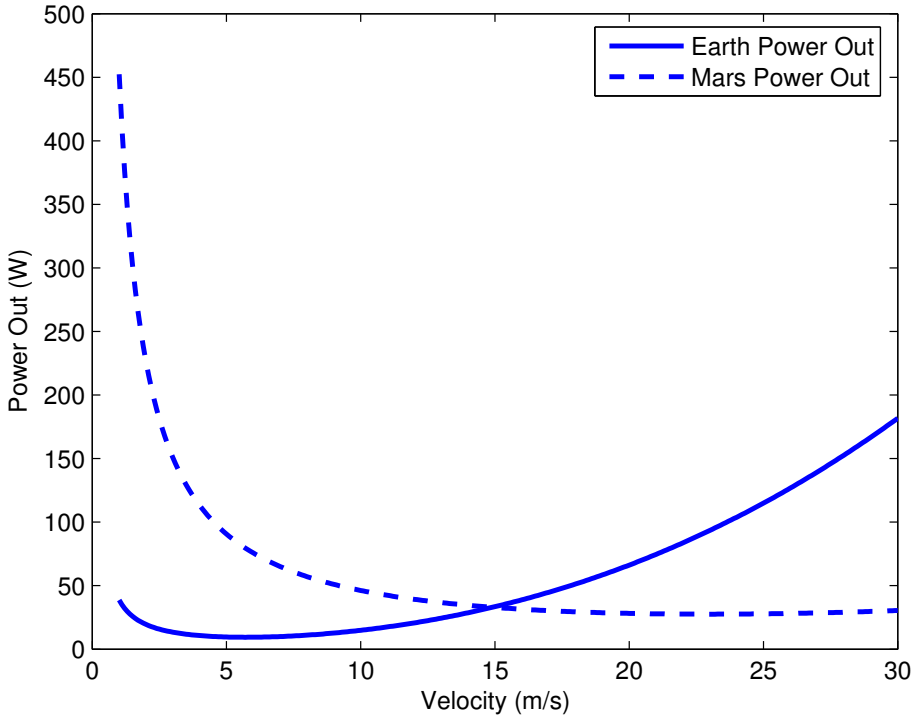

Figure G.2 Comparison of P_{out} on Earth and on Mars

G.2 Comparison of Requirements for Perpetual Endurance on Earth and Mars

The results of these sections allow us to make the following general statement:

For a given latitude and time of year, it is always easier to design an aircraft to fly perpetually on Earth than on Mars.

Several items contribute to this statement:

- The Perpetuity Thresholds for a given date and latitude are almost identical on both planets (see Section 5.6.2)
- The contribution of environmental parameters in the Power Ratio is always at least 4.9 times larger on Earth than on Mars.

G.3 Comparison of Solar Powered Aircraft

The University of Michigan SolarBubbles Student Team has been designing, building and testing an aircraft for solar-powered flight. It is named *Huitzilopochtli*, or *Hui* for short, after the sun god of the Aztecs, and is a glider-based aircraft used for engineering education and as an autonomous vehicle test platform. Details of this aircraft can be found in Appendix F. Its primary area of flight is near Ann Arbor, Michigan, at a latitude of 42.22N deg and longitude of -83.75W deg. We assume an arbitrary flight date of August 6th.

Table G.2 Perpetuity Parameters

Mean Anomaly	Ωt	136	deg
Duration of Solar Day	t_{sd}	24	hours
Duration of Daylight	$t_s - t_r$	14.2	hours
Perpetuity Threshold	P_T	1.7	
Average Elevation	$\bar{e}$	45.95	deg

From the analysis in Section G, the Power Ratio of *Hui* on Earth is 8.86. Since this Power Ratio exceeds the Perpetuity Threshold in Table G.2, *Hui* is capable of perpetual endurance on Earth. Moreover, the Power Ratio of *Hui* on Mars is 1.8. Since the Perpetuity Thresholds on Earth and Mars are very similar, we conclude that the *Hui* would also be capable of perpetual endurance on Mars.

The *Gossamer Penguin* was the first manned, solar-powered aircraft. Built in 1979, and based upon the *Pathfinder* solar panel, this aircraft was flown several times across the Mojave desert. The design parameters and assumptions about this aircraft are shown in (69). If we again compare the Power Ratio of this aircraft between Earth and Mars we find that it is 1.03 on Earth while only 0.21 on Mars. Hence, the *Gossamer* is capable of solar-powered flight on Earth but would not have that capability on Mars.

The above examples illustrate that some solar-powered aircraft are quite capable of perpetual endurance on both Earth and Mars, but others can only fly solar-powered on Earth.

G.4 Earth's Atmosphere

The Power Ratio has a strong dependence upon the environment, which can influence the capability of an aircraft to maintain extended solar-powered flight. In this section we examine the affect of altitude on the Power Ratio.

An overview of atmospheric physics can be found in Ref. (47) and Appendix H. As an illustrative example, consider Earth's atmosphere. By taking all the altitude-dependent environmental parameters into account, the total power collected by *Hui* in perpetual flight is shown in Figure G.3.

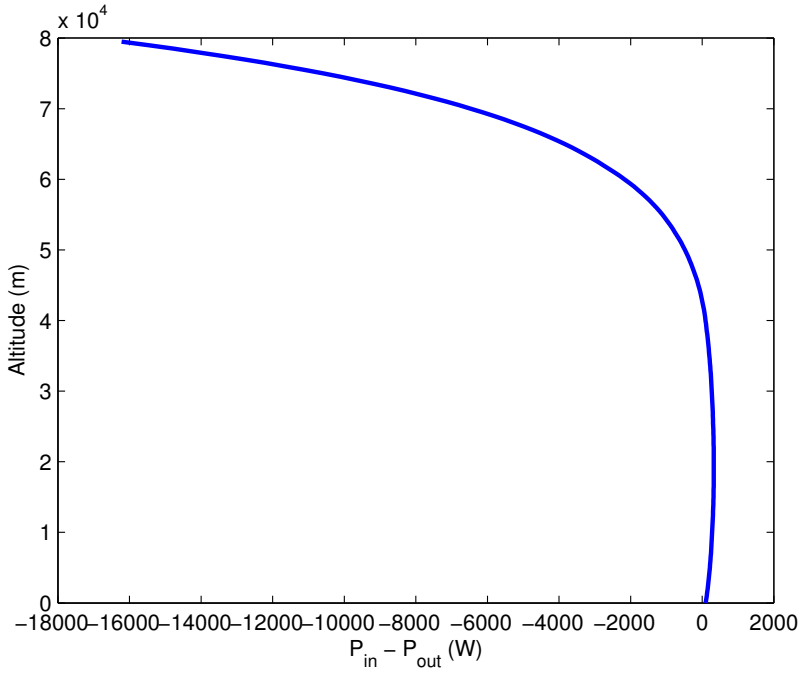

(a) Total Power

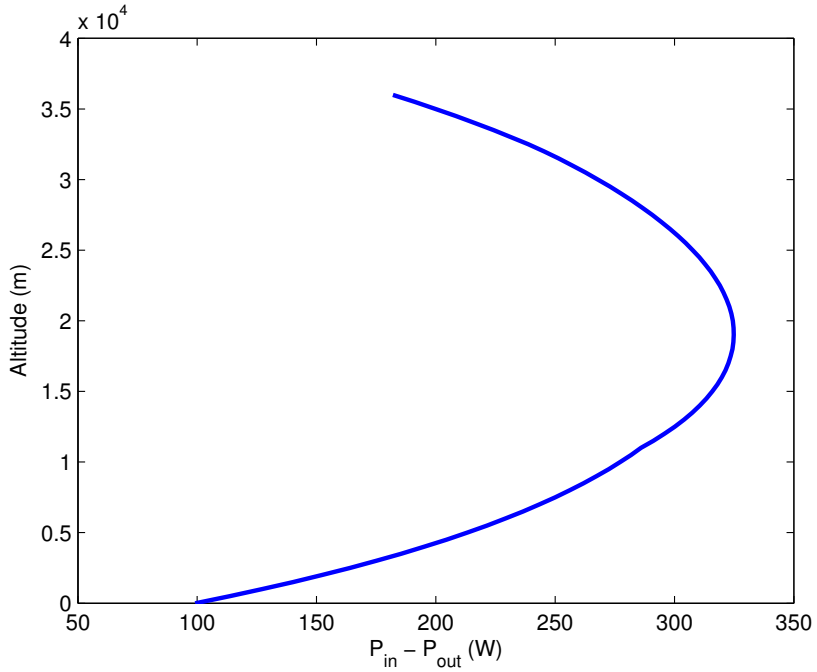

(b) Total Power (Close-up)

Figure G.3 The total power for *Hui* at altitude.

The so-called Solar Ceiling is the maximum altitude at which solar-powered aircraft can fly. There is also an optimal altitude for the aircraft to fly. These locations cannot be computed analytically but can be found numerically as in (G.3).

Appendix H

Earth's Atmosphere

The atmosphere on Earth can be divided into several layers based on temperature. These layers are the Troposphere, Stratosphere, Mesosphere, and Thermosphere. While other layers exist above an altitude of 640km, we do not consider them in this dissertation. The vertical pressure distribution can be found from the barametric equation:

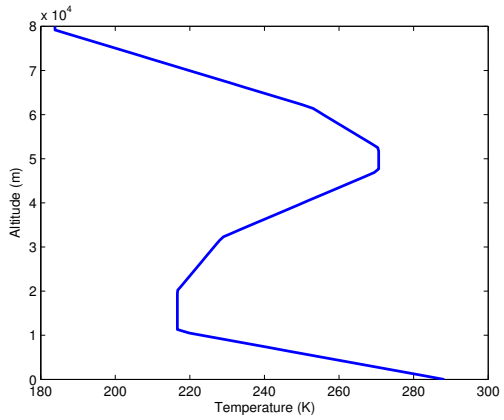

Figure H.1 Atmospheric Temperature at Altitude

$$p(h) = p_o e^{\frac{M}{R_m T(h)}}, \tag{H.1}$$

where $p(h)$ is the pressure at altitude h, p_o is the pressure at sea level, M is the molar mass of Earth's air, R_m is the molar universal gas constant and $T(h)$ is the temperature at altitude

h. Pressure as a function of altitude is shown in Figure H.2.

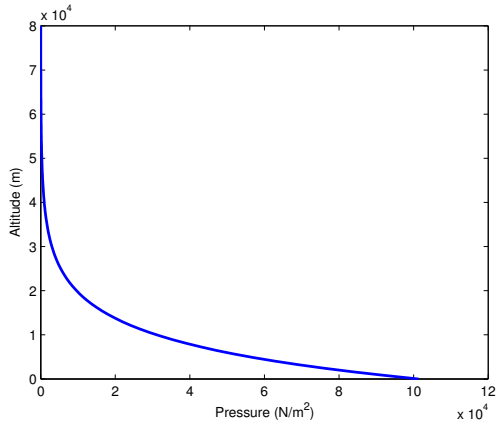

Figure H.2 Atmospheric Pressure as a function of Altitude

The density of the atmosphere is very important to any aircraft. Before flight, airline pilots must look at the density altitude, or the equivalent altitude based on the current density of the location. Density is directly dependent on temperature and pressure through the ideal gas law shown in (H.2). As temperature increases, density decreases. This is why in many tropical countries, many international airlines take off at night (when it is cooler and thus denser) to save fuel.

$$\rho = \frac{p}{RT}, \tag{H.2}$$

where R is the universal gas constant. The change of density with altitude is shown in Figure H.3.

C_{D_o} depends on the Reynolds number and velocity of the flight. The Reynolds number depends on the density of the fluid as well as its viscosity. Viscosity changes with altitude, shown in Figure H.4, roughly as

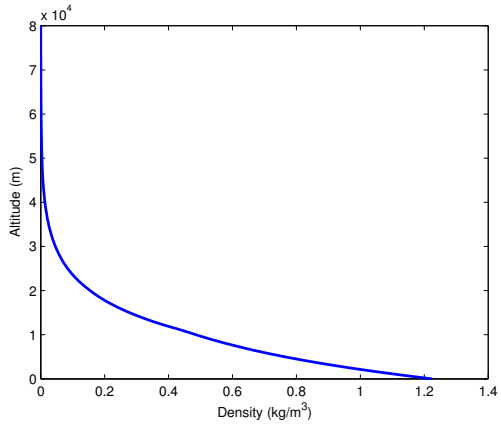

Figure H.3 Atmospheric Density at Altitude

$$\mu = 1.458e-6\frac{\sqrt{T(h)}}{(1+110.4/T(h)}. \tag{H.3}$$

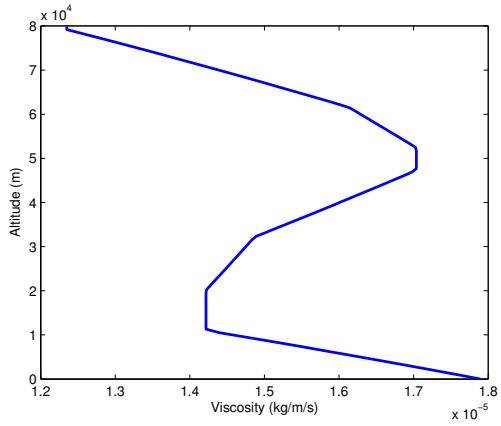

Figure H.4 Atmospheric Viscosity at Altitude

At $V_{Power_{min}}$, C_{D_o} for the *Hui* aircraft is shown in Figure H.5.

Gravitational pull also fades with altitude according to the equation

$$g(h) = g_o(1-2h/R_E), \tag{H.4}$$

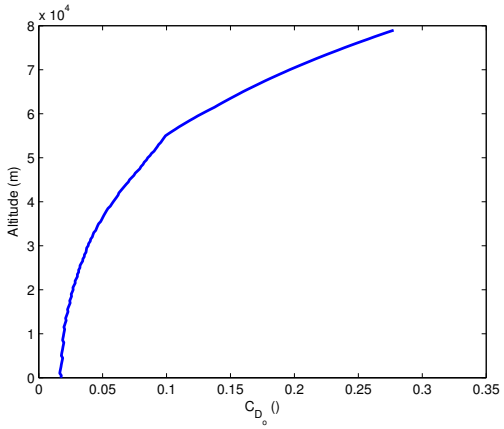

Figure H.5 Parasitic Drag at Altitude

where $g(h)$ is the gravitational acceleration as a function of altitude, g_o is gravitational pull at seal level, and R_E is the mean radius of the Earth at sea level. The decrease of gravity as a function of altitude is shown in Figure H.6.

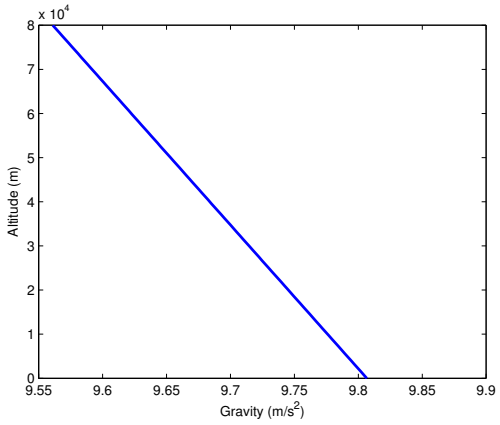

Figure H.6 Gravitational Acceleration at Altitude

The power spectral density of starlight increases with altitude. Though no definitive study has been completed (since solar-flight is a rarity), here we assume a proportional relationship between P_sd and air density. P_{sd} also depends on the location on Earth and the amount of cloud cover in the area. Typically, most cloud cover occurs below high altitude aircraft. If cloud cover is present, it can be accounted for through η_{sol}, the efficiency of the solar cells.

Bibliography

[1] Michael J. Allen. Updraft model for development of autonomous soaring uninhabited air vehicles. In *Proceedings of the ICAE 2003 Conference*. ICAE, 1996.

[2] Michael J. Allen. Autonomous soaring for improved endurance of a small uninhabited air vehicle. In *Proceedings of the 43rd Aerospace Sciences Meeting*. AIAA, 2005.

[3] Michael J. Allen. Guidance and control of an autonomous soaring uav. NASA Technical Memorandum 214611, NASA, February 2007.

[4] A. Almeida, G. Ramalho, H. Santana, P. Tedesco, T. Menezes, V. Corruble, and Y. Chevaleyre. Recent Advances on Multi-agent Patrolling. *Lecture Notes in Computer Science*, pages 474–483, 2004.

[5] B. Anderson, J.B. Moore, and M. Eslami. Optimal Filtering. *Systems, Man and Cybernetics, IEEE Transactions on*, 12(2):235–236, 1982.

[6] John D. Anderson. *Aircraft Performance and Design*. McGraw-Hill, international edition edition, Jun 1999.

[7] P. Arcara and C. Melchiorri. Control schemes for teleoperation with time delay: A comparative study. *Robotics and Autonomous Systems*, 38(1):49–64, 2002.

[8] E. Arkin, S. Fekete, and J. Mitchell. Approximation algorithms for lawn mowing and milling. In *Transportation Science (Submitted)*, 2007.

[9] N. Baldock and M. R. Mokhtarzadeh-Dehghan. A study of solar-powered, high-altitude unmanned aerial vehicles. *Aircraft Engineering and Aerospace Technology*, 78(3):187–193, 2006.

[10] J.F. Barman and H. Erzberger. Fixed-Range Optimum Trajectories for Short-Haul Aircraft. *Journal of Aircraft*, 13(10):748–754, 1976.

[11] J. Barraquand and J. C. Latombe. Robot motion planning: A distributed representation approach. *International Journal of Robotics Research*, 10:628–649, 1991.

[12] M. Batalin and G. Sukhatme. Coverage, Exploration, and Deployment by a Mobile Robot and Communications Network. *Second International Workshop on Information Processing in Sensor Networks*, pages 376–390, 2003.

[13] M. Batalin and G. Sukhatme. Efficient Exploration without Localization. *Proceedings of the 2003 ICRA, IEEE International Conference on Robotics and Automation*, pages 2714–2719, 2003.

[14] R. Beard, T. McLain, D. Nelson, and D. Kingston. Decentralized Cooperative Aerial Surveillance using Fixed-Wing Miniature UAVs. *Contract*, 5:0621, 2006.

[15] D. Ben-Arieh, G. Gutin, M. Penn, A. Yeo, and A. Zverovitch. Transformations of Generalized ATSP into ATSP: experimental and theoretical study. *Oper. Res. Lett*, 31:357–365, 2003.

[16] Patrick Berry. The Sunriser - A design study in solar powered flight. In *2000 World Aviation Conference*. AIAA and SAE, Oct 2000.

[17] D.P. Bertsekas and S. Shreve. Stochastic Optimal Control: The Discrete-TIme Case. *Optimization*, 1996.

[18] Robert J. Boucher. History of Solar Flight. In *20th Joint Propulsion Conference*. SAE and ASME, Jun 1984.

[19] F. Bourgault, AA Makarenko, SB Williams, B. Grocholsky, and HF Durrant-Whyte. Information based adaptive robotic exploration. *Intelligent Robots and System, 2002. IEEE/RSJ International Conference on*, 1, 2002.

[20] Steven A. Brandt and Fred T. Gilliam. Design Analysis Methodology for Solar-Powered Aircraft. *Journal of Aircraft*, 32(4):703–709, 1995.

[21] W. Brown. The History of Power Transmission by Radio Waves. *IEEE Transactions on Microwave Theory and Techniques*, 32(9):1230–1242, Sep 1984.

[22] M. Bryson and S. Sukkarieh. Active airborne localisation and exploration in unknown environments using inertial SLAM. *Aerospace Conference, 2006 IEEE*, page 13, 2006.

[23] Arthur E. Bryson, Jr. and Yu-Chi Ho. *Applied Optimal Control*. Hemisphere Publishing Corporation, New York, revised printing edition, 1975.

[24] David Burns and Yang Li. Study of Aerodynami Losses due to Solar Cells on Wing surfaces. University of Michigan Solarbubbles Student Team, University of Michigan, Dec 2006.

[25] J.W. Burrows. Fuel Optimal Trajectory Computation. *Journal of Aircraft*, 19(2):324–329, 1982.

[26] A.J. Calise, D.D. Moerder, Langley Research Center, United States National Aeronautics, Space Administration. Scientific, Technical Information Branch, and Drexel University Dept. of Mechanical Engineering & Mechanics. *Singular Perturbation Techniques for Real Time Aircraft Trajectory Optimization and Control*. National Aeronautics and Space Administration, Scientific and Technical Information Branch; For sale by the National Technical Information Service, 1982.

[27] L. Cesari. *Optimization-theory and applications: problems with ordinary differential equations*. Springer-Verlag, 1983.

[28] B. Chandra, H. Karloff, and C. Tovey. New results on the old k-opt algorithm for the TSP. In *Proceedings of the fifth annual ACM-SIAM symposium on Discrete algorithms*, pages 150–159. Society for Industrial and Applied Mathematics Philadelphia, PA, USA, 1994.

[29] Weisheng Chen. Directed Study Solar-Powered Unmanned Air Vehicle. University of Michigan Solarbubbles Student Team, University of Michigan, May 2006.

[30] D. F. Chichka and J. L. Speyer. Solar-powered, formation-enhanced aerial vehicle systems for sustained endurance. In *1998 American Control Conference*. IEEE, Jun 1998.

[31] T.H. Chung, V. Gupta, J.W. Burdick, and R.M. Murray. On a decentralized active sensing strategy using mobile sensor platforms in a network. *IEEE Conf. on Decision and Control*, pages 1914–1919, 2004.

[32] J.C. Clements. Minimum-time turn trajectories to fly-to points. *OPTIMAL CONTROL APPLIC. METHODS.*, 11(1):39–50, 1990.

[33] Nicholas J. Colella and Gordon S. Wenneker. Pathfinder and the Development of Solar Rechargable Aircraft. *Energy and Technology Review*, pages 1–9, 1994.

[34] A. Colozza. Solid State Aircraft. *Phase I Final Report, prepared for NASA Institute for Advanced Concepts, Nov*, 2002.

[35] Anthony J. Colozza. Effect of Power System Technology and Mission Requirements on High Altitude Long Endurance Aircraft. NASA Contractor Report 194455, NASA, Feb 1994.

[36] Anthony J. Colozza. Effect of Date and Location on Maximum Achievable Altitude for a Solar Powered Aircraft. NASA Contractor Report 202326, NASA, Mar 1997.

[37] Anthony J. Colozza. Convective Array Cooling for a Solar Powered Aircraft. NASA Contractor Report 212084, NASA, Jan 2003.

[38] Anthony J. Colozza, David A. Scheiman, and David J. Brinker. GaAs/Ge Solar Powered Aircraft. NASA Technical Memorandum 1998-208652, NASA, Oct 1998.

[39] M. A. Dornheim. Get me through the night. *Aviation Week and Space Technology*, 159(11):66, 68, 70, Sep 2003.

[40] Michael. A. Dornheim. SoLong Solar-Powered Drone Stays Aloft for 48 Hr. *Aviation Week and Space Technology*, Jun 2005.

[41] Michael A. Dornheim. Solar Powered Research and Dryden. *Webpage, Available at: http://www.nasa.gov/centers/dryden/news/FactSheets/FS-054-DFRC.html*, 2006.

[42] J.J. Dougherty and J.L. Speyer. Near-Optimal Guidance Law for Ballistic Missile Interception. *J. of Guidance, Control and Dynamics*, 20, 1997.

[43] L. E. Dubins. On curves of minimal length with a constraint on average curvature, and with prescribed initial and terminal positions and tangents. *American Journal of Mathematics*, 79:497–517, 1957.

[44] J. Enright and E. Frazzoli. UAV Routing in a Stochastic Time-Varying Environment. In *Proceedings of the International Federation of Automatic Control*, 2005.

[45] Y. Fan, F.H. Lutze, and E.M. Cliff. Time-optimal lateral maneuvers of an aircraft. *Journal of Guidance, Control, and Dynamics*, 18(5):1106–1112, 1995.

[46] R.A. Fisher. Theory of statistical estimation. In *Proceedings of the Cambridge Philosophical Society*, volume 22, pages 700–725. Cambridge: Coambridge Univ. Press, 1925.

[47] Robert G. Fleagle and Joost A. Businger. *An Introduction to Atmospheric Physics*. Academic Press, Inc., New York, 1st edition edition, 1963.

[48] Kirk Flittie and Bob Curtin. Pathfinder solar-powered aircraft flight performance. In *Atmospheric Flight Mechanics Conference and Exhibit*. AIAA, Aug 1998.

[49] G. Frulla. Preliminary reliability design of a solar-powered high-altitude very long endurance unmanned air vehicle. *Proceedings of the Institution of Mechanical Engineers, Part G: Journal of Aerospace Engineering*, 216(4):189–196, 2002.

[50] MP Golombek, JA Grant, TJ Parker, DM Kass, JA Crisp, SW Squyres, AFC Haldemann, M. Adler, WJ Lee, NT Bridges, et al. Selection of the Mars Exploration Rover landing sites. *J. Geophys. Res*, 108:8072, 2003.

[51] J.J. Grefenstette, R. Gopal, B.J. Rosmaita, and D. Van Gucht. Genetic Algorithms for the Traveling Salesman Problem. *Proceedings of the 1st International Conference on Genetic Algorithms table of contents*, pages 160–168, 1985.

[52] W. Grimm, KH Well, and HJ Oberle. Periodic Control for Minimum Fuel Aircraft Trajectories. *Journal of Guidance, Control, and Dynamics*, 9(2):169–174, 1986.

[53] B. Grocholsky. Information-theoretic control of multiple sensor platforms. 2006.

[54] G. Gutin and D. Karapetyan. Generalized Traveling Salesman Problem Reduction Algorithms. *Arxiv preprint arXiv:0804.0735*, 2008.

[55] D. W. Hall, D. A. Watson, R. P. Tuttle, and S. A. Hall. Mission analysis of solar powered aircraft. NASA Contractor Report 172583, NASA, Jul 1985.

[56] David W. Hall, Charles D. Fortenbach, Emanual V. Dimiceli, and Robert W. Parks. A Preliminary Study of Solar Powered Aircraft and Associated Power Trains. NASA Contractor Report 3699, NASA, Dec 1983.

[57] Z. Hao, H. Huang, and R. Cai. Bio-inspired Algorithms for TSP and Generalized TSP. *Travelling Salesman Problem*, page 35, 2008.

[58] S.S. Haykin et al. *Kalman Filtering and Neural Networks*. Wiley Chichester, 2001.

[59] M. Hebert, C.E. Thorpe, and A. Stentz. *Intelligent unmanned ground vehicles: autonomous navigation research at Carnegie Mellon*. Kluwer Academic Publishers, 1997.

[60] AL Henry-Labordere. The record balancing problem: A dynamic programming solution of a generalized traveling salesman problem. *RAIRO B*, 2:43–49, 1969.

[61] S.L. Holmes. The New Close Air Support Weapon: Unmanned Combat Aerial Vehicle in 2010 and Beyond, 1999.

[62] Peter C. Hughes. *Spacecraft Attitude Dynamics*. Dover Publications, Dec 2004.

[63] I.I. Hussein. Kalman Filtering with Optimal Sensor Motion Planning. In *Proceedings of the American Control Conference*, 2008.

[64] F. G. Irving and D. Morgan. The feasibility of an aircraft propelled by solar energy. In *2nd International Symposium on the Technology and Science of Low Speed and Motorless Flight*. AIAA, Sep 1974.

[65] K. Jaradat and R. Langari. Line map construction using a mobile robot with a sonar sensor. *Advanced Intelligent Mechatronics. Proceedings, 2005 IEEE/ASME International Conference on*, pages 1251–1256, 2005.

[66] R.E. Kalman. A new approach to linear filtering and prediction problems. *Journal of Basic Engineering*, 82(1):35–45, 1960.

[67] L. E. Kavraki, P. Latombe, and M. Overmars. Probabilistic roadmaps for path planning in high-dimensional configuration spaces. *IEEE Transactions on Robotics and Automation*, 12:566–580, 1996.

[68] D. Kingston, R. Beard, T. McLain, M. Larsen, and W. Ren. Autonomous vehicle technologies for small fixed wing UAVs. In *AIAA 2nd Unmanned Unlimited Systems, Technologies, and Operations–Aerospace, Land, and Sea Conference and Workshop & Exhibit*, pages 2003–6559, 2003.

[69] Andrew Klesh and Pierre Kabamba. Solar-powered aircraft: Energy-optimal path planning and perpetual endurance. University of Michigan Control Group Report CGR 09-01, University of Michigan, Jan 2009.

[70] Andrew T. Klesh. SolarBubbles Sponsorship Packet. University of Michigan Solarbubbles Student Team, University of Michigan, 2006.

[71] Craig A. Kluever. Feedback control for spacecraft rendevouz and docking. *Journal of Guidance, Control and Dynamics*, 22(4), 1999.

[72] D. E. Koditschek. Exact robot navigation by means of potential functions: Some topological considerations. In *Proceedings of the 1987 International Conference on Robotics and Automation*. IEEE, 1987.

[73] J.B. Kruskal. On the shortest spanning subtree of a graph and the traveling salesman problem. *Proceedings of the American Mathematical Society*, 7(1):48–50, 1956.

[74] S. Kullback. *Information Theory and Statistics*. Courier Dover Publications, 1997.

[75] H.J. Kushner and P. Dupuis. *Numerical Methods for Stochastic Control Problems in Continuous Time*. Springer, 2001.

[76] J. C. Latombe. *Robot Motion Planning*. Kluwer Academic Publishers, 1991.

[77] S. M. LaValle and J. J. Kuffner. Randomized kinodynamic planning. In *Proceedings of the IEEE International Conference on Robotics and Automation*. IEEE, 1999.

[78] E.L. Lawler. *The Traveling Salesman Problem: A Guided Tour of Combinatorial Optimization*. Wiley, 1985.

[79] E. B. Lee and L. Markus. *Foundations of Optimal Control Theory*. University of Minnesota - Minneapolis, Minnesota, 1967.

[80] D. Leonard and N. van Long. *Optimal Control Theory and Static Optimization in Economics*. Cambridge University Press, 1992.

[81] S. Lin and B.W. Kernighan. An effective heuristic algorithm for the traveling salesman problem. *Operations Research*, 21(2):498–516, 1973.

[82] T.J. Loredo and D.F. Chernoff. Bayesian adaptive exploration. *Statistical Challenges in Astronomy*, pages 57–70, 2003.

[83] T. Lozano-Perez. Automatic planning of manipulator transfer movements. *IEEE Transactions on Systems, Man and Cybernetics*, 11:681–698, 1981.

[84] T. Lozano-Perez and M.A. Wesley. An algorithm for planning collision-free paths among polyhedral obstacles. *Communications of the ACM*, 22:681–698, 1979.

[85] P. B. MacCready, P. B. S. Lissaman, W. R. Morgan, and J. D. Burke. Sun Powered Aircraft Design. In *Annual Meeting and Technical Display on Frontiers of Achievement*. AIAA, May 1981.

[86] S. Martínez and F. Bullo. Optimal sensor placement and motion coordination for target tracking. *Automatica*, 42(4):661–668, 2006.

[87] I. Maza and A. Ollero. Multiple UAV Cooperative Searching Operation using Polygon Area Decomposition and Efficient Coverage Algorithms. *7th International Symposium on Distributed Autonomous Robotic Systems*, 2004.

[88] TG McGee and JK Hedrick. Path planning and control for multiple point surveillance by an unmanned aircraft in wind. In *American Control Conference, 2006*, page 6, 2006.

[89] PK Menon, E. Kim, and VHL Cheng. Optimal Trajectory Planning for Terrain Following Flight. *Journal of Guidance, Control and Dynamics*, 14(4):807–813, 1991.

[90] Darryl E. Metzger and J. Karl Hedrick. Optimal flight paths for soaring flight. In *Proceedings of the 2nd International Symposium on the Technology and Science of Low Speed and Motorless Flight*. AIAA, 1974.

[91] NASA. The Vision for Space Exploration, Feb 2004.

[92] P. Newman, M. Bosse, J. Leonard, and C. MIT. Autonomous feature-based exploration. *Robotics and Automation, 2003. Proceedings. ICRA'03. IEEE International Conference on*, 1, 2003.

[93] A. Noth, W. Engel, and R. Siegwart. Design of an Ultra-Lightweight Autonomous Solar Airplane for Continuous Flight. *Proceedings of Field and Service Robotics, Port Douglas, Australia*, 2005.

[94] Andre Noth, W. Engel, and R. Siegwart. Flying Solo and Solar to Mars - Global Design of a Solar Autonomous Airplane for Sustainable Flight. *IEEE Robotics and Automation Magazine*, 13(3):44–52, Sep 2006.

[95] N. Nourani-Vatani, M. Bosse, J. Roberts, and M. Dunbabin. Practical Path Planning and Obstacle Avoidance for Autonomous Mowing. *Proc. of the Australasian Conference of Robotics and Automation*, 2006.

[96] Office of the Secretary of Defense. Unmanned aircraft systems roadmap, 2005 – 2030. 2005.

[97] J. Ousingsawat and M.E. Campbell. Establishing Trajectories for Multi-Vehicle Reconnaissance. In *AIAA Guidance, Navigation, and Control Conference and Exhibit, Providence, Rhode Island*, pages 1–12, 2004.

[98] J.T. Pado. Remotely operated underwater vehicle, January 26 1988. US Patent 4,721,055.

[99] C Palazzi, C Roseti, M Luglio, M Gerla, M Sanadidi, and J Spepanek. Satellite Coverage in Urban Areas using Unmanned Airborne Vehicles (UAVs)," . *Vehicular Technology Conference*, 2004.

[100] C. K. Patel, H. Arya, and K. Sudhakar. Design, Build and Fly a Solar Powered Aircraft. In *International Seminar and Annual General Meeting of the Aeronautical Society of India*. Aeronautical Society of India, 2002.

[101] F. Plastria and V.U. Brussel. Mixed zero-one Programming.

[102] Y. Qi and Y. Zhao. Energy-efficient trajectories of unmanned aerial vehicles flying through thermals. *Journal of Aerospace Engineering*, pages 84–92, April 1996.

[103] G. Reinelt. TSPLIB-A Traveling Salesman Problem Library. *ORSA Journal on Computing*, 3(4):376–384, 1991.

[104] K. C. Reinhardt, T. R. Lamp, J. W. Geis, and A. J. Colozza. Solar-powered unmanned aerial vehicles. In *31st Intersociety Energy Conversion Engineering Conference*. IECEC, Aug 1996.

[105] B. Rhine. Solar-powered Gossamer Penguin in flight. *Webpage, Available at: http://www.dfrc.nasa.gov/Gallery/Photo/Albatross/HTML/ECN-13413.html*, 2002.

[106] C. Roberts, M. Vaughan, and W. J. Bowman. Development of a Solar Powered Micro Air Vehicle. In *40th Aerospace Sciences Meeting and Exhibit*. AIAA, Jan 2002.

[107] G. Romeo, G. Frulla, E. Cestino, and F. Borello. SHAMPO: Solar HALE Aircraft for Multi Payload and Operations. *Aerotecnica Missili e Spazio*, 85, Sep 2005.

[108] Giulio Romeo and Giacomo Frulla. HELIPLAT: Aerodynamic and Structural Analysis of HAVE Solar Powered Platform. In *1st Technical Conference and Workshop on Unmanned Aerospace Vehicles*. AIAA, May 2002.

[109] D.J. Rosenkrantz, R.E. Stearns, P.M. Lewis, et al. An Analysis of Several Heuristics for the Traveling Salesman Problem. *SIAM Journal on Computing*, 6:563, 1977.

[110] G. Sachs and T. Christodoulou. Reducing fuel consumption of subsonic aircraft by optimal cyclic cruise. *J. AIRCRAFT.*, 24(9):616–622, 1987.

[111] K Savla, F. Bullo, and E. Frazzoli. On Traveling Salesperson Problem for Dubins' Vehicle: Stochastic and Dynamic Environments. In *Proceedings of the 44th IEEE Conference on Decision and Control and the European Control Conference 2005*. IEEE, 2005.

[112] D. Scheler. Introduction to electronic warfare, 1986.

[113] R.L. Schultz and N.R. Zagalsky. Aircraft Performance Optimization. *Journal of Aircraft*, 9(2):108–114, 1972.

[114] J. T. Schwartz and M. Sharir. On the piano mover's problem: I. the case of a two-dimensional rigid polygonal body moving admist polygonal barriers. *Communications on Pure and Applied Mathematics*, 36:345–398, 1983.

[115] J. T. Schwartz and M. Sharir. On the piano mover's problem: Ii. general techniques for computing topological properties of real algebraic manifolds. *Advances in Applied Mathematics, Academic Press*, 4:51–96, 1983.

[116] J. T. Schwartz and M. Sharir. On the piano mover's problem: Iii. coordinating the motion of several independent bodies: The special case of circular bodies. *Planning, Geometry, and Complexity of Robot Motion*, 1987.

[117] Claude Shannon. A Mathematical Theory of Communication. *The Bell System Technical Journal*, 27:379–423, 623–656, 1948.

[118] TB Sheridan and C. MIT. Space teleoperation through time delay: review and prognosis. *Robotics and Automation, IEEE Transactions on*, 9(5):592–606, 1993.

[119] R. Sim. To Boldly Go: Bayesian Exploration for Mobile Robots, 2000.

[120] R. Sim and N. Roy. Global A Optimal Robot Exploration in SLAM. *log*, 2(1):2.

[121] C. SNYDER and V. MOROZ. Spacecraft exploration of Mars. *Mars(A 93-27852 09-91)*, 1992.

[122] P. Soueres and J. P. Laumond. Shortest paths synthesis for a car-like robot. *IEEE Transactions on Automatic Control*, pages 672–688, 1996.

[123] J.L. Speyer. Nonoptimality of the Steady-State Cruise for Aircraft. *AIAA Journal*, 14(11):1604–1610, 1976.

[124] Paul M. Stella and Dennis J. Flood. Photovoltaic Options for Solar Electric Propulsion. NASA Technical Memorandum 103284, Jul 1990.

[125] R.F. Stengel. *Optimal control and estimation*. Dover Publications.

[126] V.A. Sujan and M.A. Meggiolaro. On the Visual Exploration of Unknown Environments using Information Theory Based Metrics to Determine the Next Best View. *Mobile Robots: New Research*, 2006.

[127] P. Svestka and M. Overmars. Coordinated motion planning for multiple car-like robots using probabilistic roadmaps. In *Proceedings of the IEEE International Conference on Robotics and Automation*. IEEE, 1995.

[128] Colin R. Theodore, Mark B. Tischler, and Jason D. Colbourne. Rapid Frequency-Domain Modeling Methods for Unmanned Aerial Vehicle Flight Control Applications. *Journal of Aircraft*, 41(4):735–743, Aug 2004.

[129] S. Thrun, Y. Liu, D. Koller, A.Y. Ng, Z. Ghahramani, and H. Durrant-Whyte. Simultaneous Localization and Mapping with Sparse Extended Information Filters. *The International Journal of Robotics Research*, 23(7-8):693, 2004.

[130] O. Trifu and G. Savu. Unmanned solar powered aerial surveyor configured with an aerodynamic optimization procedure. In *15th AIAA Applied Aerodynamics Conference*. AIAA, Jun 1997.

[131] S. Udupa. Collision detection and avoidance in computer controlled manipulators, 1977.

[132] E. van der Meulen. A survey of multi-way channels in information theory: 1961-1976. *Information Theory, IEEE Transactions on*, 23(1):1–37, 1977.

[133] J.L. Vian and J.R. Moore. Trajectory optimization with risk minimization for military aircraft. *Journal of Guidance, Control, and Dynamics*, 12(3):311–317, 1989.

[134] R. Vinter and S. Sieniutycz. Optimal Control. *Applied Mechanics Reviews*, 54:B82, 2001.

[135] J.P. Watson, C. Ross, V. Eisele, J. Denton, J. Bins, C. Guerra, D. Whitley, and A. Howe. The Traveling Salestep Problem, Edge Assembly Crossover, and 2-opt. *LECTURE NOTES IN COMPUTER SCIENCE*, pages 823–834, 1998.

[136] William H. Phillips. Some Design Considerations for Solar-Powered Aircraft. NASA Technical Report 1675, Jun 1980.

[137] C. Wilson, J. Nutbean, and I. Bond. Aerodynamic and Structural Design of a Solar-Powered Micro Unmanned Air Vehicle. *Proceedings of the Institution of Mechanical Engineers, Part G: Journal of Aerospace Engineering*, 214(2):97–106, 2000.

[138] J. W. Youngblood and T. A. Talay. Solar-powered airplane design for long-endurance, high altitude flight. In *2nd International Verh Large Vehicles Conference*. AIAA, May 1982.

[139] J. W. Youngblood, T. A. Talay, and R. J. Pegg. Design of long-endurance unmanned airplanes incorporating solar and fuel cell propulsion. In *20th Joing Propulsion Conference*. SAE and ASME, Jun 1984.

[140] A. Zelinsky, RA Jarvis, JC Byrne, and S. Yuta. Planning paths of complete coverage of an unstructured environment by a mobile robot. In *Proceedings of International conference on Advanced Robotics*, pages 533–538, 1993.